NASA Technical Memorandum 104146

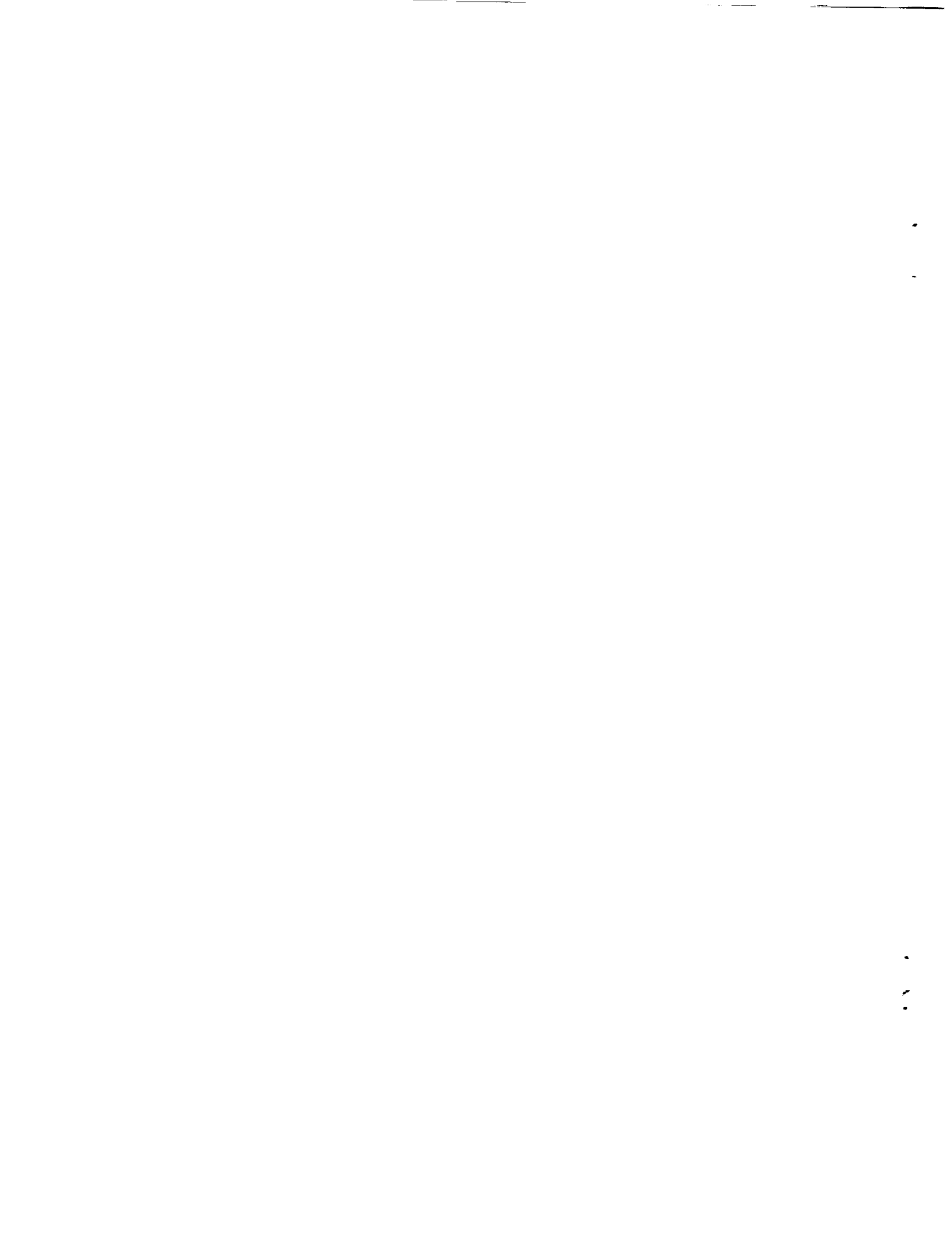# TECHNICAL ACTIVITIES OF THE CONFIGURATION AEROELASTICITY BRANCH

Stanley R. Cole, Editor

October 1991

NASA

National Aeronautics and
Space Administration

Langley Research Center
Hampton, Virginia 23665

PREFACE

This compilation is a summary of a technical review of the Configuration Aeroelasticity Branch of the Structural Dynamics Division. The Configuration Aeroelasticity Branch is one of five branches in the Structural Dynamics Division. Each of these branches participates in periodic technical reviews to improve inter-branch communication and dissemination of technical developments and information concerning the work being conducted. This compilation contributes further to this goal of the technical reviews as well as providing a thorough overview of the Configuration Aeroelasticity Branch for other interested individuals and organizations.

The papers presented herein are assembled according to the various working units within the Configuration Aeroelasticity Branch. The first paper, authored by Rodney H. Ricketts (branch head), provides a full description of the branch and its associated facilities and program efforts. The following ten papers cover specific projects conducted or underway in the branch. The final paper describes the primary facility operated by the branch, the Langley Transonic Dynamics Tunnel, and is authored by the facility safety head, Bryce M. Kepley.

The following Configuration Aeroelasticity Branch engineers also deserve specific recognition for their contributions to this publication:

- Frank W. Cazier, Jr., Michael H. Durham, Donald F. Keller, and Ellen C. Parker of the Aircraft Aeroelasticity Group

- Paul H. Mirick, Matthew L. Wilbur, and W. Keats Wilkie of the Rotorcraft Aeroelasticity Group

- Bryan E. Dansberry, Clinton V. Eckstrom, Moses G. Farmer, and José A. Rivera, Jr. of the Aircraft Aeroelastic Validation Group

- Renee C. Lake and Howard E. Hinnant of the Rotorcraft Structural Dynamics Group.

Special thanks are extended to the Configuration Aeroelasticity Branch secretary, Christine Caldwell, for the many hours of work that she contributed to make this publication possible.

Stanley R. Cole
Technical Review Editor

i

CONTENTS

V - ROTORCRAFT STRUCTURAL DYNAMICS GROUP

VI - FACILITY OVERVIEW

CONFIGURATION AEROELASTICITY BRANCH OVERVIEW

Rodney H. Ricketts
NASA Langley Research Center
Hampton, VA

CONFIGURATION AEROELASTICITY

AIRCRAFT
DEVELOPMENT TESTS

ROTORCRAFT
AEROELASTICITY

TRANSONIC DYNAMICS TUNNEL

BASIC STUDIES

STRUCTURAL DYNAMICS
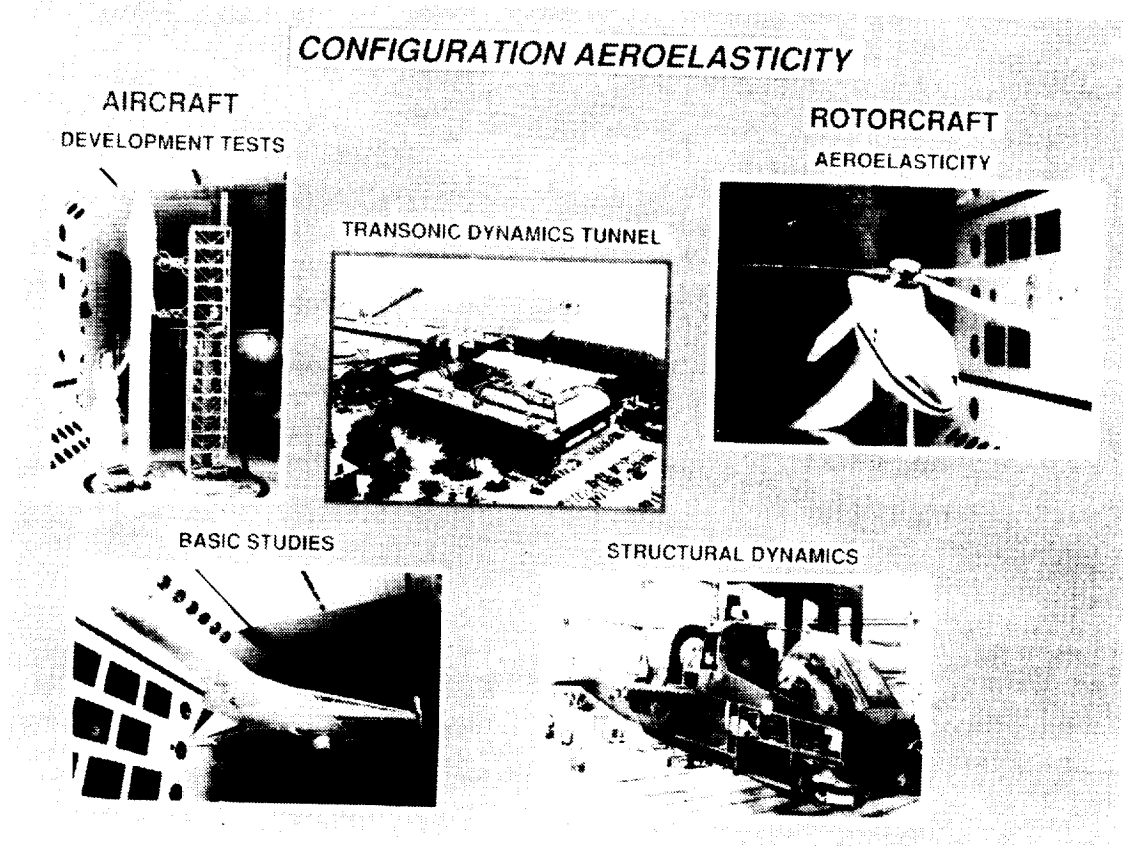
The Configuration Aeroelasticity Branch (CAB) is one of five branches in the Structural Dynamics Division at NASA Langley Research Center. Research is conducted in the areas of aeroelasticity and structural dynamics in support of a wide variety of aerospace vehicles, including aircraft, rotorcraft and space launch systems. Basic research to determine fundamental physics of aeroelastic phenomena and tests to support full-scale vehicle development are conducted in the Transonic Dynamics Tunnel (TDT) by branch personnel.

Four Necessary "P's"

People

Ph(F)acilities

Program

Ph(F)unding

The four elements necessary for viable research include people, facilities, program, and funding. With any element missing, the research cannot be successfully conducted. These elements can be called the Four P's when the "F"-words are misspelled by substituting Ph for F. This paper describes the people, facilities and the research program of the CAB.

Research/Operations/Management

Aircraft Aeroelasticity Group (7)	**Rotorcraft Aeroelasticity Group (9)**	**Facilities Operations Group (9)**
Aircraft Aeroelastic Validation Group (4)	**Rotorcraft Structural Dynamics Group (6)**	**Branch Office (4)**

The CAB is organized into five groups which report to the branch office. Two of the groups conduct research related to aircraft, two groups conduct research related to rotorcraft, and one group is responsible for facility operations. The numbers in parentheses define the number of personnel in each group. The personnel include 25 NASA and Army civil servants and 12 non-personnel service (NPS) contractors. NPS contractors represent the following companies: Lockheed Engineering and Sciences Company, Wyle Laboratories, and Vigyan Associates.

Facilities

Transonic Dynamics Tunnel (TDT)

Hover Lab

Data Acquisition System

The CAB conducts research using its three facilities, namely, the Transonic Dynamics Tunnel (TDT), the General Rotor Aeroelastic Laboratory (GRAL) and the data acquisition system. Each of these is described in the following charts.
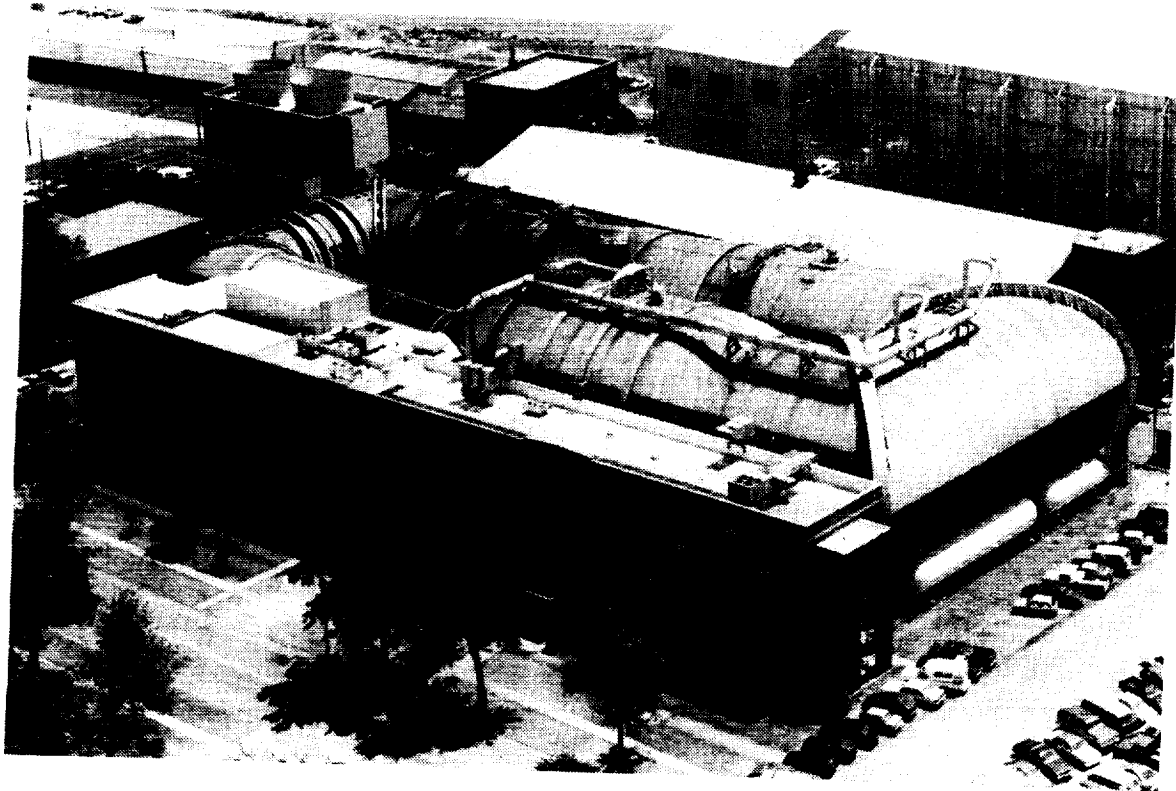
The TDT (shown above) is a major national wind-tunnel facility for conducting aeroelastic tests in the transonic regime. It is a closed-circuit, single return tunnel with a 16' by 16' test section. The TDT uses Freon or air as a medium for testing to Mach number 1.2. When Freon gas is used in tests, it must be reclaimed and stored as a liquid for future use. The reclamation processing system is currently being upgraded through a $6.5 million Construction of Facility (CoF) project.

ARES HOVER FACILITY
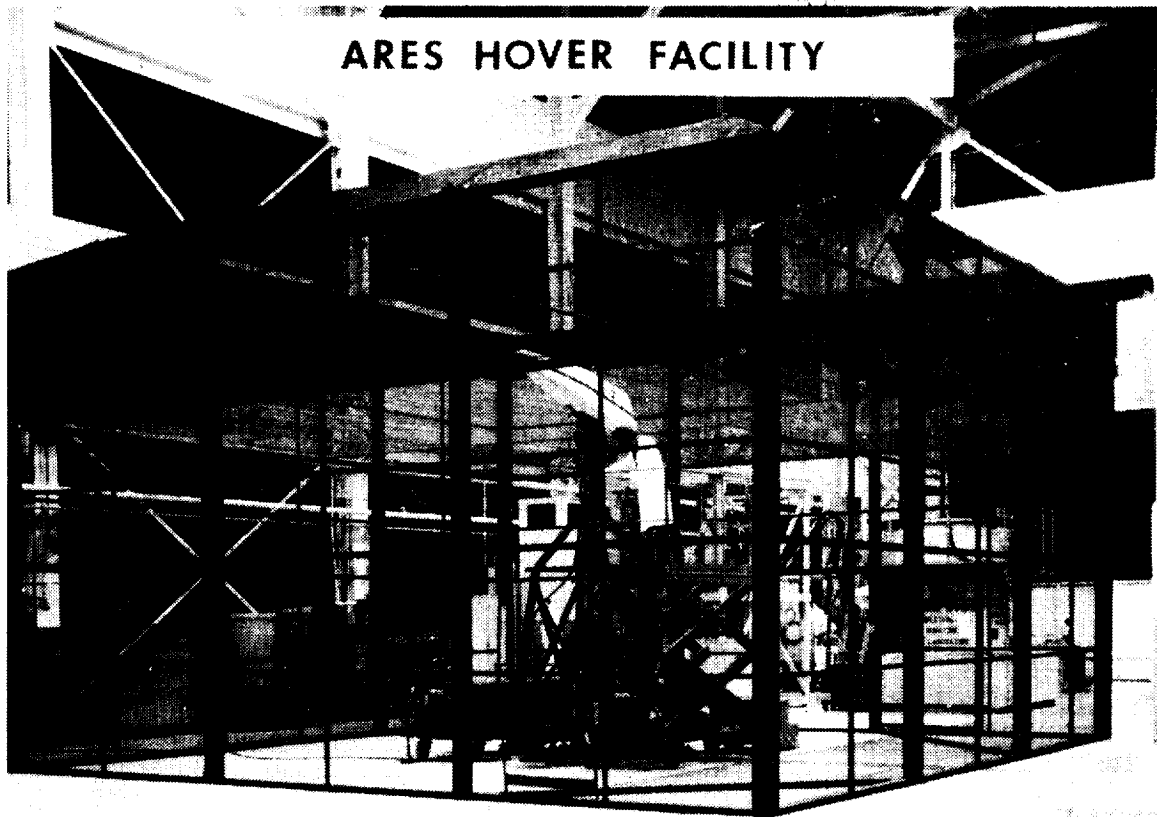
The helicopter GRAL is located in a high-bay area of Building 647. It consists of a room for model build up and checkout and a large (30'x 30'x 20' high) screened area for testing the rotor in hover. The models are elevated 15' above the floor during testing. The helicopter rotor testbed (ARES) is shown in the screened area pictured above.
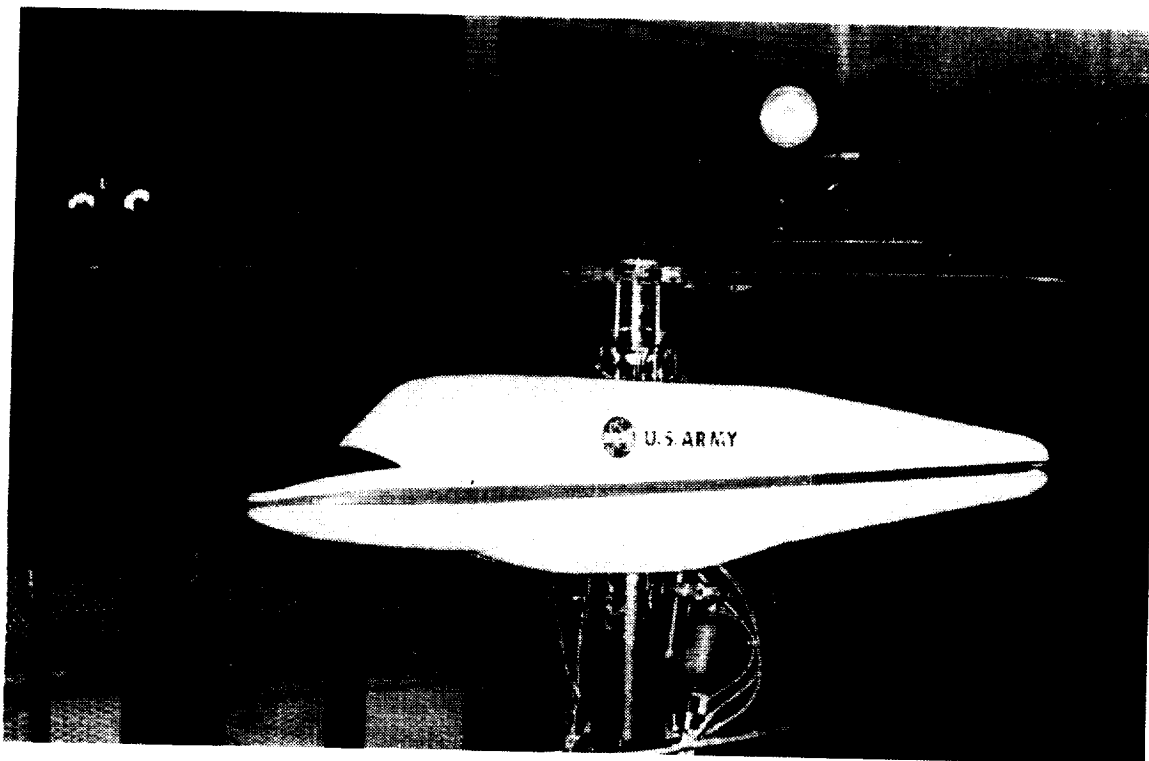
The Aeroelastic Rotor Experimental System (ARES) is the testbed used in rotor research. Advanced blades and hubs are mounted on ARES and first tested in the GRAL before being tested in the TDT. A hingeless rotor system being tested on ARES is shown above.

A new MODCOMP data acquisition system (DAS) became operational in the spring of 1988. It supports research testing in the TDT, GRAL, and calibration laboratories. The view of the DAS above shows the array of hard disk drives present in the system.

Data Acquisition -- TDT vs NTF

	NTF	TDT	RATIO
NUMBER OF COMPUTERS	4	3	
SPEED (mips), per CPU	0.9	2.5	
total	3.6	7.5	2+
HARD DISKS, number	4	8	
capacity, megabytes	1	2	2
DIGITAL TAPES, number	6	6	
speed, kilobytes/sec	120	750	6+
ANALOG SAMPLING RATE			
kilosamples/sec	40	287	7+

In comparison to the data acquisition system of the National Transonic Facility (NTF), the TDT data acquisition system has more than twice the speed, twice the hard disk storage capacity, more than six times the digital tape capacity and more than seven times the data sampling rate. The TDT system is used to acquire data, to reduce it at "near realtime" speeds, and to provide on-line measurements of aerodynamic performance, model loads and aeroelastic stability characteristics.

- **Determine aeroelastic characteristics and develop databases for validating new computational codes**

| 1989 | 1990 | 1991 | 1992 |

HiMARCS rotors

Benchmark aeroelastic models

NASP buzz/panel flutter

AFW active controls

Planform/wing-tip flutter effects

ARES vibration (mass) & noise (BVI) reduction
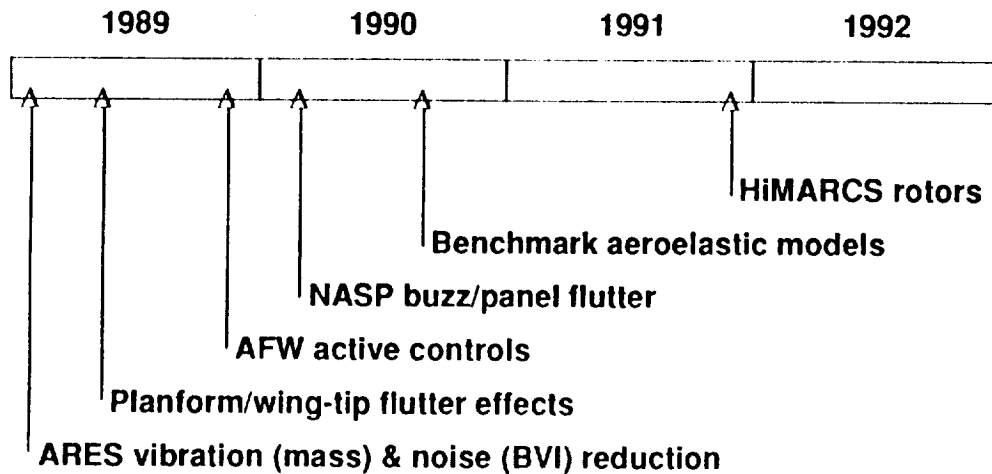
One technical objective of the CAB is to determine the aeroelastic characteristics of new aerospace configurations. Another objective is to develop experimental databases for use in validating new computational aeroelastic codes. Some of the milestones to meet these objectives are shown on the chart above for the years 1989 to 1992.

Aileron buzz and panel flutter model tests and analyses are being conducted to support the National Aerospace Plane (NASP) program. Aeroelastic models are being developed for measuring benchmark data for code validation. Highly maneuverable and agile rotor/control systems (HiMARCS) will be developed and tested in support of advanced Army rotorcraft programs. Active Flexible Wing (AFW) model and NASP model studies are described in the following charts.

OPEN- AND CLOSED-LOOP FLUTTER CHARACTERISTICS OF MODIFIED AFW MODEL DETERMINED IN TDT
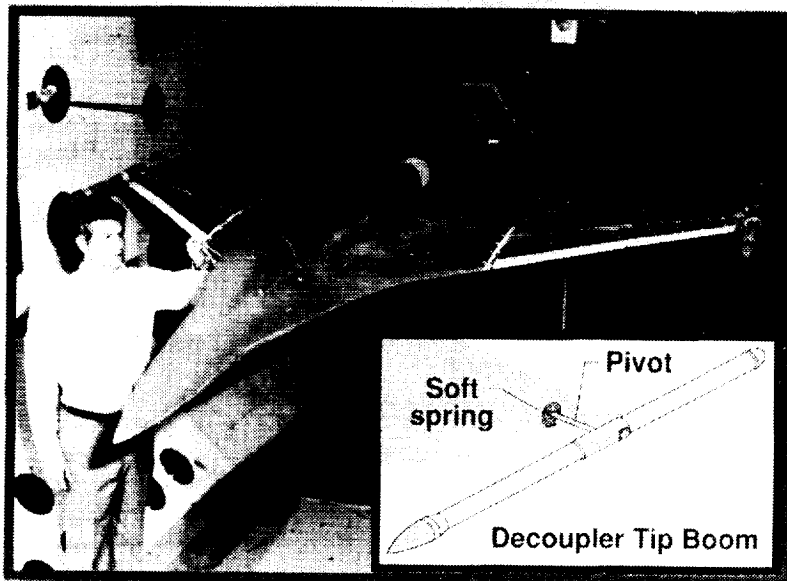
The Active Flexible Wing (AFW) model was tested in the TDT to define the open-loop and closed-loop flutter characteristics of the model. The AFW was modified with a tip boom to allow flutter of the model to be achieved within the tunnel operational envelope. The wing tip boom had a decoupler device that allowed a soft-spring suspension in addition to the normal stiff condition. The model with the soft spring condition had a substantially higher flutter speed than the stiff condition. Therefore, the tip boom also served as a flutter stopper when the soft suspension was engaged. Three flutter suppression system (FSS) control laws were tested. One law was able to suppress flutter to 24 percent above the open-loop condition.

The next test of AFW is scheduled for February 1990, and will integrate FSS control laws with rolling maneuver load alleviation (RMLA) Control laws.

NASP AEROELASTICITY STUDIES IN TDT

ALL-MOVEABLE WING MODEL

AILERON BUZZ MODEL

PANEL FLUTTER MODEL

FUSELAGE SHAPE STUDY

All-moveable
70 sweep delta wing

Wing tip fins

Fiberglass shell
fuselage wrapped
around aluminum
flat plate

Sting
mounted with
pitch plunge
freedom
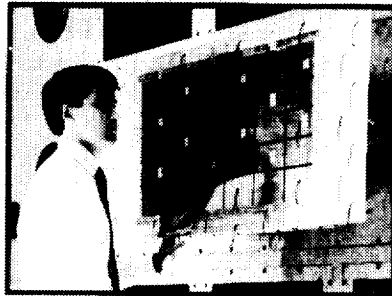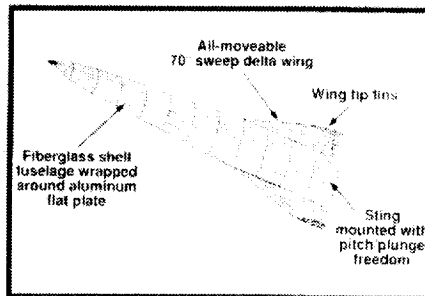
The CAB has conducted a number of flutter model studies in support of the NASP. These studies have been conducted in cooperation with McDonnell Douglas and Rockwell International. Three of the studies are shown above. One test determined the flutter and divergence characteristics of an all-moveable wing. Another test determined the buzz characteristics of a full-span aileron. A third study investigated the panel flutter characteristics in the transonic region. A fourth study to investigate the fuselage shape effects on flutter has been initiated.

• **Insure new vehicle designs are safe from aeroelastic problems**

1989   1990   1991   1992

A12 flutter clearance

F106 VF flight flutter tests

ATLAS II ground-wind loads

ATF flutter clearance

Navy ATF

F16 Agile

LHX
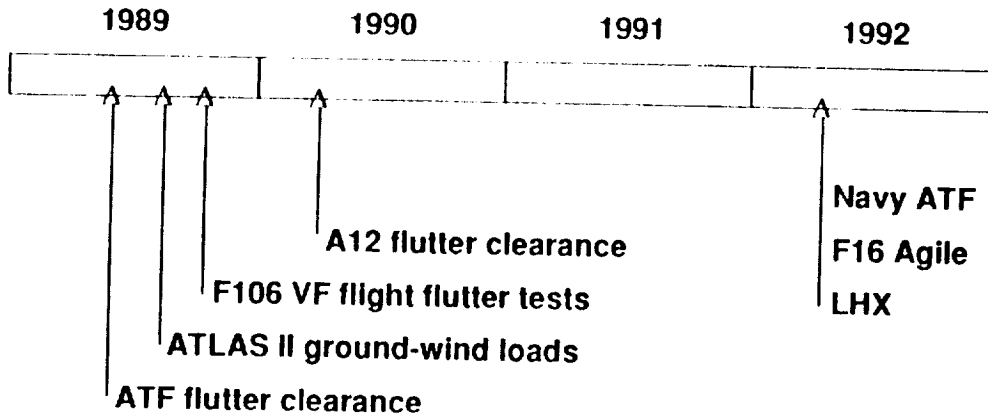
The second technical objective of the CAB is to insure that new full-scale vehicle designs are free of aeroelastic problems. These tests are conducted in cooperation with the Department of Defense. Several milestones are shown in the chart above. They include testing Navy A-12 and Advanced Tactical Fighter (ATF) models for flutter clearance and an LHX helicopter model for aeromechanical stability. The ATLAS II ground wind loads test and the F106 vortex flap fight flutter tests are described in the following charts.

TDT TESTS SHOW THAT GROUND WIND LOADS ARE NO PROBLEM FOR ATLAS II
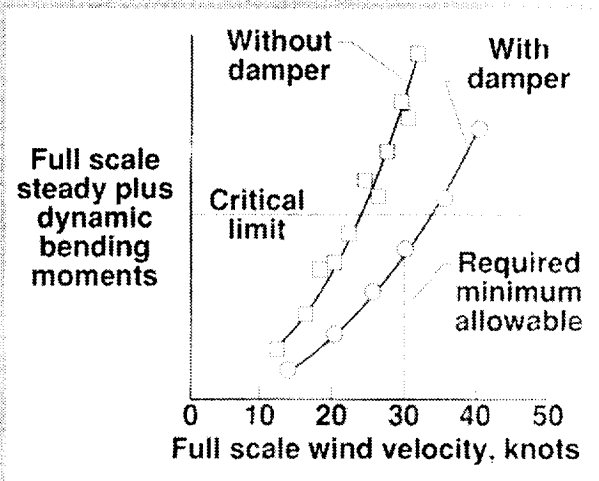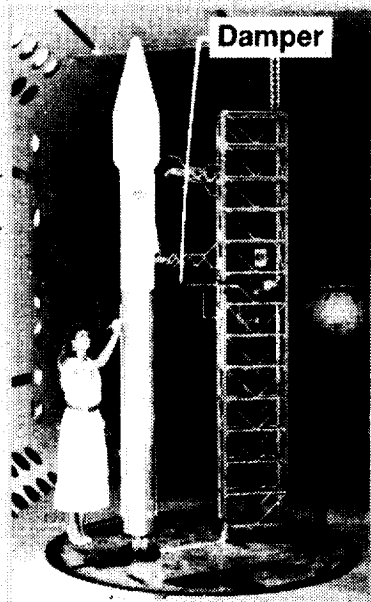
A model of the ATLAS II launch vehicle was tested in the TDT to determine the ground-wind-load characteristics of the launch complex. The model was attached to a floor-mounted turntable to allow various orientations of the model launch complex to the wind direction. Tests were conducted with and without a new damper system to determine response characteristics. Results indicate that the damper is required to meet minimum allowable wind criteria without exceeding the critical load unit.

F-106B FLIGHT ENVELOPE FLUTTER CLEARED FOR VORTEX FLAP EXPERIMENTS

WALLOPS TELEMETRY STATION

The CAB participated in flight testing of the F106B vortex flap vehicle to expand the envelope for follow-on performance tests. The added flap changed the aerodynamic and structural characteristics of the original vehicle, and, therefore, changed the flutter characteristics of the aircraft. For this reason, flutter clearance tests were required. Test engineers monitored aircraft instrumentation during flight and evaluated the vehicle flutter stability. Through a series of systematic flights which gradually expanded the envelope, a flutter-free flight regime was defined.

- **Develop improved methods for predicting and reducing rotorcraft vibrations**
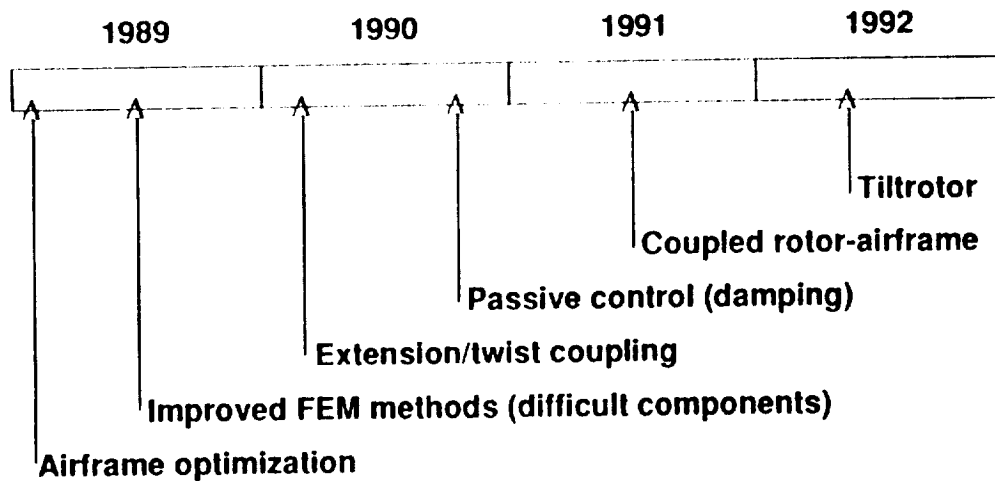
A third technical objective of the CAB is to develop improved methods for predicting and reducing rotorcraft vibrations. This is achieved through airframe structural optimization and through passive means such as damping treatment of structures.

In addition, composite materials are being used in aeroelastic tailoring applications to improve twist performance through extension twist coupling of helicopter and tiltrotor blades. Improved finite element methods (FEM) are achieved through validation and comparisons with experimental data. Results of ground vibration testing of a helicopter airframe to identify difficult-to-model components are shown in the following figure.

GROUND VIBRATION TEST OF HELICOPTER AIRFRAME
IDENTIFIES IMPORTANT CONTRIBUTORS
TO VIBRATORY RESPONSE

COMPLETE AIRFRAME

STRIPPED-DOWN AIRFRAME

SECONDARY PANEL EFFECTS
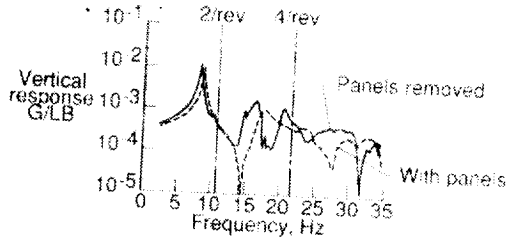
CANOPY GLASS EFFECTS
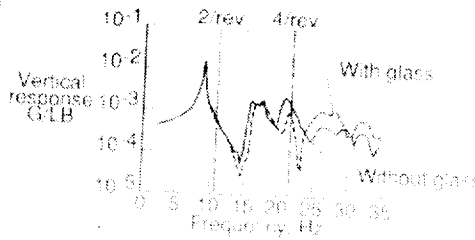
A cooperative NASA/industry program to improve FEM methods has been in place since 1984. Difficult components studies are being conducted as a part of this program. In these studies, various configurations of a full-scale helicopter are tested to determine the vibration characteristics. In the example shown above, effects of secondary panels and canopy glass were determined. Results from NASTRAN finite element models (not shown) were then compared with the experimental results to indicate area of agreement and non-agreement. Based on these comparisons, the FEM methods were updated to improve predictions.

EXPERIMENTAL TRANSONIC FLUTTER CHARACTERISTICS OF

SUPERSONIC CRUISE CONFIGURATIONS

M. H. Durham, S. R. Cole, F. W. Cazier, Jr., D. F. Keller
NASA Langley Research Center
Hampton, VA

E. C. Parker
Lockheed Engineering and Sciences Co.
Hampton, VA

W. K. Wilkie
USAARTA-AVSCOM, ASTD
NASA Langley Research Center
Hampton, VA

OVERVIEW

- **Background**
- **Objectives**
- **Model description**
- **Results**
- **Video**
- **Summary**

This figure presents an overview of the presentation. The presentation begins with background information that led to the experimental study concerning transonic flutter of supersonic cruise configurations. The program objectives are then defined including some description of the approach taken to meet the objectives. The development and physical characteristics of the wind-tunnel models are then discussed, followed by experimental results from the wind-tunnel test. In the actual presentation at the CAB technical review, a short video was shown of actual flutter for one configuration. The presentation concludes with a brief summary.

BACKGROUND

- **Renewed interest in SST's**
  - **HSCT , NASP**

- **Advanced SST designs of the 70's**
  - **SCAR, AST**
  - **flutter deficiencies**

- **Related Studies**
  - **Semispan arrow wing**
  - **Full-span SCAT-15**

The High Speed Civil Transport and the National Aero-Space Plane (NASP) programs have brought a renewed interest in the flutter characteristics of highly-swept low-aspect-ratio wings. Looking back at the supersonic transport (SST) studies of the late 1970's there were documented flutter deficiencies in strength-designed SST's. This presentation covers results from a NASA study, conducted in the Langley Transonic Dynamics Tunnel, to determine the flutter characteristics of a generic arrow-wing configured supersonic transport.

OBJECTIVE/APPROACH

- **OBJECTIVE**
  - **Extend experimental flutter database**
  - **Understand arrow wing flutter mechanism**

- **APPROACH**
  - **Develop aeroelastic model and test in TDT**

The objectives of this study were to extend the SST experimental flutter database and to better understand the arrow wing flutter mechanisms. Some earlier test results of simple small-scale arrow wings can be found in the literature. The current study builds on earlier results by investigating the effects of additional airplane design parameters and by using a structural model more representative of proposed flight vehicles.

The approach taken to accomplish these objectives was to develop aeroelastic arrow wing models and to test them in the Langley Transonic Dynamics Tunnel (TDT).

WIND-TUNNEL MODEL IN TDT
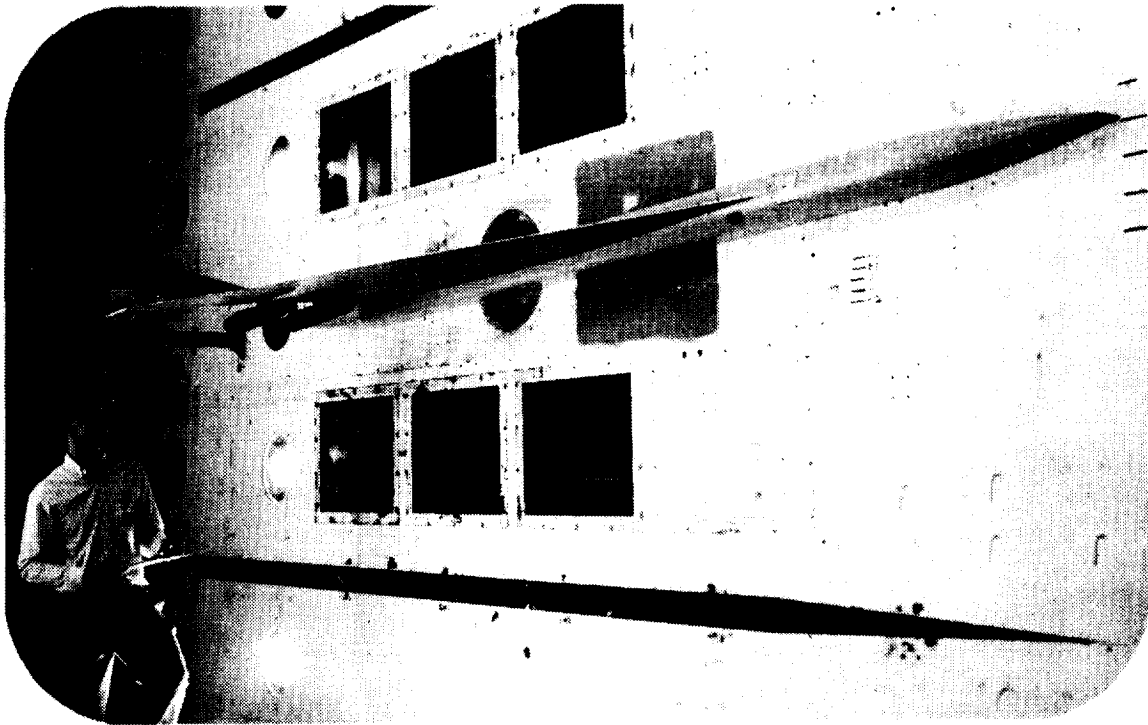
    Semispan cantilevered models were used for this generic arrow-wing study. The photograph shows an arrow-wing flutter model side-wall mounted in the TDT. The flutter models were designed as twentieth scale geometric representations of a Langley Advanced Supersonic Technology series (AST-200) arrow-winged SST. The AST series was a refinement of an earlier Supersonic Cruise Aircraft Research transport configuration that was designed for a cruise Mach number of 2.7.

PARAMETERS STUDIED

➤ • **Fuel loadings**

➤ • **Engine nacelles**

 • *Wing-mounted vertical fin*

 • *Wing angle-of-attack*

 • *Wing-tip mass and stiffness distributions*

Configurations studied included known flutter sensitive parameters such as engine nacelles and fuel loadings. In addition, a wing-mounted vertical fin, wing angle-of-attack, and wing-tip mass and stiffness variations were tested to determine their effects on flutter. For brevity, only the results of the engine nacelle and fuel loading variations are discussed in this presentation.

The wing-tip mass and stiffness variations were included to study an anomaly encountered in a flutter test conducted during some SST work in the late 1970's. An unexpected flutter boundary for a full-span arrow-wing model was found during tests in the TDT. Post-test analyses showed that some errors in the mass modeling of the wing-tip region may have caused the flutter predictions to be unconservative by about 10 to 30 percent for this cable-mounted model. In the current study, two arrow-wing structural models were built with different wing-tip mass and stiffness distributions to investigate the flutter sensitivity to this parameter.

MODEL PLANFORM

Engine Nacelle

Vertical Fin

35.06

73 degs

60 degs

9.74

91.32

108.46
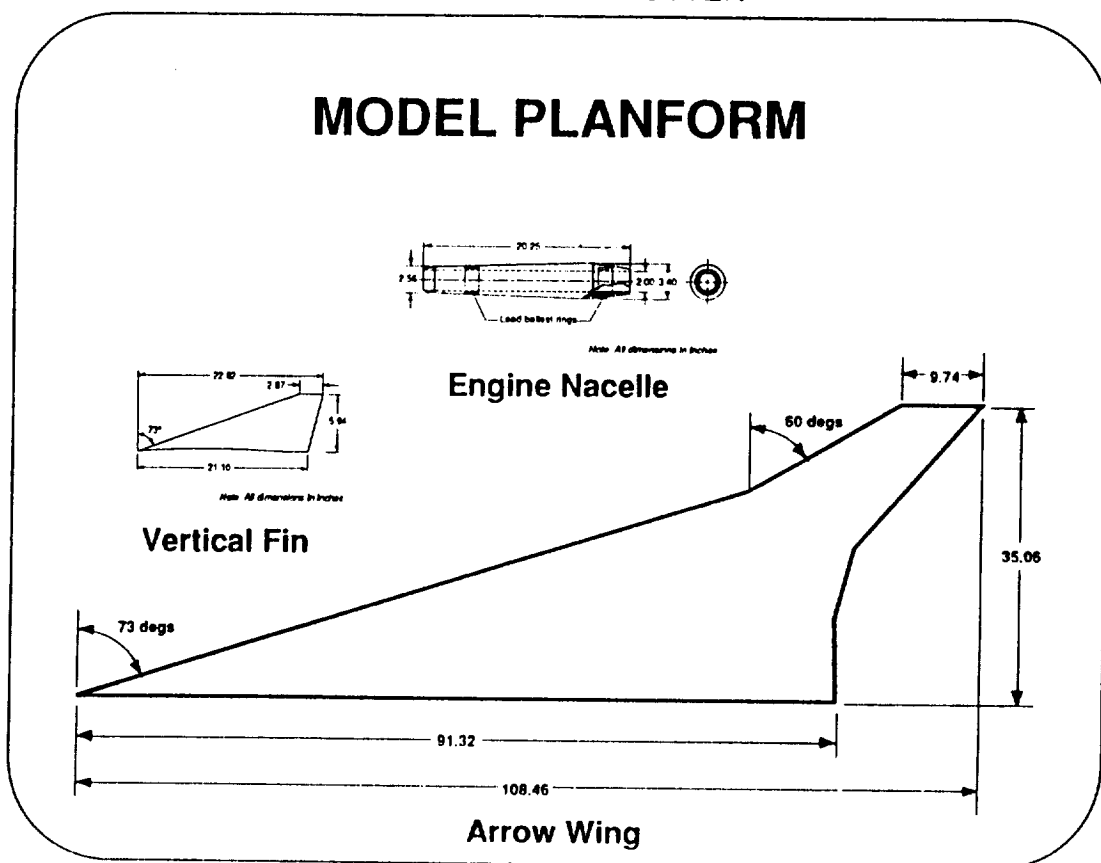
Arrow Wing

The planform shape of the arrow-wing models is shown in the figure. The leading-edge sweep was 73 degrees on the inboard 70 percent of the wing semispan and 60 degrees on the leading edge of the cranked tip (outboard 30 percent semispan). The trailing edge was cranked at two locations as shown. The models had a 3 percent thick bi-convex (symmetric circular arc) airfoil section and a wing planform area of 10.02 square feet.

The vertical fin, also shown in the figure, was mounted streamwise and perpendicular to the wing reference plane on the model upper-surface at the 70 percent wing span. The fin shown in figure 6 was constructed from a solid 0.125 inch thick aluminum plate covered with balsa to form a 3 percent bi-convex airfoil. An aluminum and a steel fin were available for these tests to study the effect of variations in the weight and inertia of the vertical fin. For the purpose of this study the solid fins were considered rigid relative to the elastic arrow-wing model.

Two flow-thru nacelles (see figure) were designed to model under-wing aircraft engines. The model nacelles were constructed of contoured aluminum tubes weighted with lead rings. The weight- and inertia-scaled nacelles were rigidly attached to the model lower-surface at the 28 and 51 percent semispan.

MODEL DESIGN
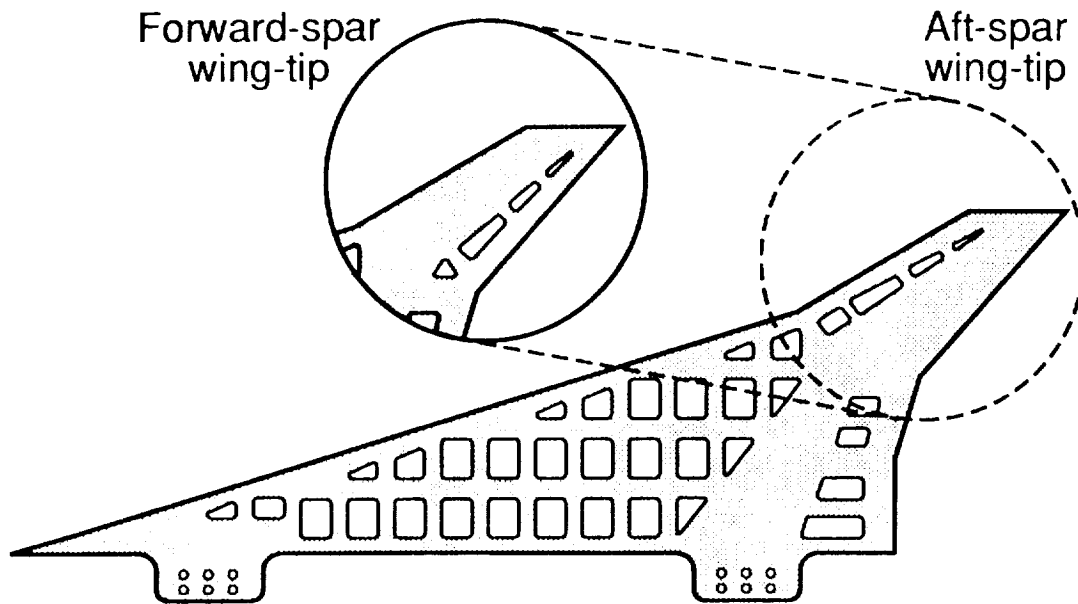
The model structural design consisted of a 0.25 inch thick aluminum alloy (7075-T651) plate covered with balsa wood. Cutout patterns in the aluminum plates were used to create a mass and stiffness distribution representative of a typical aircraft wing built with rib and spar construction. The figure provides a sketch of the cutout patterns for the aluminum plates used in the two basic wing configurations. Cutouts in the wing-tip regions were varied to model forward or aft spar mass and stiffness distributions. The plate thickness and overall cutout pattern were chosen so the model would flutter within the tunnel boundary. The balsa was bonded with its grain orientation perpendicular to the model plates to minimize any stiffening effects. The balsa was then milled to the desired airfoil shape.

To cantilever the wings, the two root tabs on the models were clamped to a steel mounting beam which was attached to the tunnel side-wall turntable. Using the two mounting tabs instead of clamping the entire root allowed a wing mid-chord root flexibility that was more representative of an elastic fuselage and blended wing aircraft. A half-fuselage fairing covered the mounting hardware and provided an aerodynamic root condition similar to a blended wing-fuselage.
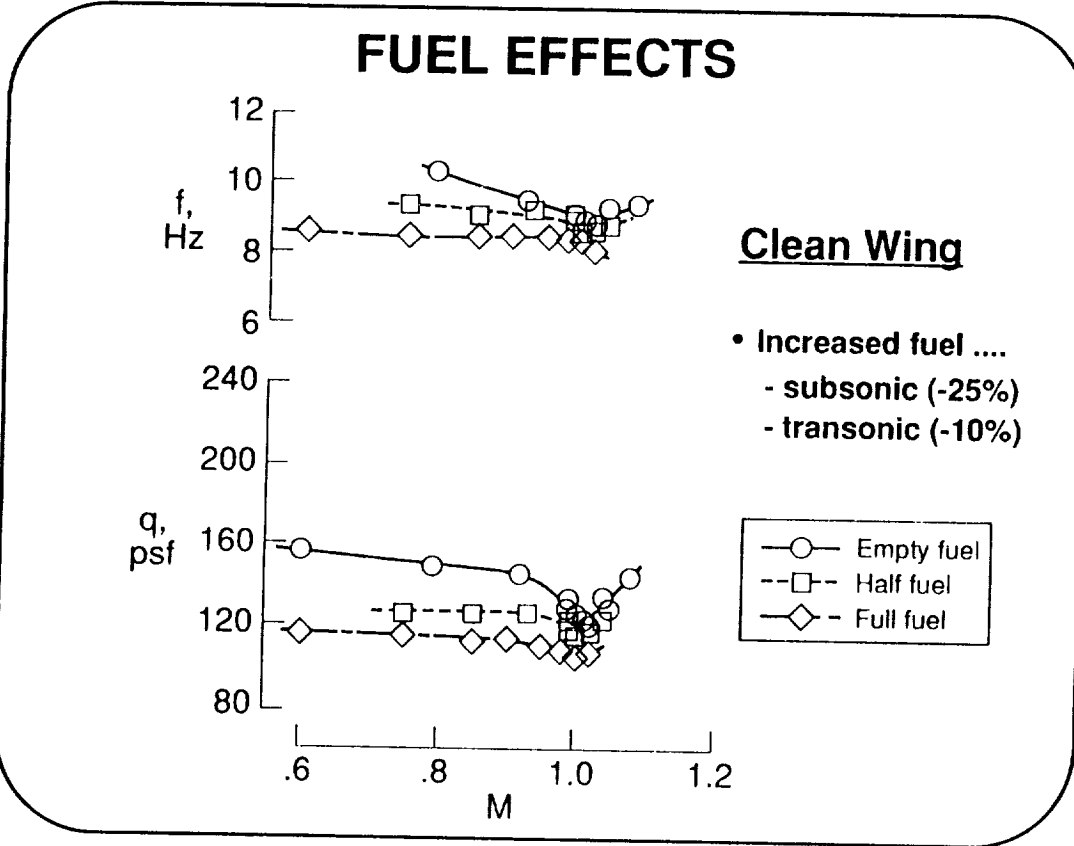
Wing fuel loadings were modeled using lead block inserts of various thicknesses distributed in the mid-wing area. Two wing fuel loadings, full-fuel and half-fuel, were tested. The full-fuel configuration represented a fuel loading approximately equal to the weight of the wing structure and corresponding systems (i.e. a wing carrying its weight again in fuel).

26

NACELLE EFFECTS
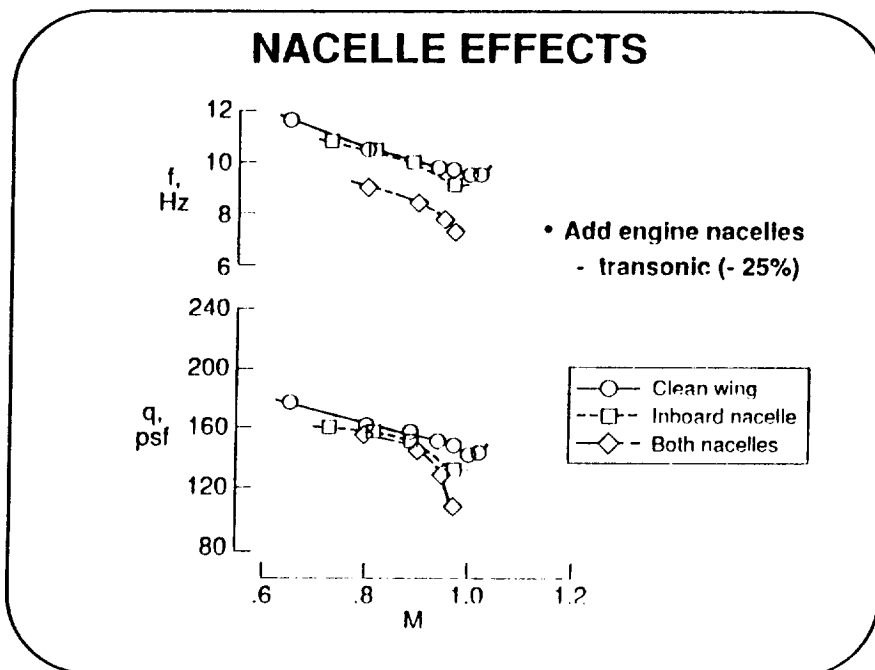
Flutter boundaries for some of the configurations tested are plotted as flutter dynamic pressure and flutter frequency versus Mach number in the following two figures. The boundaries represented by the curves faired through the flutter test points are interpretations of the finite number of experimental data points. The boundaries represent neutral flutter stability. The flutter models were stable when tested at dynamic pressures below the boundaries and would be unstable above the boundaries. No unusual flutter mechanisms were encountered. All test configurations had similar flutter behavior. The model flutter mode "shape" varied between the subsonic and transonic regions. The flutter points in the subsonic region were predominantly wing second bending motion and involved considerable mid-wing leading edge deflections. The transonic and supersonic flutter points were predominantly the first wing bending mode and were characterized by large wing tip deflections. This trend in modal content is supported by the variations of flutter frequency versus Mach number. Subsonic flutter frequencies were closer to the wind-off second wing bending frequency, while the transonic flutter frequencies approached the wing first bending mode frequency. The lowest experimental flutter frequencies corresponded to the Mach number at the minimum flutter dynamic pressures. The transonic dip occurred between a Mach number of 1.00 to 1.04.

The effect of engine nacelles on flutter of the wing with an aft-spar wing-tip cutout pattern is presented in this figure. Results are for the clean wing, wing with one inboard nacelle, and wing with both nacelles. Below a Mach number of 0.8 there is no significant effect on flutter. However in the transonic region the addition of each nacelle had a destabilizing effect on the flutter boundary. The transonic minimum flutter dynamic pressure was lowered by 23 percent with the addition of both engine nacelles.

FUEL EFFECTS

Clean Wing

- **Increased fuel ....**
  - **subsonic (-25%)**
  - **transonic (-10%)**

—O—	Empty fuel
--□--	Half fuel
—◇--	Full fuel

The fuel effects portion of this study was conducted for the forward-spar wing-tip configuration. This figure presents fuel loading effects on the flutter of the wing without nacelles. The figure shows that adding fuel had a destabilizing effect on flutter. These clean wing boundaries show that the half- and full-fuel loadings lower flutter dynamic pressures by about 18 percent and 25 percent, respectively, in the subsonic region, and as much as 10 percent for the transonic dip.

ARROW WING FLUTTER

FLUTTER VIDEO

Flutter test conditions

Mach = 1.05

q = 100. psf

Freq = 8 Hz

Mach = .65

q = 150. psf

Freq = 10. Hz

SUMMARY

- **Experimental flutter boundaries were obtained for the cantilevered semi-span models**

- **Engine nacelles reduced the transonic flutter dynamic pressures by 25-30%**

- **Wing-fuel loadings reduced subsonic dynamic pressures by 25% and the transonic dynamic pressures by as much as 10%**

- **Wing angle-of-attack produced steep transonic boundaries**

- **Addition of a vertical fin and the variations of wing-tip mass and stiffness each had small (5-10%) effects on flutter**

In summary, a generic arrow-wing configured supersonic transport was flutter tested in the Langley Transonic Dynamics Tunnel. Experimental flutter boundaries were obtained for the cantilevered semispan models. The shapes of the transonic dip in the flutter boundaries and the supersonic recoveries were well defined. Tests were performed to determine the effects on flutter of engine nacelles, fuel loadings, a wing-mounted vertical fin, wing angle-of-attack, and wing-tip mass and stiffness distributions. The flutter effects of these basic airplane parameters extend the experimental flutter database for arrow-wing configured supersonic transports.

Results of the arrow-wing configurations tested indicate the following:

1. The addition of engine nacelles reduced the transonic flutter dynamic pressures by 25 to 30 percent, with little effect on subsonic portions of the flutter boundaries.

2. Wing-fuel loadings reduced subsonic dynamic pressures by 25 percent. For the forward-spar clean wing configuration, wing fuel reduced the transonic minimum flutter dynamic pressures by 10 percent.

3. Wing angles-of-attack of 4 to 6 degrees produced steep transonic boundaries with stabilizing effects of 20 to 30 percent for Mach numbers less than 0.75, and destabilizing effects of 22 to 27 percent on the transonic minimum flutter dynamic pressures. (This result was not specifically covered in this presentation.)

4. Increasing the wing-mounted vertical fin weight and inertia had a slight stabilizing effect (5 to 10 percent) on flutter dynamic pressures. (This result was not specifically covered in this presentation.)

5. Wing-tip mass and stiffness variations tested changed flutter dynamic pressures by 5 to 10 percent. (This result was not specifically covered in this presentation.)

AEROELASTIC EFFECTS OF SPOILER SURFACES MOUNTED

ON A LOW-ASPECT-RATIO RECTANGULAR WING

Stanley R. Cole
NASA Langley Research Center
Hampton, Virginia

31

BACKGROUND

- Desirable to have flutter suppression capabilities

- Aerodynamic spoiler surfaces are one such technique

- Spoiler effects on flutter undetermined

Experimental aeroelastic wind-tunnel testing has always been risky in terms of model integrity due to the fact that aeroelastic instabilities, such as flutter or static divergence, often quickly destroy the model. Occasionally, such losses represent the only useful information obtained after a great financial and time investment has been made to explore an aeroelastic phenomenon. To make matters worse, the test facility is also at risk from the debris of a destroyed model. Many test techniques, physical mechanisms, monitoring techniques, and safety features have been developed and are being developed when possible to reduce risks to both models and test facilities during aeroelastic testing.

One such technique which has been used recently on several aeroelastically scaled flutter models is a deployable spoiler surface intended to substantially disrupt the aerodynamic forces on the model and thereby prevent flutter. This presentation describes a research study which was undertaken to specifically examine the effectiveness of such surfaces in preventing flutter.

A-6 SPOILER CONFIGURATION
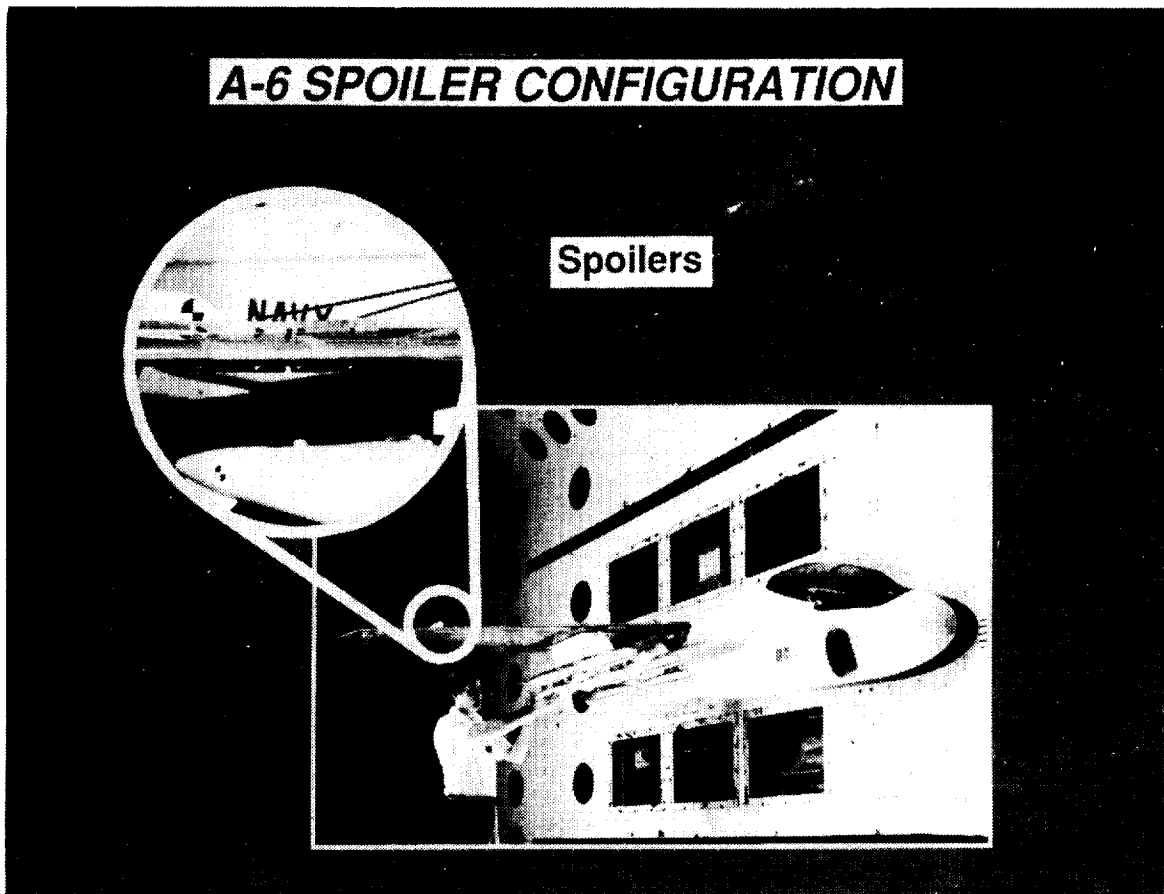
Spoilers

This photograph shows an example of a wind-tunnel model previously tested in the Langley Transonic Dynamics Tunnel (TDT) which utilized spoiler surfaces for flutter suppression. The model is a geometrically-scaled replica of a Navy attack vehicle. The wing is aeroelastically scaled to allow for flutter clearance testing. The inset in the figure shows the spoiler surfaces above and below the wing structure in the deployed state. These spoilers could be remotely deployed and retracted to allow for efficient testing.

OBJECTIVE/APPROACH

- Objective

  - Determine the effectiveness of aerodynamic spoiler surfaces in suppressing flutter

- Approach

  - Utilize an inexpensive wing model previously tested in the TDT

  - Attach fixed vertical spoiler surfaces

  - Flutter test configurations in the TDT

The objective of the project was to determine the effectiveness of aerodynamic spoiler surfaces in suppressing flutter and to develop guidelines for locating and sizing such surfaces on models to maximize their effectiveness in suppressing flutter. The approach to accomplishing this objective was to utilize an inexpensive wing model which had been previously tested in the TDT. The spoiler surfaces tested in this study were fixed in position and could not be remotely deployed as would be required for testing of an actual aeroelastic model. Identical spoiler surfaces were mounted above and below the wing surface at the same spanwise and chordwise location. The spoiler surfaces were tested on a 1.5 aspect ratio, rectangular semispan wing model in the TDT.
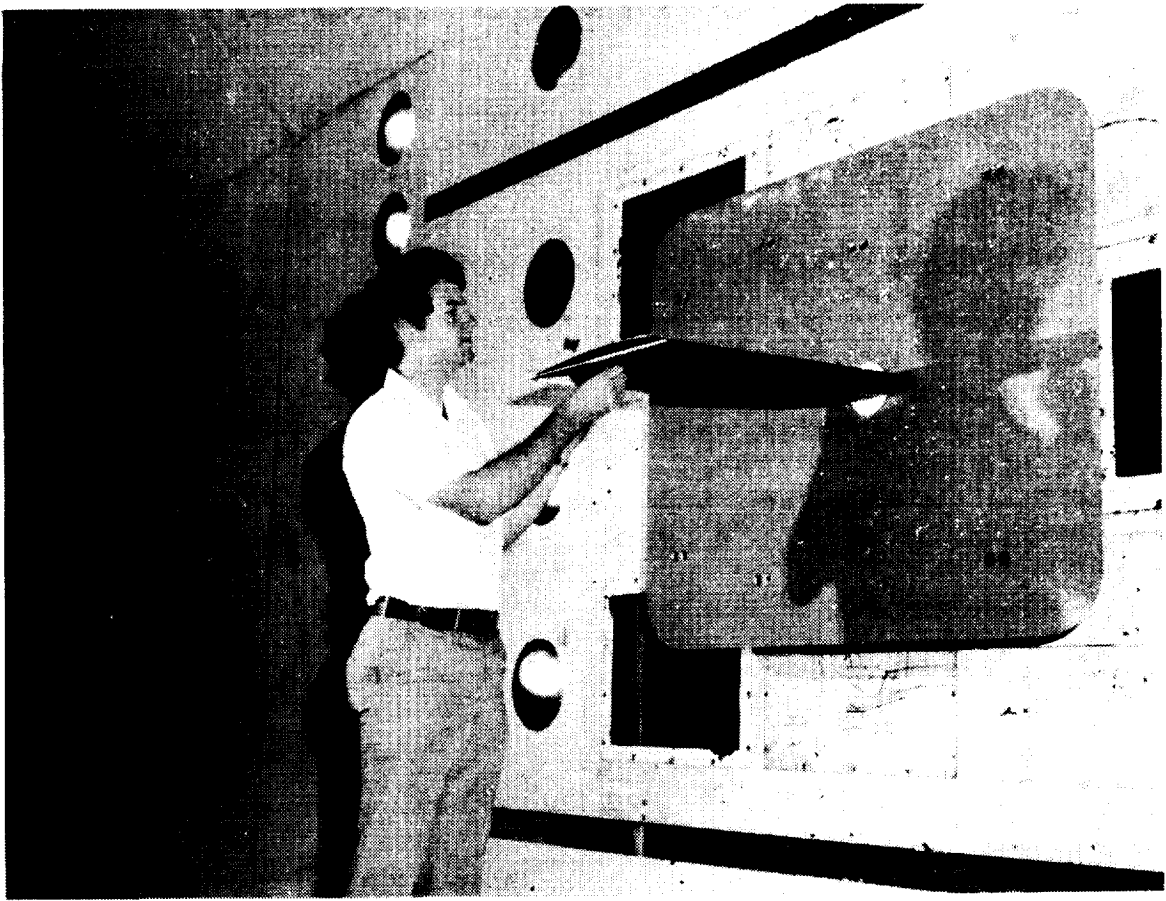
The wind-tunnel wing model is shown in the photograph from a previous flutter test (prior to the addition of the spoiler surfaces). The model co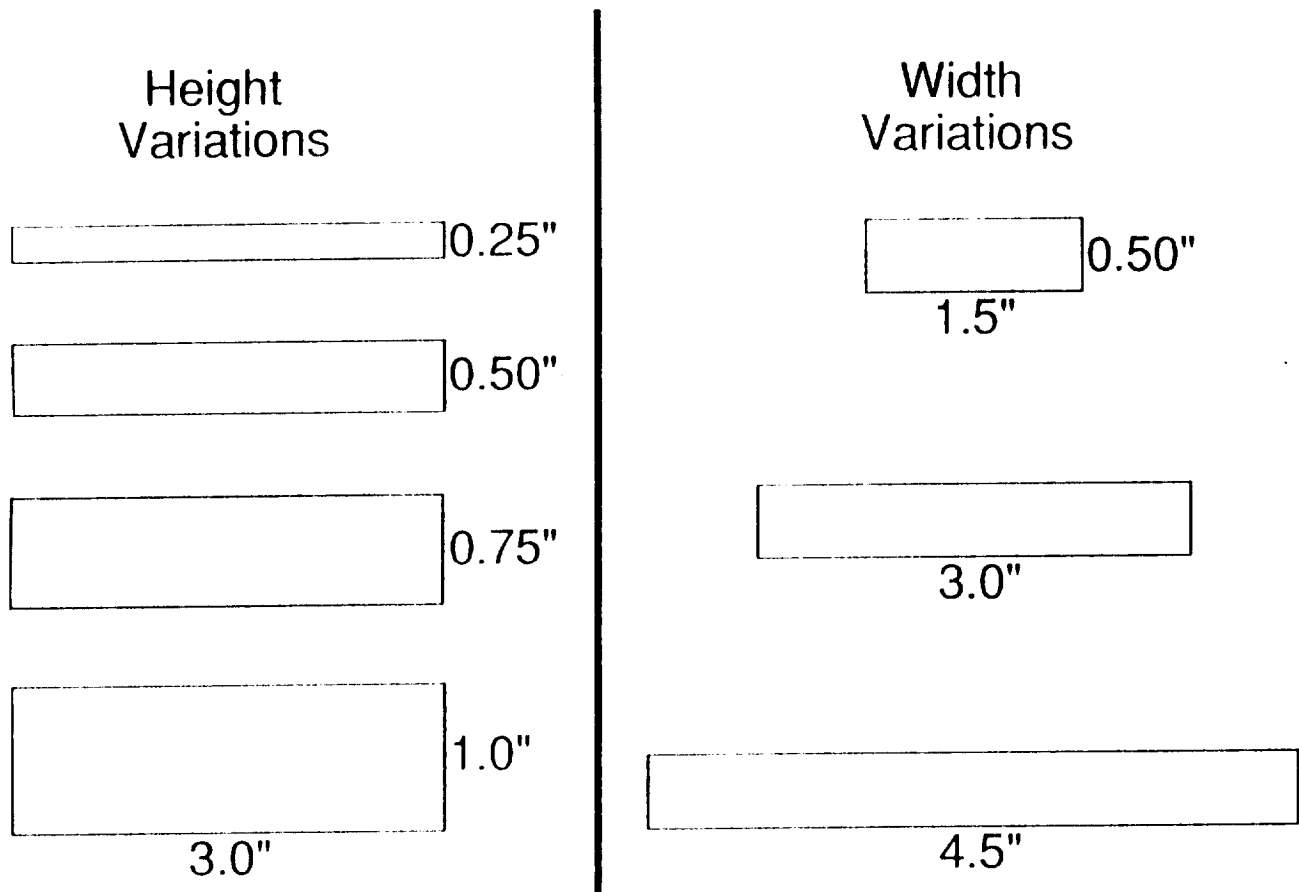nsisted of a relatively rigid wing surface which was integrally connected to a rectangular flexible support beam (shown in the following figure) at the root of the wing. The wing had zero sweep and a 1.5 panel aspect ratio. The airfoil was a NACA 64A010 symmetrical shape. The wing stiffness was provided by a flat 0.25-inch thick aluminum plate which was covered by balsa wood to provide the airfoil shape while minimizing the weight. The aft 40 percent of the wing chord contained 49 1.375 -inch holes drilled through the aluminum plate in order to reduce the weight of the wing and to shift the center of gravity of the wing forward to a chordwise position more representative of a typical wing. The wing aluminum plate was rounded at the leading edge and tapered at the trailing edge to meet the airfoil shape. The rectangular support beam extended from the wing root at the 30 percent chord location to provide the flexibility needed to test the model to flutter. This beam section consisted of a 0.25" thick aluminum core cut from the same plate as the wing structure with two 0.0625" thick aluminum plates bonded and riveted to both sides. The thin plates extended over a portion of the wing plate to relieve stress concentrations at the wing root. The bond material resulted in a total thickness of 0.391". The support beam was 2.25" wide and was 11.33" long from the wing root to the wind-tunnel wall support. The support beam was cantilevered at the tunnel wall on a turntable to allow remote control of the wing angle of attack during testing. A splitter plate was mounted at the wing root to provide a symmetry reflection plane for the wing aerodynamics. Sufficient clearance was provided between the splitter plate and the wing root and support shaft to prevent contact during testing.

SPOILER MOUNTING POSITIONS
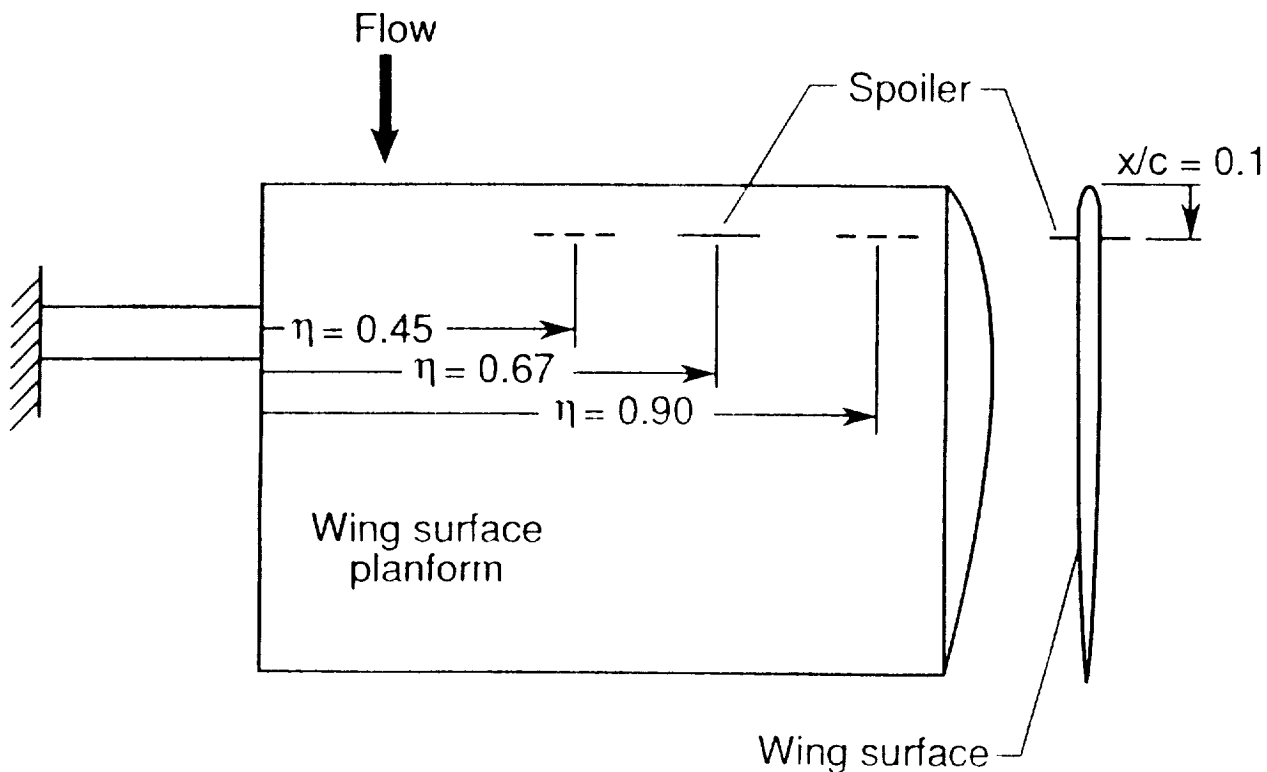
The spoiler surfaces consisted of rectangular plates which were attached directly to the top and bottom of the wing. The spoiler surfaces were constructed from 0.05" thick aluminum plate. The figure shows a planform- and an end-view line drawing representing the shape and orientation of the spoiler surfaces when mounted on the wing. For a spoiler height of 0.50" and a width (spanwise) of 3.0", variations were made in the spanwise location on the wing surface. Three mounting positions were available for the spanwise variations along the x/c=0.10 chord of the wing. These positions corresponded to h=0.45, 0.67, and 0.90 as the point at which the spoiler was centered spanwise. The dashed lines in the planform view indicate these optional locations for mounting and testing the spoiler surfaces. Rectangular segments of balsa wood were removed at each of these position options so that the spoilers could be mounted to the wing. Dummy weights were available for each of the possible test configurations so that the total weight and weight distribution of the model always remained the same regardless of the spoiler configuration being tested. The idea behind this was that the structural and inertial properties of the model would be essentially constant for all configurations so that any aeroelastic stability changes would be purely a function of aerodynamic changes. The gaps in the wing surface (where the balsa wood was removed for the spoiler mounting slots) were covered with aluminum tape to help smooth the wing aerodynamically.

SPOILER CONFIGURATIONS

Height Variations

$\boxed{}$ 0.25"

$\boxed{}$ 0.50"

$\boxed{}$ 0.75"

$\boxed{}$ 1.0"

3.0"

Width Variations

$\boxed{}$ 0.50"

1.5"

$\boxed{}$

3.0"

$\boxed{}$

4.5"

Several variations in the geometric dimensions of the spoiler surfaces were tested during the wind-tunnel test. Spoiler vertical height and width (spanwise) variations were tested at the $x/c=0.10$, $\eta=0.67$ mounting position. The spoiler heights (h_s) available for testing at this location were 0.25", 0.50", 0.75", and 1.00" (width = 3.0"). The spoiler width (w) variations were 5, 10, and 15 percent of the wing semispan (w=1.5", 3.0", and 4.5", respectively) with the height held constant at 0.5".

EXPERIMENTAL RESULTS

- Model vibration characteristics

- Wind-tunnel test results
  - Spoiler height effects
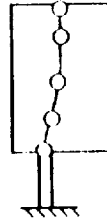 - Spoiler width effects
  - Spoiler area effects

Tests results from ground vibration tests and from the wind-tunnel test are shown in the following six figures. The wind-tunnel tests results are categorized as spoiler height effects, spoiler width effects, and a combination of these two as spoiler area effects.
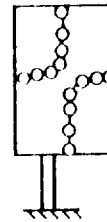
MEASURED NODE LINES

--o-- Experiment
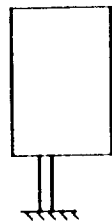
First bending
2.85 Hz

First torsion
13.1 Hz

Second bending
26.2 Hz

Second torsion
62.6 Hz

A ground vibration study was conducted on the wind-tunnel model to determine its natural frequencies and to locate modal node lines. The model was excited by an impulse air shaker to minimize distorting the modes. A lightweight roving accelerometer was used to locate the node lines of the natural vibration modes while exciting the model with the impulse air shaker.

Measured node lines determined during the ground vibration test of the model prior to the addition of the spoiler surfaces are shown in the figure. Node lines measured following the addition of the spoilers were very similar to the experimental node lines shown in the figure. The measured natural frequencies of four of the primary vibration modes of the model are also given in the figure.

SPOILER HEIGHT EFFECTS
(w=3.0")
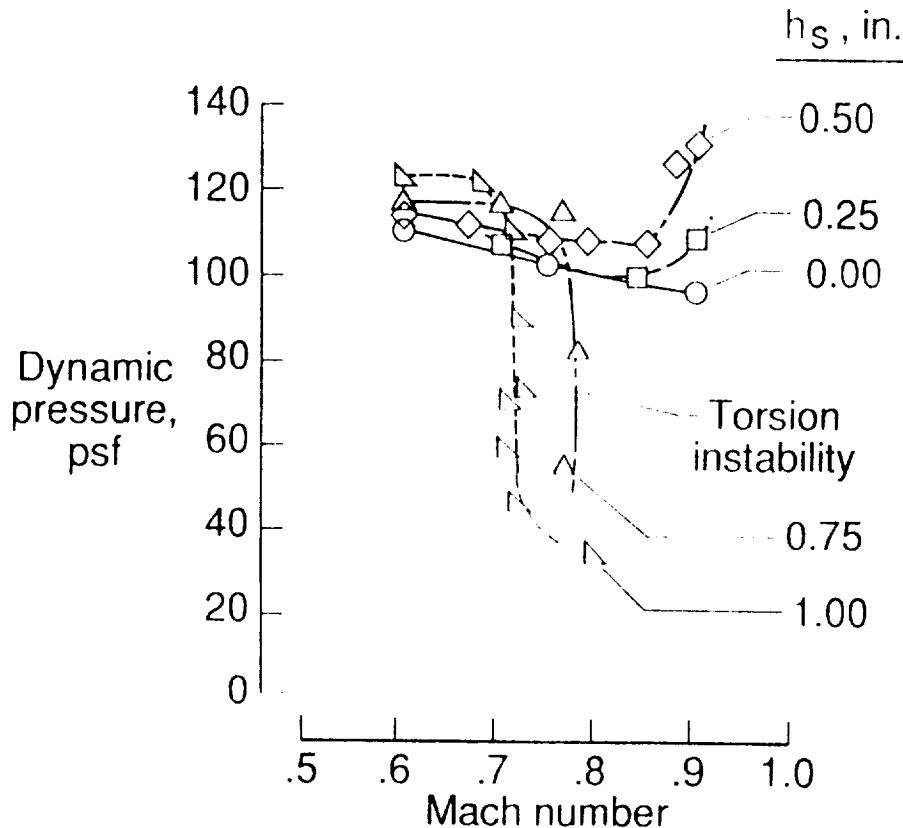
This figure indicates the effects of varying spoiler height (above the wing aerodynamic surface). The primary objective of this research at the outset was to determine the flutter suppressing capability of spoiler surfaces such as tested in this study. The figure gives insight into the flutter suppression capability of spoiler surfaces as a function of spoiler height. As the spoiler height is increased, there appears to be a stabilizing effect on the flutter condition of the model for conditions below a Mach number of approximately 0.7. For the 0.25" and 0.50" spoiler heights, this stabilizing trend is even more dramatic at transonic Mach numbers. But for spoiler heights greater than 0.50", this trend in the transonic range did not continue. In fact, a new instability was excited which does not appear to be classical flutter as was experienced at previously discussed conditions. The new instability appears to be a nearly single-degree-of-freedom torsional instability which is highly Mach number dependent and was found to occur at dynamic pressure conditions far below the expected flutter condition. The motion in this torsional instability appeared to be very similar to the wind-off first torsional mode of the wing. As the Mach number was decreased, the instability tended to transform from the torsional instability to the classical flutter instability in which the motion is primarily a coupling of the wing first bending mode and the wing first torsion mode.

SPOILER HEIGHT EFFECTS
(w =3.0")
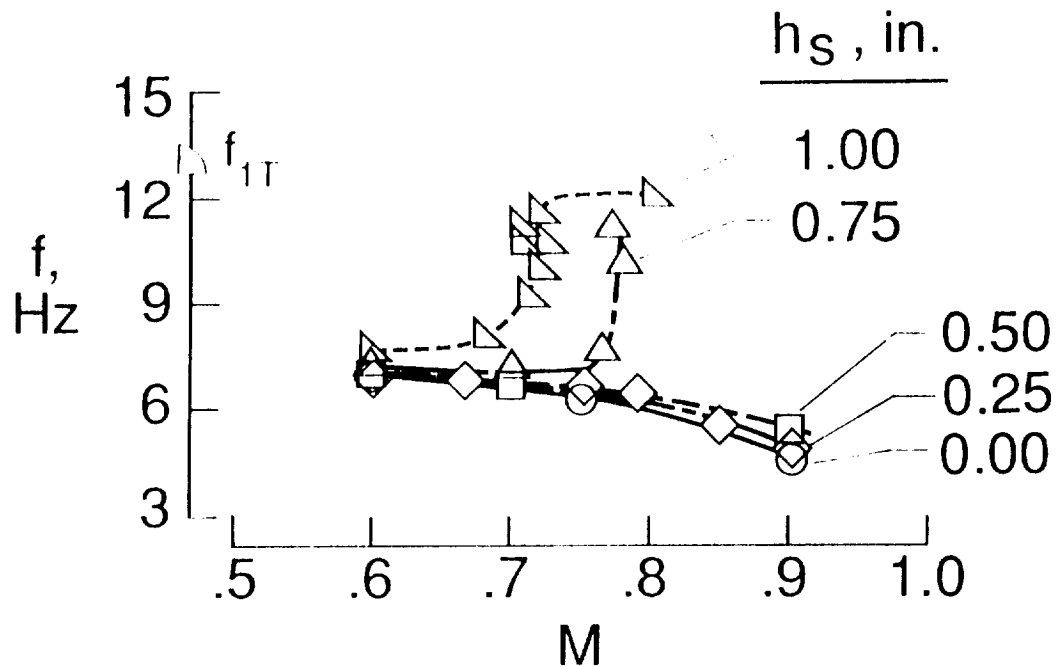
This figure provides a further indication, based on instability frequency, that the observations made for the previous figure quantify the behavior of the model due to the spoiler surfaces. The 0.00", 0.25", and 0.50" cases shown in this figure indicate slight variations in the instability frequency measured. But for the 0.75" and 1.00" spoilers, the figure shows a dramatically increasing instability frequency as Mach number is increased. This frequency rapidly approaches the wind-off first torsion mode frequency. This behavior is supportive of the observation that this Mach number-dependent instability is a single-degree-of-freedom torsional instability.

SPOILER WIDTH EFFECTS
(hs=0.5")
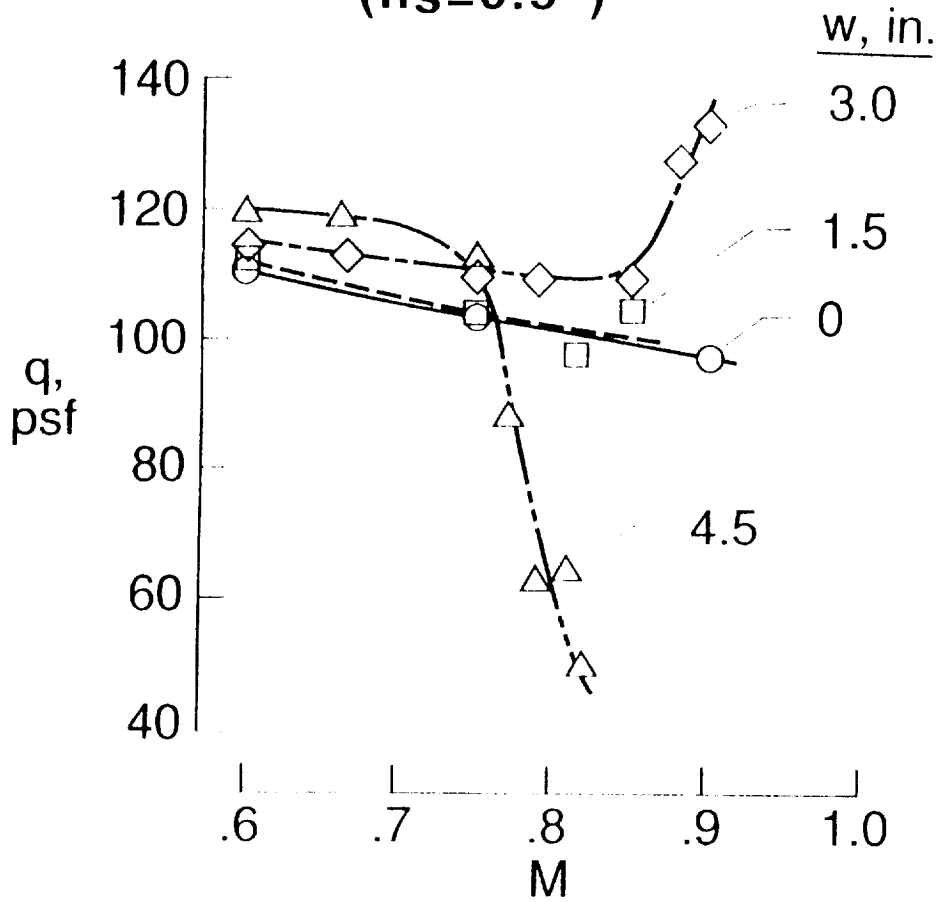
This figure and the next figure show the effects of varying spoiler width. The comments concerning the spoiler height effects from the previous two figures describe the effects of increasing spoiler width equally well. The results in this figure and in the following figure show that as the spoiler width is increased a torsional instability again predominates the flutter condition at higher Mach numbers.

42

SPOILER WIDTH EFFECTS
(hs=0.5")
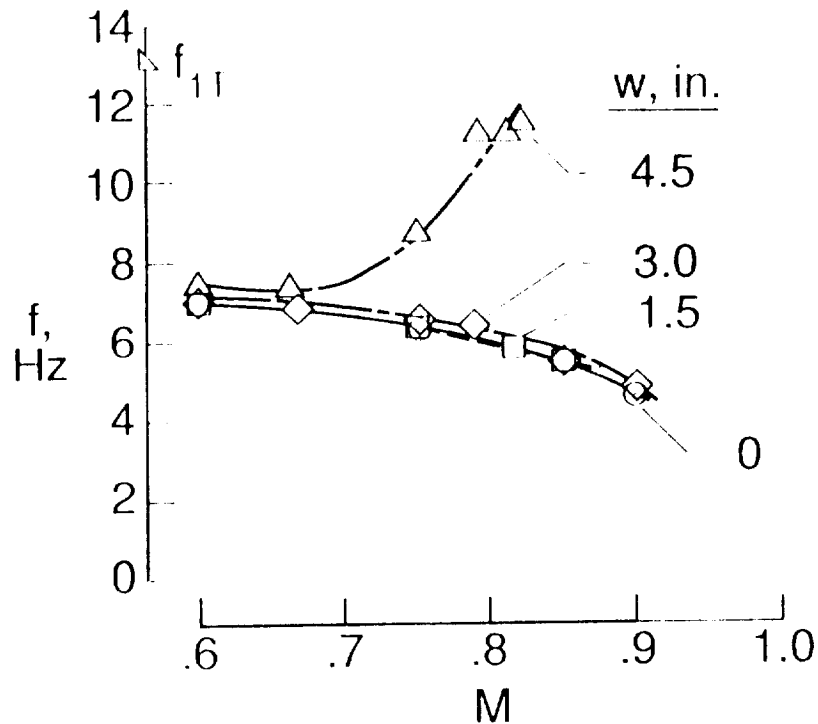
The cause of this unusual torsional instability has not been determined based on the experimental results, but a number of possible influences are suggested in related literature. Perhaps the most likely cause is a periodicity of vortex shedding related to the Strouhal number occurring about the spoiler surfaces which drives the model in the first torsion mode. A number of other studies have shown that such wing-wake frequency response develops for a range of Strouhal numbers (based on frequency in units of radians/seconds) from 0.93 to 1.32 for two-dimensional flat plates and airfoils.

The Strouhal number was calculated for the spoiler surfaces based on the total projection of the spoilers in the vertical direction perpendicular to the freestream flow. In other words, the Strouhal number is based on the sum of the upper surface spoiler's projection above the wing surface, the wing thickness at the chordwise location of the spoiler, and the lower surface spoiler's projection below the wing surface. Based on this dimension, the Strouhal number (S_h) for the torsional instability was between S_h=0.038 and 0.055 for the configurations which exhibited the torsional instability in the figures on pages 40 and 41 of this report. The Strouhal number for the torsional instability case in the above figure was calculated based on the spoiler's width along the span of the wing. The Strouhal number for the torsional instability cases with this configuration was nearly constant with an average Strouhal number (S_w) of S_w=0.068. Obviously, the Strouhal number as calculated for all of the torsional instability conditions in the current study is far below the values found in previous studies and appears to discount the possibility of the torsional instability being excited by shedding vortices.

43

EFFECT OF SPOILER AREA
ON TORSION INSTABILITY
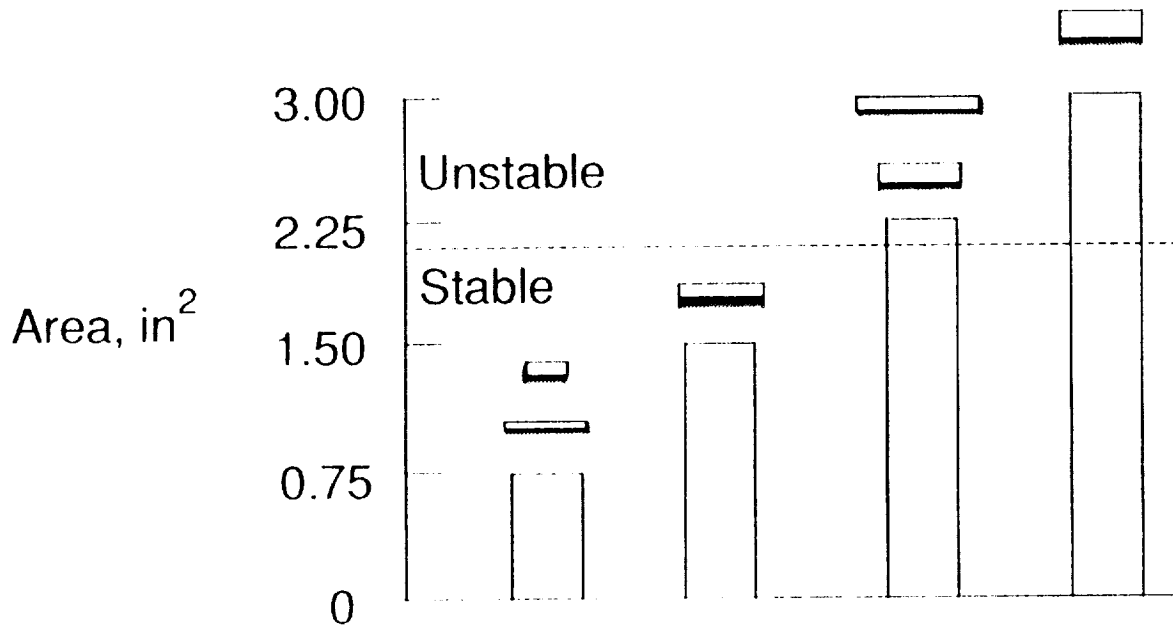
Interestingly, it is possible to categorize the spoilers as to their ability to excite the torsional instability by their planform area. The figure shows that even for several combinations of spoiler height and width, none of the spoilers excited the torsional instability if their area was equal to or less than 1.50 in² (per spoiler plate). Further, all of the spoilers generated the torsional instability if the surface area was equal to or greater than 2.25 in². Additional work would be required before stronger conclusions could be made concerning the relationship between spoiler sizes and the torsional instability.

CONCLUDING REMARKS

- Increasing spoiler height or width:
  - subsonically
    - slightly increased flutter q
  - transonically
    - substantially increased flutter q for smaller spoilers
    - induced M-sensitive torsional instability for larger spoilers

An experimental study has been conducted to determine the effectiveness of vertical spoiler surfaces located on the 10 percent chord in suppressing flutter onset for a 1.5 panel aspect ratio, rectangular wing wind-tunnel model. The study included variations in the spoiler geometry (height and width) and location (spanwise) on the wing surface.

The wind-tunnel test showed that slight increases in the flutter dynamic pressure conditions were obtained due to the spoiler surfaces at subsonic Mach numbers. This effect at subsonic Mach numbers demonstrated consistent trends in that increasing spoiler dimensions (either height or width) resulted in increasing flutter dynamic pressures. The largest spoiler surfaces tested for either height or width variations resulted in approximately 15 percent increases in the flutter dynamic pressures at subsonic conditions.

At transonic Mach numbers, much larger increases in the flutter dynamic pressure were experienced for the smaller size spoilers tested indicating that they were very effective in suppressing flutter. On the other hand, several of the larger size spoiler surfaces induced a torsional instability in this Mach number range. This detrimental torsional instability was extremely Mach number sensitive and was found to occur at dynamic pressure conditions well below the expected flutter dynamic pressures.

A limited amount of experimental data were obtained to examine the effect of spanwise location of the spoiler surfaces on flutter (not shown in this presentation). For the three spanwise locations tested in this study, no measurable effect of spoiler location was found.

PLANFORM CURVATURE EFFECTS ON FLUTTER OF

56 DEGREE SWEPT WING DETERMINED IN TDT

Donald F. Keller
NASA Langley Research Center
Hampton, VA

PRESENTATION OUTLINE

- ● Background

- ● Objectives and Approach

- ● Structural Models

- ● Aerodynamic Models

- ● Flutter Results

- ● Summary

This presentation reports on a NASA in-house study which investigated the effects of planform curvature on the flutter characteristics of a generic 56 degree swept wing model. The presentation includes results from analysis and experimental models tested in the Transonic Dynamics Tunnel (TDT).

A brief background on planform curvature and its use in a recent NASA High Speed Civil Transport (HSCT) concept is presented followed by a list of this study's objectives and the approach used to complete them. The experimental and analytical structural models are then presented along with a comparison of the natural frequencies and node line locations obtained from them. A figure showing the aerodynamic model and the method used in the flutter analysis is also shown. Next, the flutter results obtained in the TDT are compared to those obtained from the flutter analysis. This figure also shows the effects that planform curvature had on the flutter characteristics of the models tested. Finally, a brief summary of the results is presented.

BACKGROUND
HSCT - High Speed Civil Transport
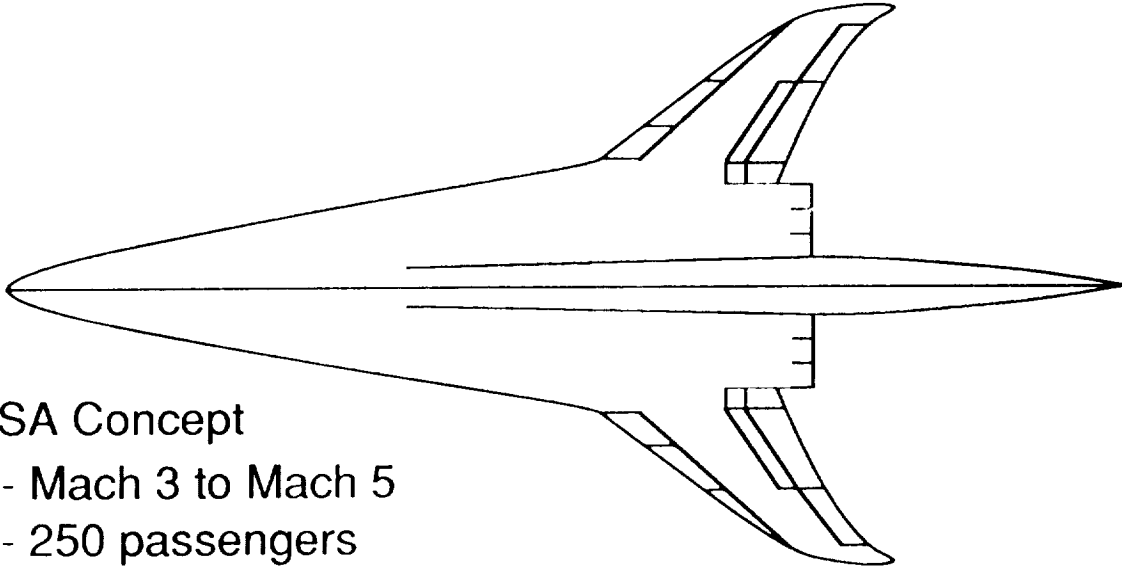
- **NASA Concept**
  - Mach 3 to Mach 5
  - 250 passengers
  - 6500 nautical miles
- **Previous strength designed HSCT's flutter deficient**
- **Planform curvature**
  - Increased low speed performance and pitch stability

Due to a recent increase of interest in HSCT's, NASA and several airframe manufacturers have developed new designs to meet the configuration requirements of a Mach 3+ HSCT. A sketch of a NASA concept currently being studied is presented in the figure. A HSCT of this design would cruise at Mach 3 to Mach 5, carry 250 passengers, and have a range of 6500 miles. Many previous HSCT designs, however, have had serious flutter deficiencies, especially in the transonic region. This NASA concept currently being studied involves curving the leading and trailing edges of the outboard portion of a high speed transport wing. This is to improve aerodynamic performance and to help reduce the pitch up instability associated with highly swept wings.

As a result, this study was conducted at the TDT to investigate the effects of planform curvature, the curving of the leading and trailing edges of a wing, on the flutter of a generic HSCT wing.

WING PLANFORM CURVATURE STUDY

Objectives:

- Determine the effects of planform curvature on the flutter characteristics of a cantilevered wing
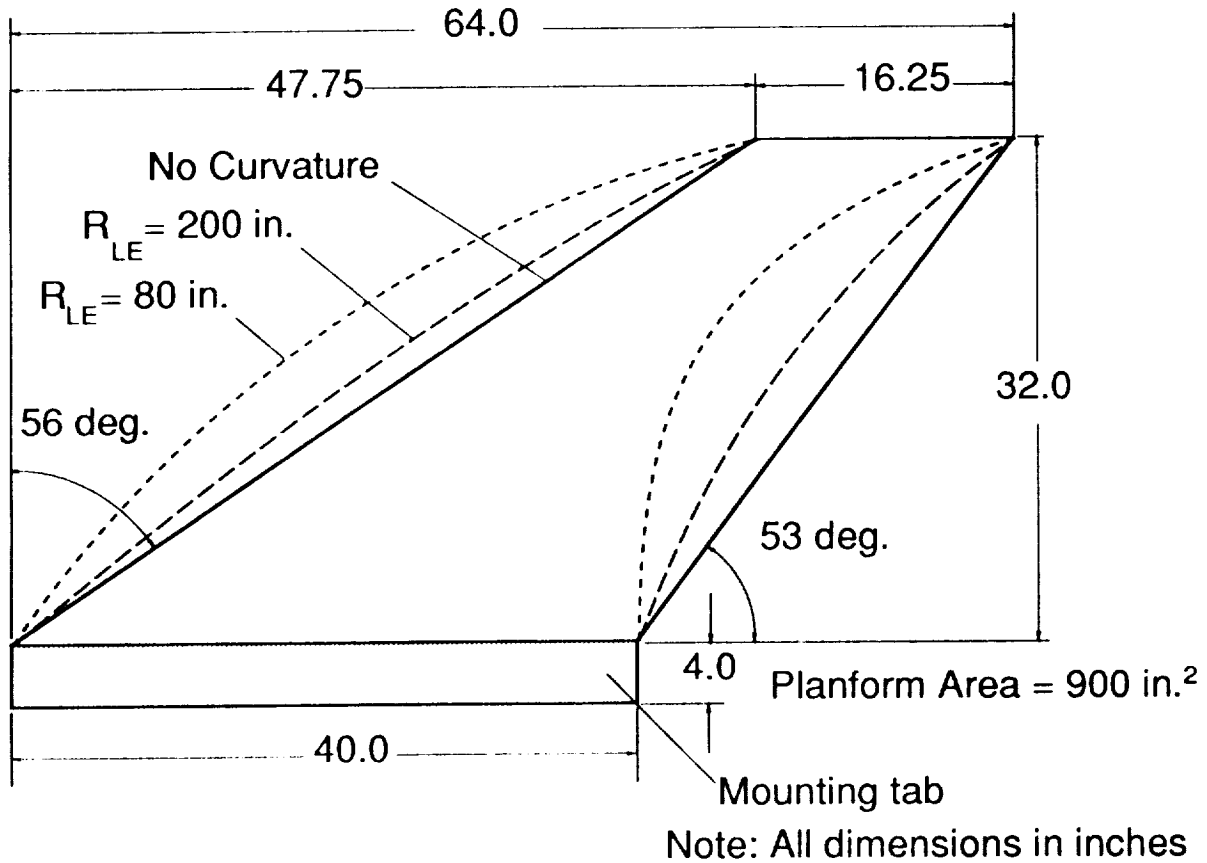
- Correlate test results with analysis

Approach:

- Design models

- Perform a flutter analysis using finite element models

- Determine flutter characteristics in TDT

The first objective of the study was to experimentally determine the effects of planform curvature on the flutter of a generic swept wing model. This model would represent the outboard portion of the wing of the recent NASA HSCT concept and would provide some general information on how planform curvature could effect the flutter characteristics of an actual HSCT wing. The second objective of the study was to correlate the experimental flutter data with analytical results obtained from an unsteady aerodynamics flutter prediction program.

Three models were designed that would flutter within the TDT operating envelope. The first model had straight leading and trailing edges (i.e. no planform curvature) and served as the baseline model. The other two models, however, had different degrees of planform curvature. Following design, the models were constructed and a flutter analysis was performed using information obtained from a ground vibration test and a finite element analysis. The three models were then flutter tested in the TDT and the experimental results compared with the analytical results.

Model Planforms

64.0

47.75 16.25

No Curvature

$R_{LE} = 200$ in.

$R_{LE} = 80$ in.

56 deg.

32.0

53 deg.

4.0

Planform Area = 900 in.^{2}

40.0

Mounting tab

Note: All dimensions in inches

The planforms of the three models tested are shown overlayed in the figure. The baseline model, no planform curvature, had a leading edge sweep of 56 degrees and a trailing edge sweep of 37 degrees. The radius of curvature of the leading edge of the other two models was 200 in. and 80 in., respectively. The radius of curvature of the trailing edge was determined so that the planform area of each model was 900 in.^{2}. The span for all three models was 32 in. which gave each model a panel aspect ratio of 1.14. The length and location of the root and tip chords were also the same for all three models. In addition, each model had a 4 in. mounting tab which was clamped between a steel plate and steel beam when the models were mounted in the TDT.

A photograph looking downstream at the moderately curved wing (R_{LE}=200 in.) mounted in the TDT is presented in the figure. The three semi-span cantilevered models used during the test consisted of a 0.188-inch-thick aluminum plate to which balsa wood was bonded and contoured to form a 3% thick bi-convex airfoil. The models were mounted cantilevered along their entire root to a splitter plate assembly which was then attached to the side-wall turntable in the TDT. The splitter plate was located outside the tunnel wall boundary layer to provide freestream flow conditions over the models.
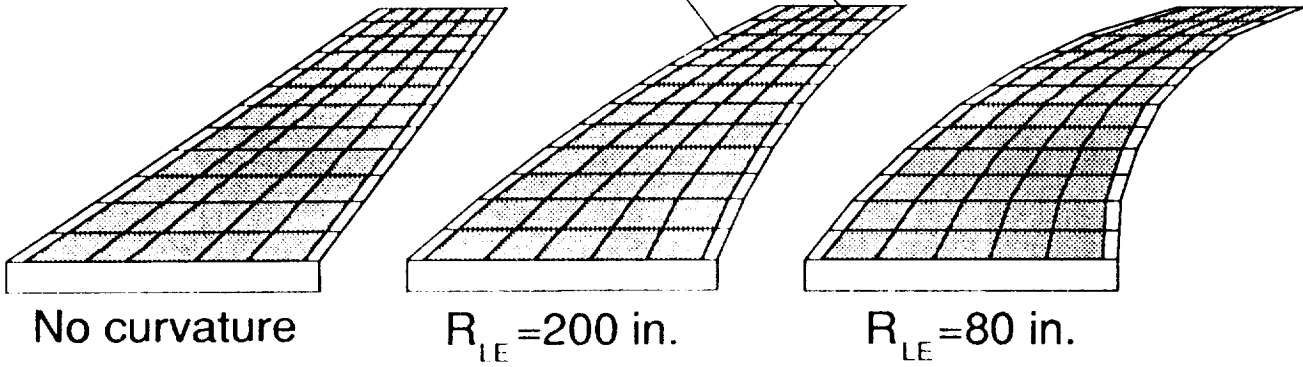
STRUCTURAL MODELS
FINITE ELEMENT MODELS

Aluminum and balsa elements

Aluminum elements

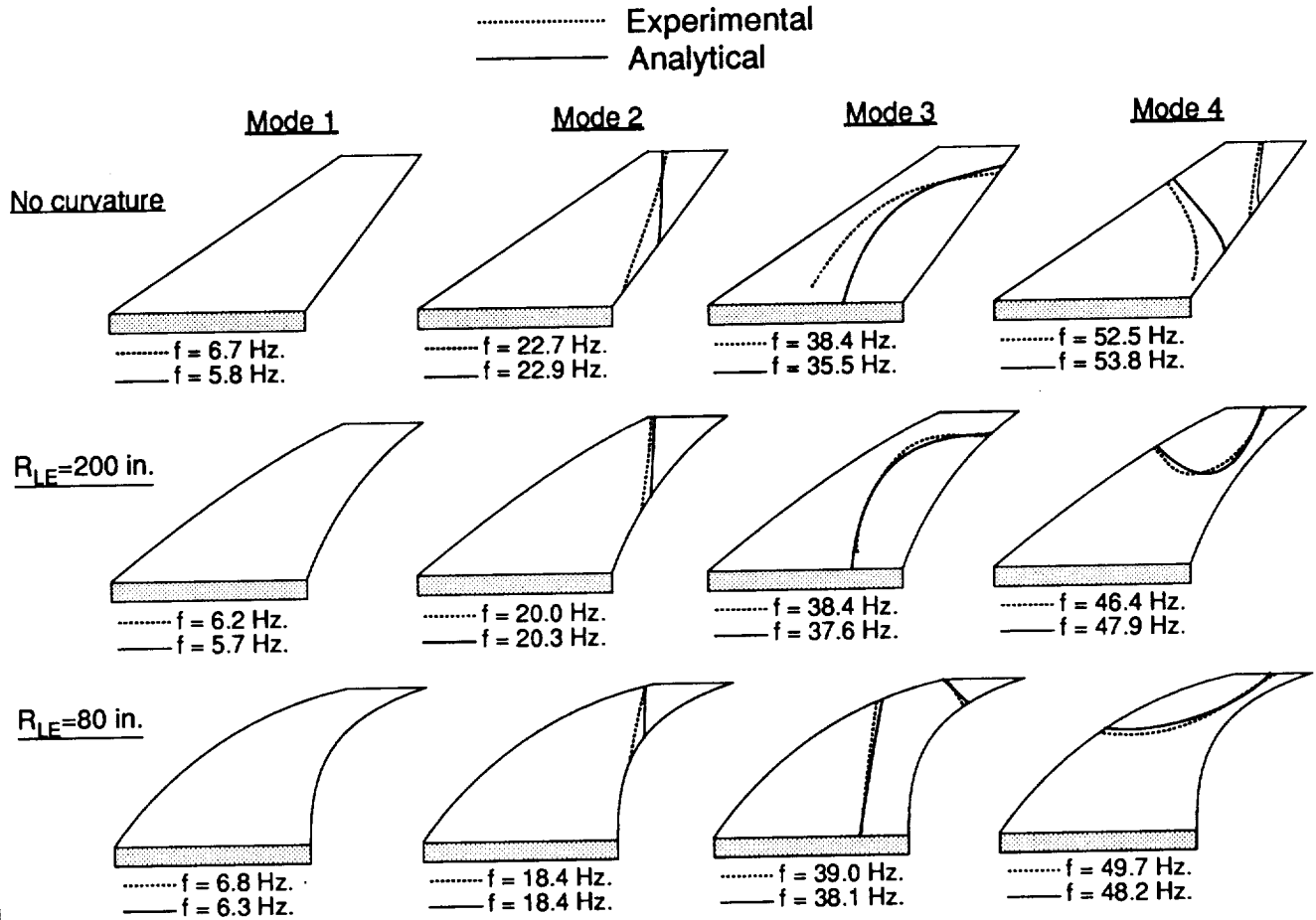No curvature $R_{LE} = 200$ in. $R_{LE} = 80$ in.

- **MSC NASTRAN**
- **Provide input for flutter analysis**
- **Quadrilateral (CQUAD4) plate elements**
- **Separate elements used to model aluminum plate and balsa**

Three finite element models representing the experimental models used in this study were developed using the MSC NASTRAN finite element program. These were used primarily to provide input for the flutter analysis. The models were constructed of quadrilateral (CQUAD4) plate elements. Separate elements were used to model the aluminum plate and the balsa wood which formed the airfoil shape. Regions where elements representing the aluminum and balsa were both employed are depicted by the shaded areas.

Comparison of Frequencies and Node Lines

.... Experimental
───────── Analytical

| Mode 1 | Mode 2 | Mode 3 | Mode 4 |

No curvature

- f = 6.7 Hz.
- f = 5.8 Hz.

- f = 22.7 Hz.
- f = 22.9 Hz.

- f = 38.4 Hz.
- f = 35.5 Hz.

- f = 52.5 Hz.
- f = 53.8 Hz.

R_{LE}=200 in.

- f = 6.2 Hz.
- f = 5.7 Hz.

- f = 20.0 Hz.
- f = 20.3 Hz.

- f = 38.4 Hz.
- f = 37.6 Hz.

- f = 46.4 Hz.
- f = 47.9 Hz.

R_{LE}=80 in.

- f = 6.8 Hz.
- f = 6.3 Hz.

- f = 18.4 Hz.
- f = 18.4 Hz.

- f = 39.0 Hz.
- f = 38.1 Hz.

- f = 49.7 Hz.
- f = 48.2 Hz.

A comparison of the experimental and analytical structural models is illustrated in the above figure. The figure presents the experimental and analytical natural frequencies and node line locations for the three models studied. The frequencies and node lines were important in understanding the vibrational modes involved in the flutter of each model (primarily mode 1 and mode 2) and in determining the accuracy of the analytical structural models which were used in the flutter analysis. The experimental frequencies were obtained by exciting the models while mounted in the TDT and recording the resulting frequency spectrum output from an accelerometer mounted in each model. A modal survey was also conducted on each of the three experimental models to determine the location of the node lines for each of the first four vibrational modes. The analytical natural frequencies and node line locations were output from MSC NASTRAN using the three structural models shown in the previous figure. The analytical results correlated well with the measured data as all but one of the analytical natural frequencies were within 10 percent of the experimental frequencies and the analytical node lines generally agreed with the experimental data.

AERODYNAMIC MODELS

64 Collocation Points (8x8 array)

No curvature $R_{LE} = 200$ in. $R_{LE} = 80$ in.
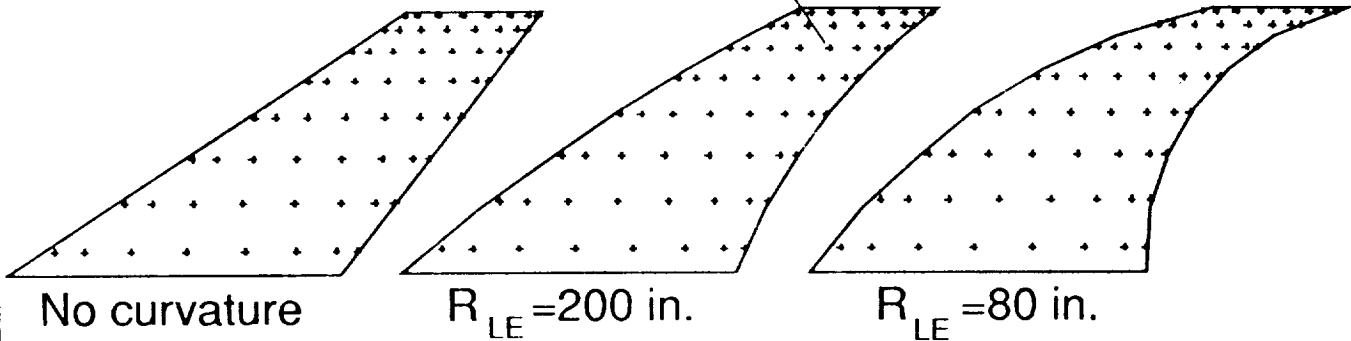
- ● FAST Flutter Analysis Program
    - Subsonic kernel function aerodynamics
    - Analytical mode shapes and generalized masses
    - Experimental natural frequencies
    - Match point flutter solution

A flutter analysis for each of the three models tested was performed using the FAST flutter analysis program. The aerodynamic models used in the flutter analysis are shown in the figure. Using calculated mode shapes, the program was used to calculate the unsteady aerodynamic forces for the natural vibration modes at each of the 64 collocation points (8X8 array) using a subsonic kernel function. Next, experimental natural frequencies and calculated generalized masses were input into the program. A match point flutter solution was then performed using FAST which output the correct density and flutter frequency for a specified flutter velocity.

Planform Curvature Effects
Experimental and analytical results
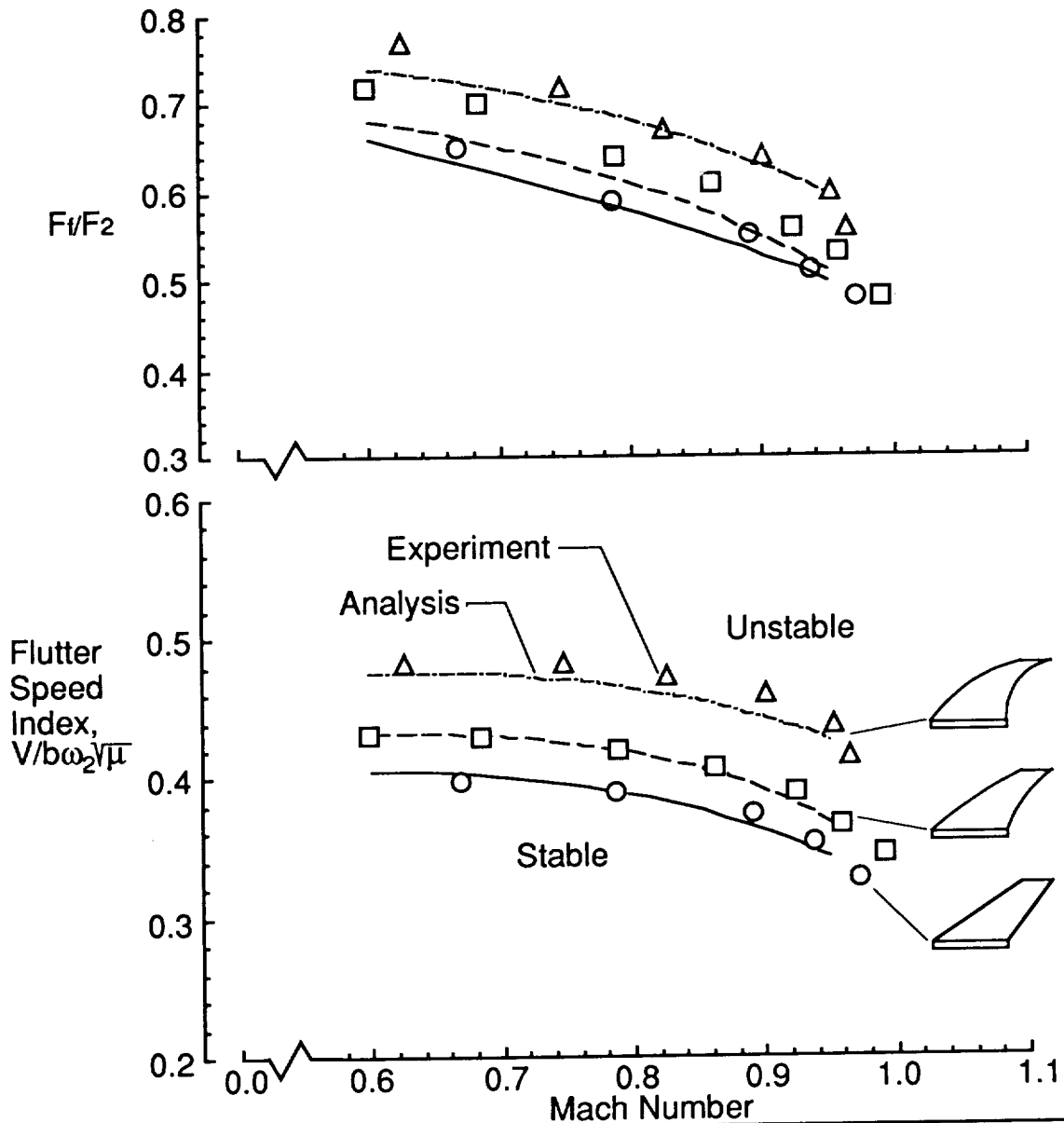
The experimental and analytical flutter boundaries presented in the figure are plotted as Flutter Speed Index (FSI) and flutter frequency ratio versus Mach number. The FSI is a non-dimensional velocity parameter used to correlate flutter results obtained for different models. Its value depends on the flutter velocity, V, root semi-chord, b, first torsional frequency, ω_2, and the square root of the mass ratio, μ. The value of flutter frequency ratio depends on the flutter frequency, Ff, and the first torsional frequency, F2. The experimental boundaries were obtained over a Mach number range of 0.60 to 1.00 using air as the test medium while the analytical boundaries were calculated over a Mach number range of 0.60 to 0.95 using FAST. The experimental flutter results presented in the figure show that the FSI and flutter frequency ratio increased as the planform curvature was increased. Both of these trends are also seen in the analytical flutter results which correlate very well with the experimental results. The flutter analysis also revealed that the participation of the second mode (first torsion) in the flutter increased as the planform curvature was increased.

55

SUMMARY

- Structural and flutter analysis agreed well with the experimental data

- Flutter speed index increased as planform curvature increased

In summary, both the structural and flutter analysis agreed well with the experimental results. Also, flutter speed index was shown to increase as planform curvature was increased for a series of generic flutter models used to represent the outboard portion of the wings for a recent NASA HSCT concept. This beneficial effect means that curving the leading and trailing edges of the outboard portion of a HSCT wing would not only improve the aerodynamic performance of the aircraft but could also improve its flutter characteristics.

AN INTRODUCTION TO ROTORCRAFT TESTING IN TDT

Paul H. Mirick
USAARTA-AVSCOM, ASTD
NASA Langley Research Center
Hampton, VA

OUTLINE

RESEARCH OBJECTIVES & AREAS

ARES MODEL DESCRIPTION

EXAMPLES OF RESEARCH WITH ARES

ARES ENHANCEMENTS UNDERWAY

SUMMARY

This presentation covers the research areas and objectives of the Rotorcraft Aeroelasticity Group. The Aeroelastic Rotor Experimental System (ARES), which is the primary test bed for rotorcraft testing in the TDT is described and three examples of research conducted are given. The enhancements of the ARES which are currently underway are also described.

TESTING OBJECTIVES

- **PERFORM RESEARCH INTO FUNDAMENTAL ROTORCRAFT PHENOMENA**

- **INVESTIGATE ADVANCED ROTORCRAFT CONCEPTS**

- **DEVELOP HARDWARE AND TEST TECHNIQUES TO TAKE ADVANTAGE OF UNIQUE CAPABILITIES OF TDT**

The objectives of rotorcraft testing in the TDT are usually one of the following:
a. Investigate a fundamental rotorcraft phenomena.
b. Investigate a new concept.
c. Develop new hardware or test techniques which will take advantage on the unique capabilities of the TDT.

ROTOR RESEARCH AREAS IN TDT
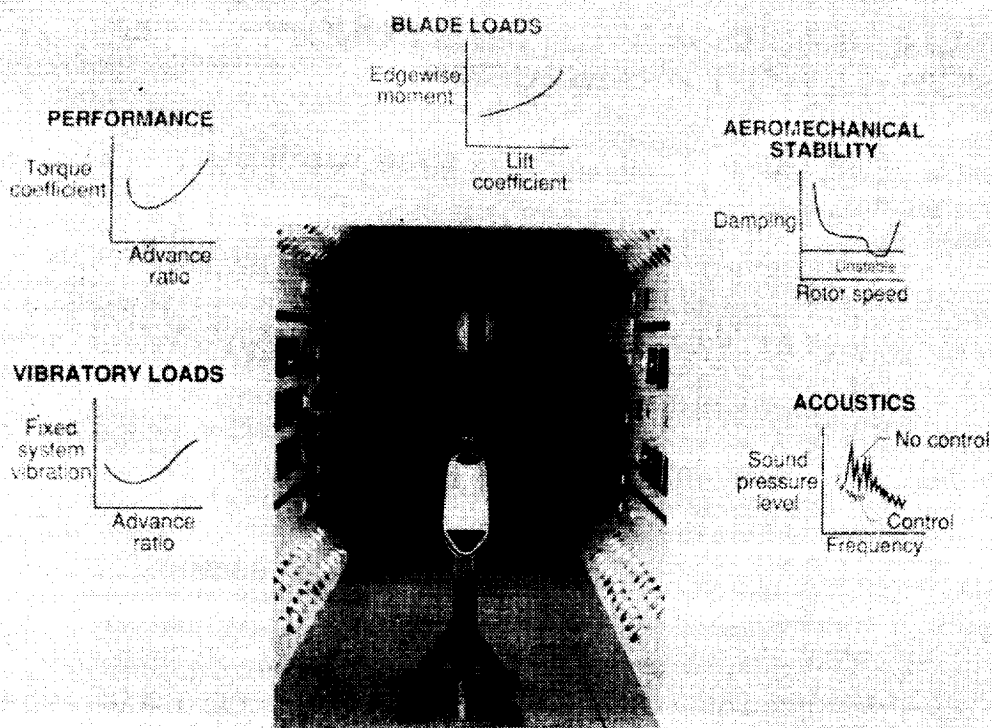
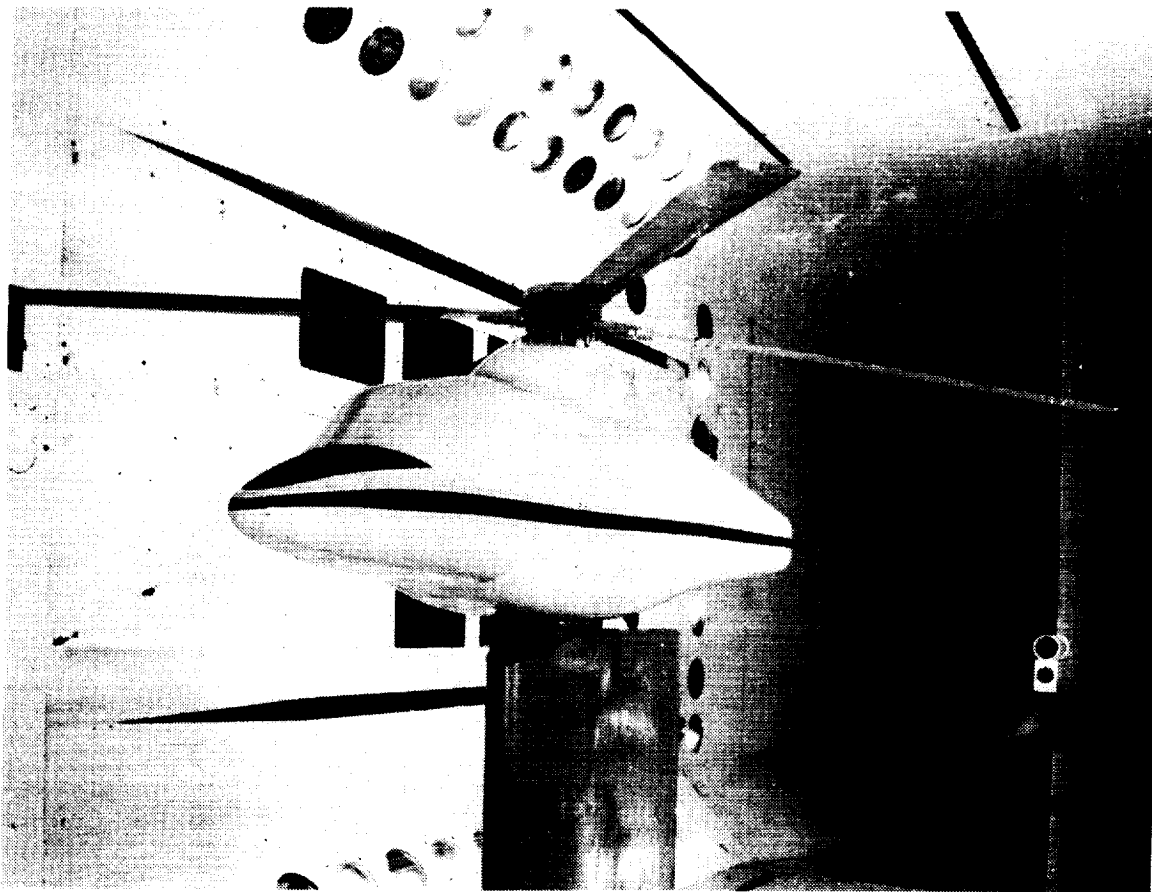The research areas covered by the Rotorcraft Aeroelasticity Group include:
a. Fixed system vibratory load
b. Rotor performance
c. Blade loads
d. Aeromechanical stability and
e. Acoustics

60

AEROELASTIC ROTOR EXPERIMENTAL SYSTEM (ARES)

- MODEL DEVELOPED - 1976 BY NASA/ARMY

- STAND MOUNTED

- NOMINAL 9 FOOT DIAMETER ROTORS

- SKINS - AERODYNAMIC FAIRING

The primary test bed for rotorcraft tests conducted in the TDT is the ARES model. This model was first developed by the Army and NASA in 1976. Since then, a number of modifications have been made which have improved the model's capability. The model is stand mounted to the TDT test section floor. The nominal rotor diameter of rotors tested on the ARES is 9 feet. The model has skins to provide an aerodynamic fairing around the drive system.
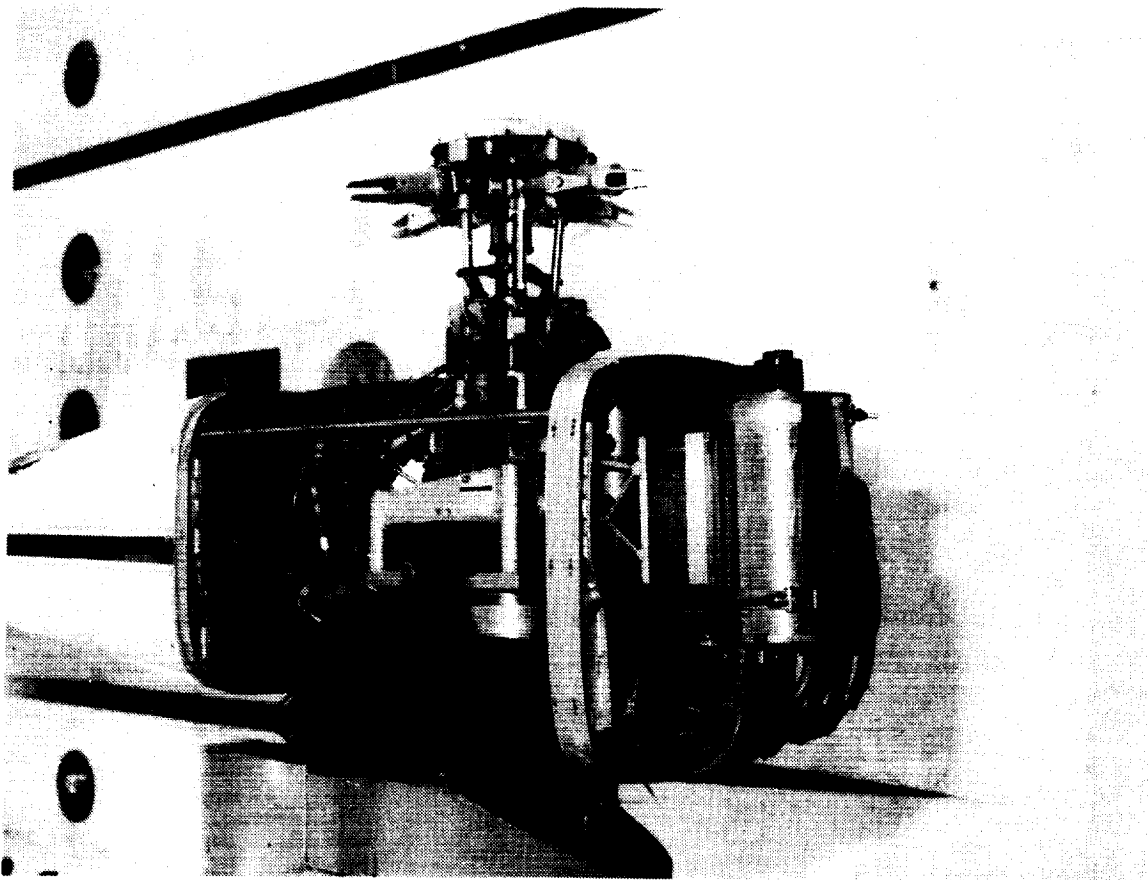
ARES

POWER: ELECTRIC MOTOR

- 47 HP @ 12000 RPM
- WATER COOLED

DRIVE: 2 STAGE BELT DRIVE

CONTROL SYSTEM: HYDRAULIC - FLY BY WIRE

- CONVENTIONAL SWASHPLATE
- ROTOR SHAFT ANGLE

Power is provided to the rotor by a water cooled electric motor which is capable of producing 47 HP and 12000 RPM. The motor RPM is controlled by a motor generator set which allows the desired rotor RPM to be obtained. Power is transmitted to the rotor through a two-stage belt drive system which provides a reduction ratio of about 14 to 1. Typical model rotor RPM are between 600 and 700 RPM. Control of the model is by the use of a hydraulic fly-by-wire system. The model uses a conventional swashplate which is driven by three hydraulic actuators. By adjusting the swashplate position, the rotor collective and cyclic pitch are changed to either trim the model rotor or to simulate desired rotor loading conditions. The whole model can also be pivoted about a pitch bearing by another hydraulic actuator. This angle is referred to as the rotor shaft angle.

ARES

INSTRUMENTATION:

- FIXED SYSTEM - SIX COMPONENT STRAIN GAGE BALANCE

  - MEASURES ROTOR FORCES AND MOMENTS
  - METRIC SECTION ISOLATED FROM SKINS

- ROTATING SYSTEM - 30 CHANNEL SLIP RING

  - MEASUREMENTS ARE TEST DEPENDENT

65
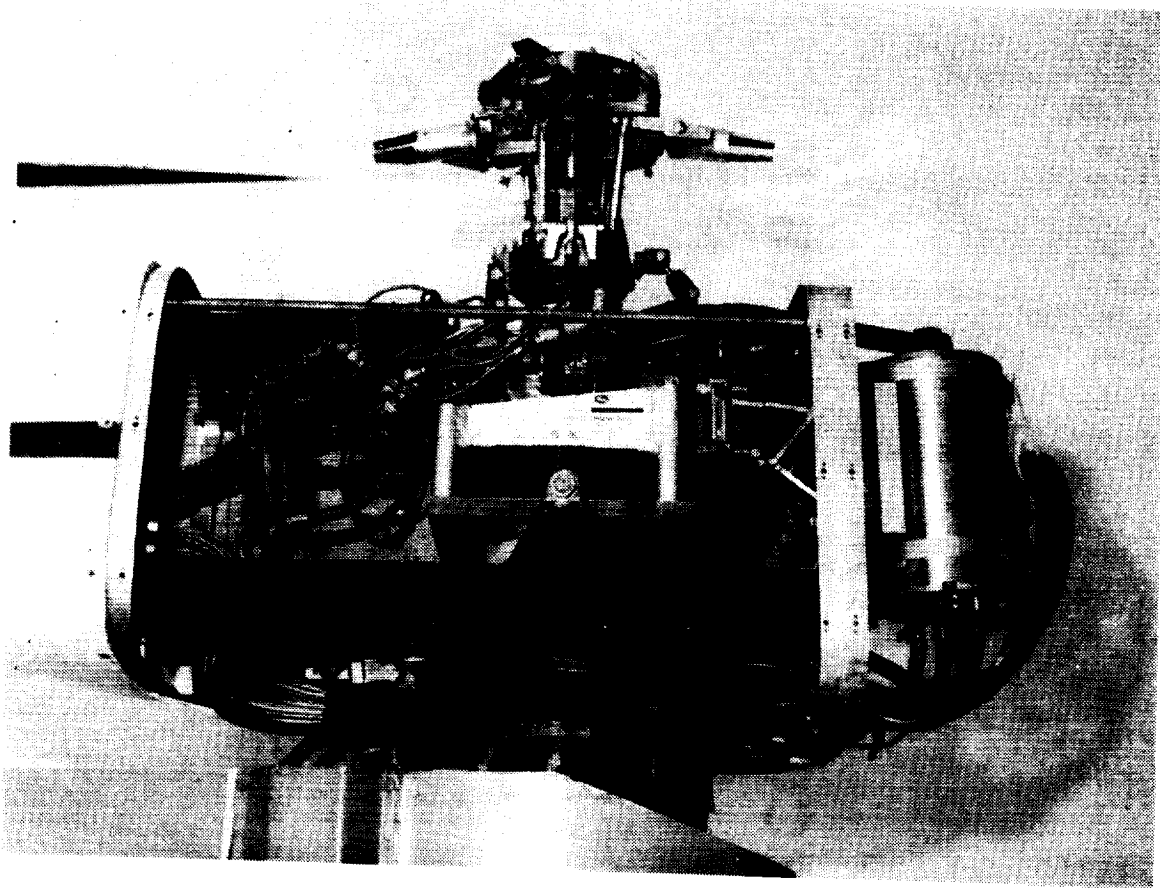
ARES instrumentation consists of a six component strain gage balance. The motor, rotor drive system, and the rotor control system are on the metric side of the balance. However, the skins are attached to the bulkheads which are on the ground side of the balance. Therefore, the measured forces and moments provided by the balance are due to the rotor and do not include any contribution from the fuselage skins. For measurements in the rotating system there is a 30 channel slip ring located at the base of the rotor shaft. The rotating system parameters measured are taylored to each test. Typical measurements are blade angles, blade strain gage readings, and pitch link loads.
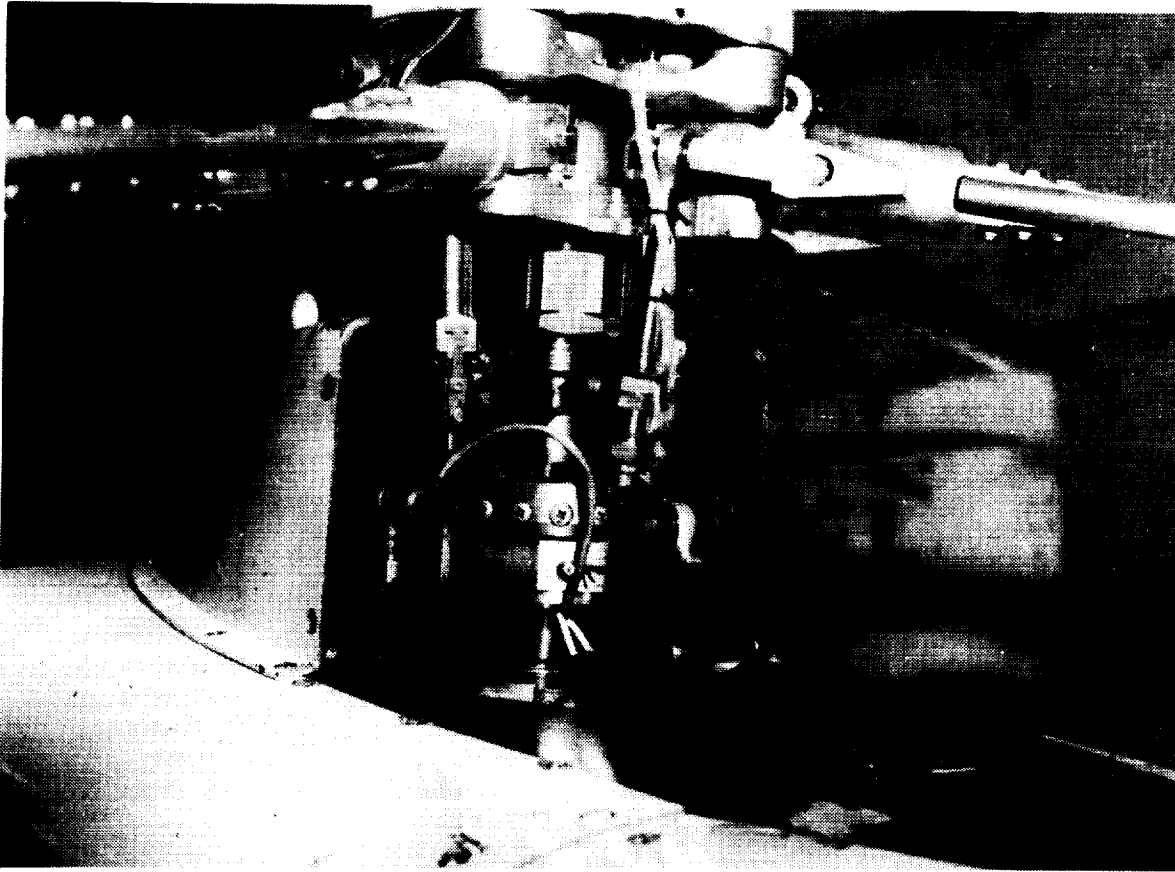
ARES VERSATILITY

SHAFT DESIGNED TO ACCEPT DIFFERENT HUBS

HUBS DESIGNED TO ACCEPT DIFFERENT BLADES

CONTROL INPUTS MAY BE VARIED

67

What makes the ARES a valuable tool in rotorcraft research is its versatility. The rotor shaft is threaded which allows different hubs to be easily adapted to the rotor shaft. Likewise, the hub blade attachment cuffs are designed to accept different blades. The third attribute of the ARES is the control system. The fly-by-wire system allows for high frequency control inputs to the rotor blades.

BLADE MOTION
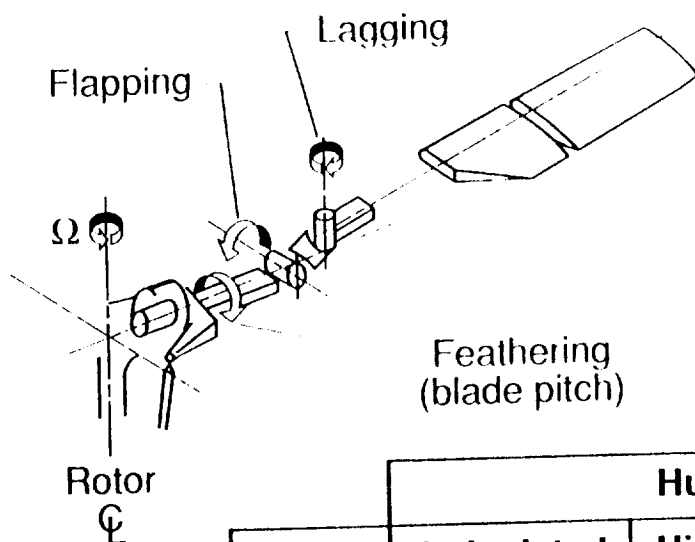
| Motion	Hub Type		
	Articulated	**Hingeless**	**Bearingless**
Flap	Hinge	Flexure	Flexure
Lag	Hinge	Flexure	Flexure
Pitch	Hinge	Hinge	Flexure

The purpose of this diagram is to explain the differences in types of rotor hubs. Each blade has three degrees of freedom which the hub must allow. A back and forth movement in the horizontal plane of a rotor which is referred to as lead-lag or as lag. An up and down motion which is referred to as blade flapping and a degree of freedom to allow the blade angle of attack or pitch to be changed which is referred to as pitch or feathering. The simplest way to allow these motions is to use hinges or bearings. This design is known as an articulated hub and it has hinges or bearings which allows flap, lag, and pitch. While the articulated is simple in concept, its design is complex. Each hinge consists of many parts which have limited life, require lubrication, and require periodic inspection. This requires many maintenance manhours which is undesirable. With improvements in materials technology, two rotor hub types which replace the hinges with flexible structural members have become more feasible. These are the hingeless and the bearingless rotor hubs. The hingeless rotor hub replaces the flap and lag hinges with flexbeams which flex to allow the flap and lag motion but retains the bearings to allow blade pich changes. The bearingless rotor hub replaces all hinges with a flexbeam to allow blade flap, lag, and pitch.
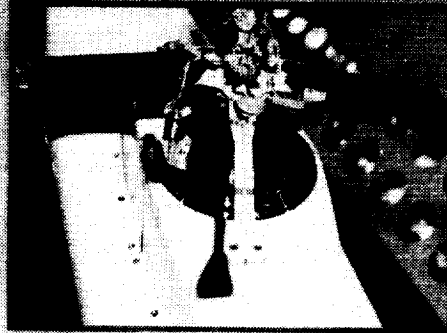
69

HUBS TESTED ON ARES
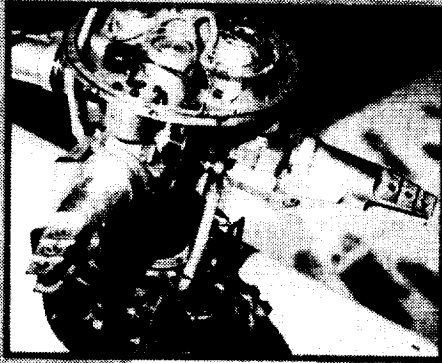
ARTICULATED
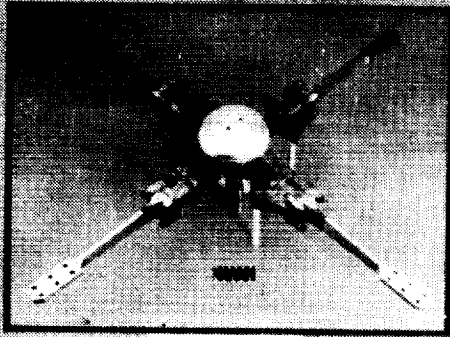
HINGELESS

BEARINGLESS

This figure shows an example of each type of hub that has been tested on the ARES. The articulated hub has a coincident flap and lag hinge with the feathering bearings outboard. The hingeless hub shown has a flap flexure inboard, then the feathering bearing, and finally the flap flexure. The bearingless hub has a single flexure which allows the flap, lag, and feathering motion. Each type of rotor hub has different dynamic characteristics and problems. Therefore, it is necessary to have the capability to test the different types of hubs.

BLADE DESIGN VARIABLES

- **PLANFORM**

- **TIP GEOMETRY**

- **AIRFOILS**

- **TWIST DISTRIBUTION**

- **MASS DISTRIBUTION**

- **STIFFNESS DISTRIBUTION**
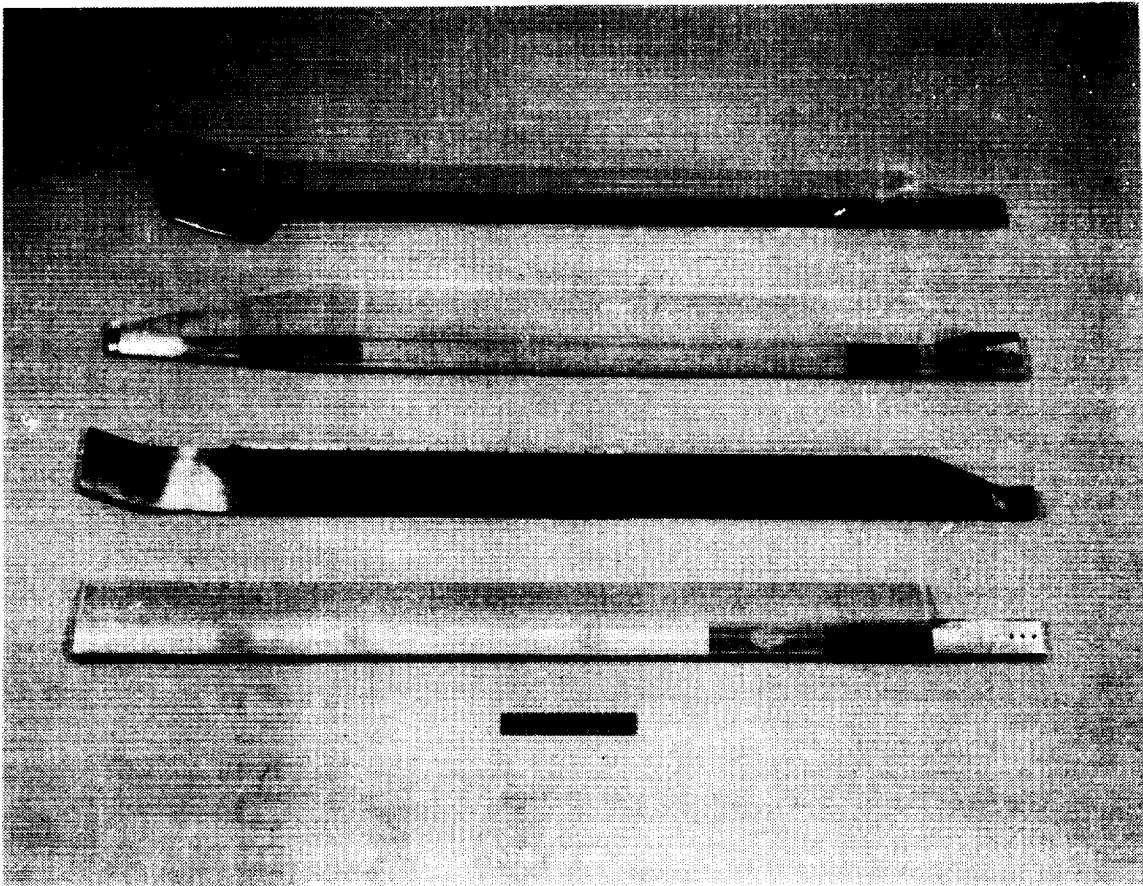
The figure shows four different blades which were built for testing on ARES. Descriptions of each blade follows starting from the bottom of the figure. The first blade has a simple rectangular planform with a NACA 0012 airfoil. The second blade is shown with a swept tip but has provisions for installation of different tips. This blade also has tabs which can be adjusted to change pitch moment. A companion blade was designed with different internal torsional stiffness to investigate this effect. The third blade (referred to as the Growth Blackhawk Blade or GBH which will be discussed later) has a tapered tip and has different airfoils at different radial stations in order to obtain the desired performance from the blade. A companion blade was designed that allows the blade mass distribution to be varied. The fourth blade has an experimental tip geometry based on a British design called the BERP tip. Due to the restrictions on testing in R-12, this blade has not been tested in the TDT.

ARES CONTROL SYSTEM

HYDRAULIC / FLY BY WIRE

- **COLLECTIVE AND CYCLIC FOR ROTOR TRIM**
- **SIGNAL MAY BE ADDED TO TRIM**

  - **EXCITE ROTOR FOR STABILITY TESTS**
  - **HIGHER HARMONIC CONTROL INPUT**

The ARES control system also allows for flexibility in testing. The model uses electrically controlled hydraulic actuators to drive the swashplate. As illustrated on the following page, it is possible to add an arbitrary signal such as the higher harmonic pitch signal to the trim signal. This capability is used in stability testing to excite frequencies of interest in the rotor system. Other investigations which use this capability have been conducted to examine the effect of higher harmonic inputs on rotor loads, fixed system vibrations and rotor acoustic signal.

74
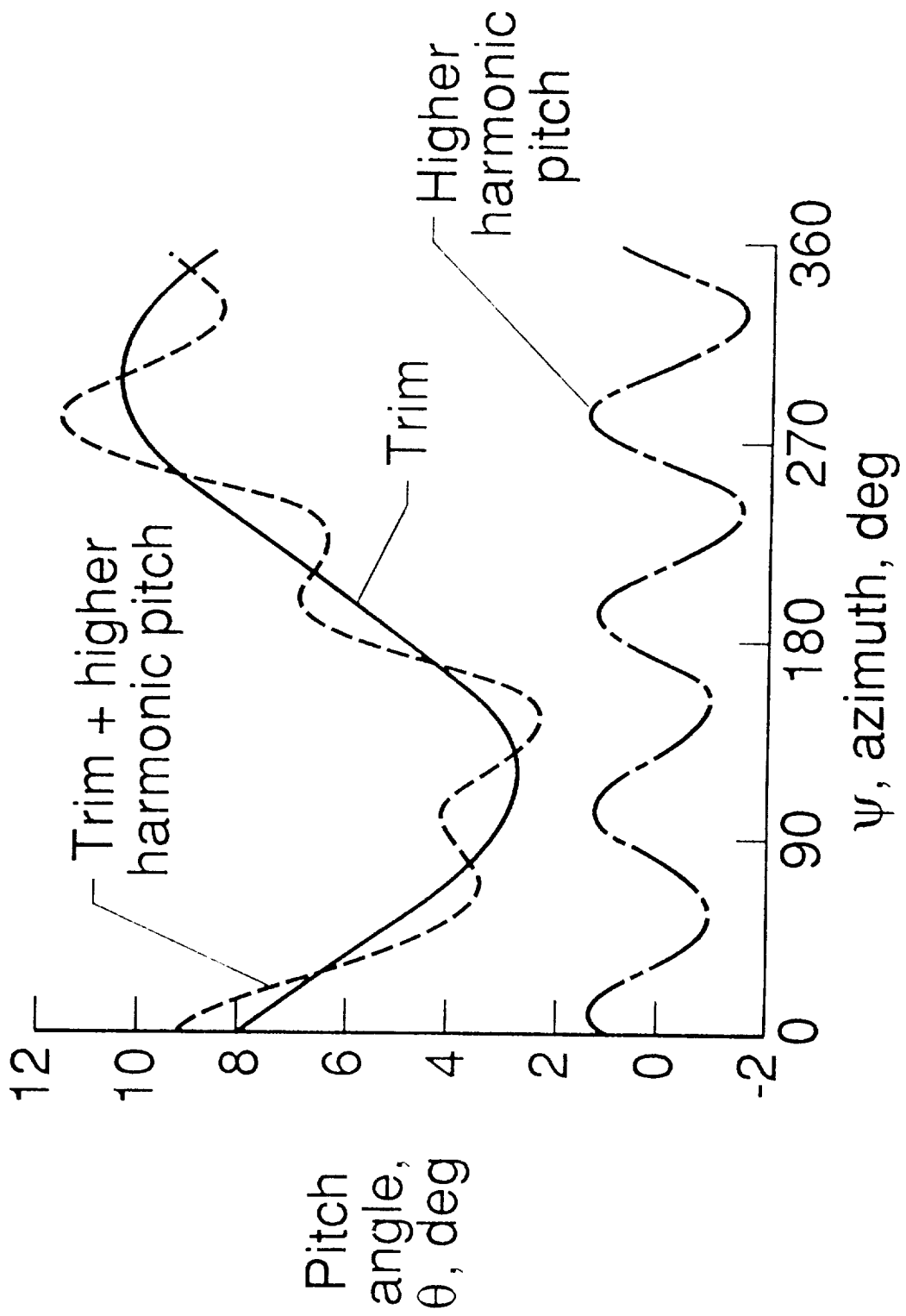
HINGELESS ROTOR EXPERIMENTS VALIDATE ANALYTICAL METHOD

HINGELESS ROTOR MODEL IN TDT

HOVER
(COLLECTIVE PITCH = 8°)

FORWARD FLIGHT
(ADVANCE RATIO = 0.2)
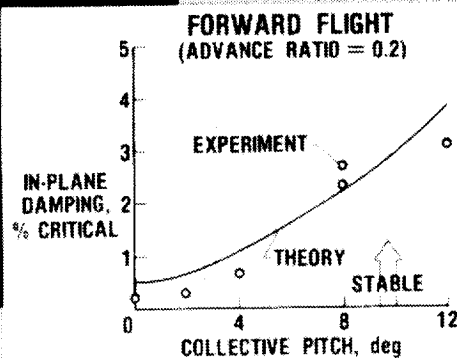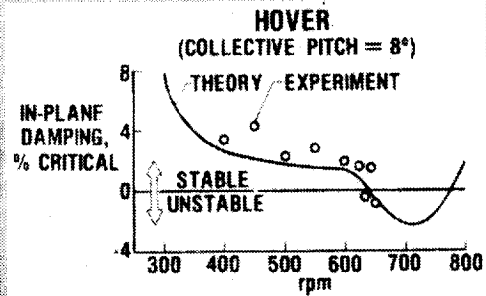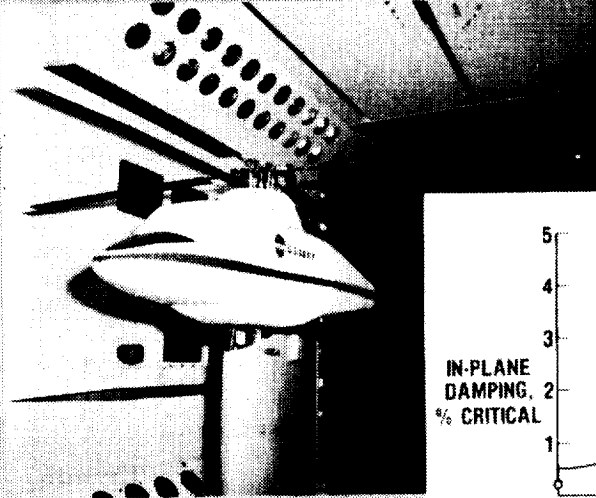
The previous figures have covered ARES capability. The next three figures are examples of how the ARES capability is used to accomplish a research objective. The first example is a test of a hingeless rotor design. This test was conducted to obtain data to be used for validation of an analytical method. A hingeless rotor similar to the one shown earlier was installed on ARES. The control system was used to excite in-plane motion of the blade. Once the motion was excited, the control input was turned off and the rotor in-plane motion was then examined with a moving block analysis to determine its damping characteristic. This procedure was repeated over a combination of rotor RPMs, collective pitch settings, and forward flight conditions. The two plots show typical data obtained and the correlation with pretest analytical predictions.

75
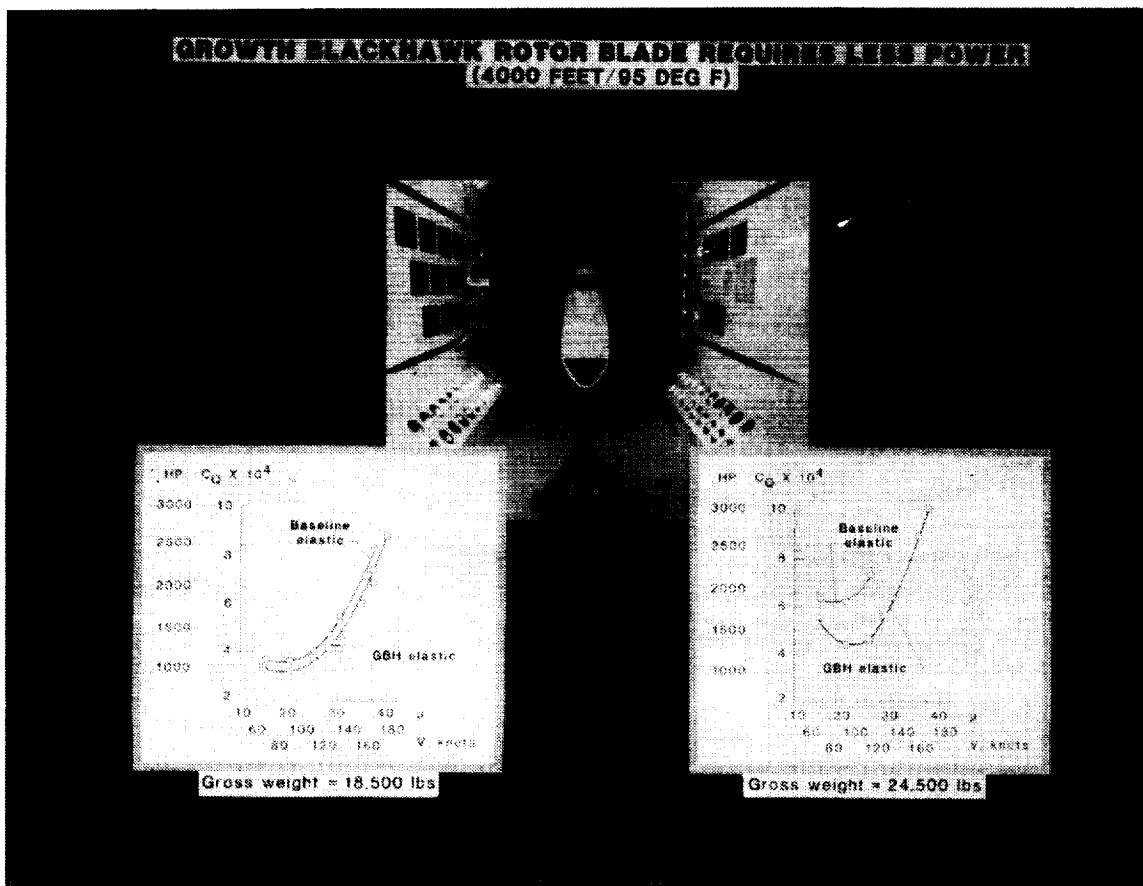
The second example is a test conducted with the GBH rotor blade. The blade was designed for the Army's UH60 (Blackhawk) helicopter. The original Blackhawk design was for an aircraft gross weight of 18,500 lbs at a density altitude of 4000ft/95°F. The army had a requirement to increase the Blackhawk's capability to 24,500 lbs at a density altitude 4000ft/95°F. A rotor was designed by the Army Aerostructures Directorate at NASA Langley Research Center to meet this mission. A baseline rotor representative of the current Blackhawk rotor and the new rotor design were tested in the TDT. The two graphs compare the rotors at their design condition. These graphs examine power as a function of forward speed. As shown, the GBH performed better than the baseline at both design conditions.

BVI NOISE REDUCED USING HIGHER-HARMONIC PITCH CONTROL

HHP/BVI TEST IN TDT

ROTOR MODEL

MICROPHONES

HHP CONCEPT

FLOW

REDUCED VORTEX
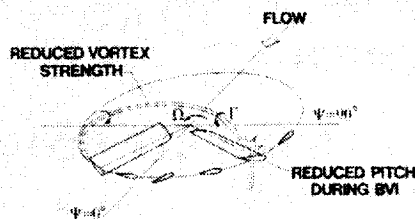STRENGTH

REDUCED PITCH
DURING BVI
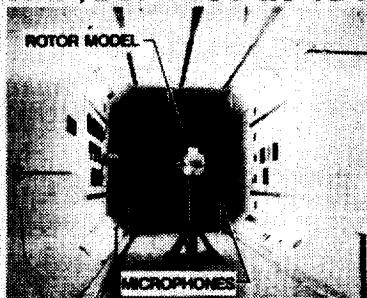
NOISE LEVEL (dB) WITH HELICOPTER FLIGHT CONDITION

WITHOUT HHP

HIGH LEVELS

WITH HHP

REDUCED LEVELS

DESCENT
ANGLE,
deg.

DESCENT

LEVEL
FLIGHT

CLIMB

ADVANCE RATIO
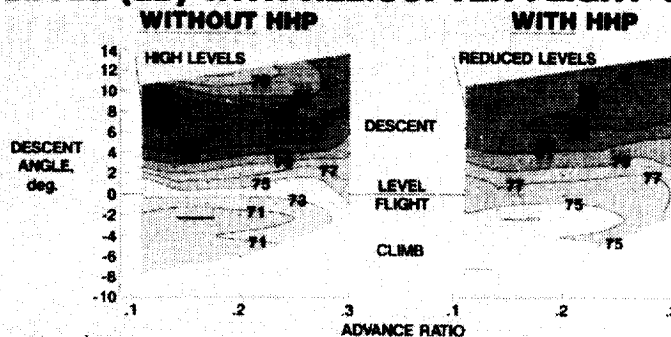
The third example is an experimental program to modify the noise produced by blade vortex interaction (BVI). BVI is the result of a blade passing through or near the vortex generated by another blade. A higher harmonic pitch (HHP) control signal which was added to the normal rotor collective and cyclic was developed to reduce the blade pitch in the region where BVI occurs and thereby reduce the noise associated with the BVI. BVI is most noticeable during low speed descending flight and therefore this was the area of primary interest. The two diagrams show the measured noise level with and without the HHP over a range of advance ratios and descent angles. The noise level in the primary area of interest (low speed descending flight) was reduced from 87db to 81db.

ARES ENHANCEMENTS

ABILITY TO CHANGE MODEL BODY FREQUENCIES

- TUNE MODEL TO AVOID UNDESIRABLE FREQUENCIES

ABILITY TO SIMULATE ROTOR BODY DYNAMIC INTERACTIONS

- IMPROVES CAPABILITY TO INVESTIGATE AEROMECHANICAL STABILTIY AND VIBRATION OF A COUPLED ROTOR/AIRFRAME SYSTEM

While the ARES is an excellent testbed for rotorcraft tests, there are some improvements that are desired. With the current ARES model it is very difficult to change the model body frequencies in order to avoid any undesirable frequencies or to simulate rotor and body interaction. The easiest way to change the model dynamics is to modify the way the balance is mounted to the stand. The current ARES has the balance rigidly mounted to the longeron with the ability to change rotor shaft angle about a pivot point. Two refinements to the ARES model are being developed which will change the way the balance is mounted and thereby give the desired enhancements to the ARES.

ARES 1.5

SAME AS ARES FROM BALANCE UP

METRIC SECTION IS SUPPORTED ON A SPHERICAL BEARING AND TWO ELASTOMER SPRINGS

SPRINGS AND DAMPERS FOR PITCH AND ROLL

PASSIVE MEANS OF ADJUSTING MODEL FREQUENCIES AND DAMPING

ARES 1.5

ARES 1.5 BALANCE MOUNTING

FRONT MOUNT

REAR MOUNT
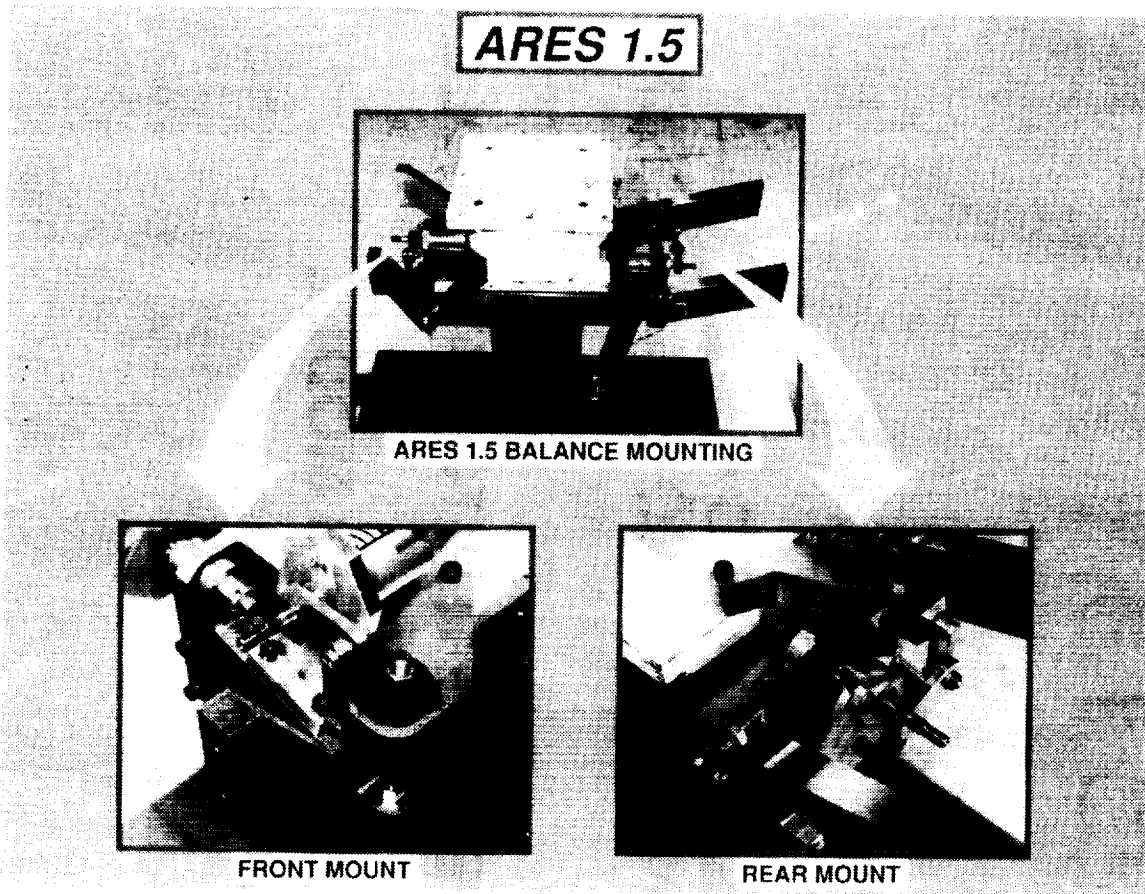
The first modification (ARES 1.5) has the balance mounted on a spherical bearing at the front of the balance. The model is also supported in the pitch and roll directions by two elastomer springs and two dampers. From the balance up the model is unchanged from the basic ARES model. By making changes in the springs and dampers, it is possible to adjust model frequencies and damping.

ARES II

- SAME AS ARES FROM BALANCE UP

- METRIC SECTION SUPPORTED BY SIX ACTUATORS

- CONTROLLER COMMANDED ACTUATOR POSITION

- ACTIVE MEANS OF CONTROLLING MODEL
  RIGID BODY DYNAMICS
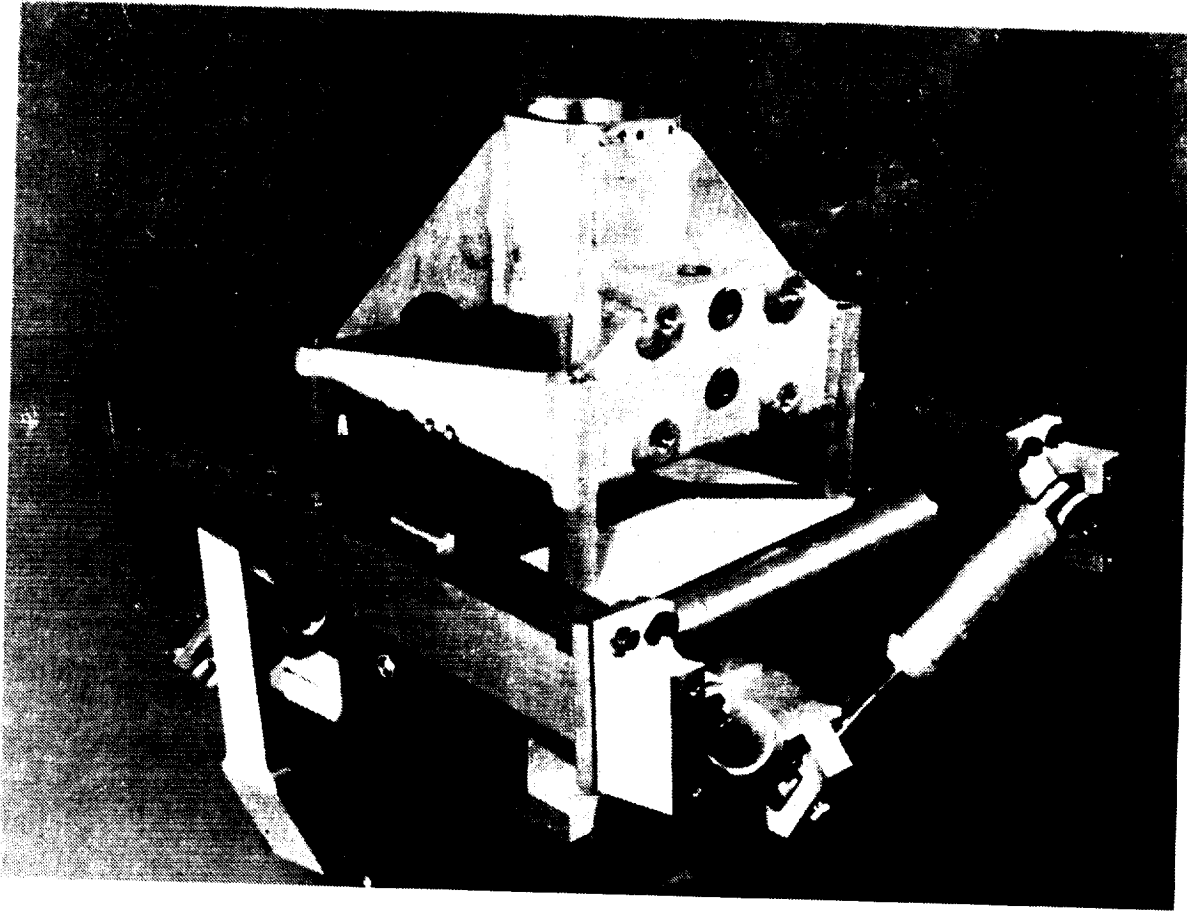
The second modification (ARES II) has the balance supported on six hydraulic actuators. A controller will command the actuator positions which will drive the balance and rotor system in a desired manner. This will give an active means of controlling the model rigid body dynamics. A wooden mock up of the ARES II is shown in the figure.

SUMMARY

- **ARES IS THE PRIMARY TEST BED FOR ROTORCRAFT TESTING IN TDT**

- **ARES PROVIDES FLEXIBILITY TO CONDUCT ROTORCRAFT RESEARCH**

- **ENHANCEMENTS TO ARES WILL PROVIDE NEW AND IMPROVED CAPABILITY FOR CONDUCTING ROTORCRAFT RESEARCH**

The ARES is the primary test bed for rotorcraft testing in the TDT. The ARES model provides the flexibility to conduct rotorcraft research in many areas. With the new enhancements underway, the ARES will have new and improved capability for conducting rotorcraft research.

# ROTORCRAFT VIBRATION REDUCTION RESEARCH AT THE TDT

Matthew L. Wilbur
USAARTA-AVSCOM, ASTD
NASA Langley Research Center
Hampton, VA

BACKGROUND

- **Rotorcraft vibrations are a continuing problem**

- **Historically, vibration problems have been corrected in post-design phases**

- **Current trends are to address vibrations throughout the design phase**

- **Failure has shown that analyses are not accurate/sophisticated enough**

Helicopters have always had vibration problems, and such problems continue today. Historically, severe vibration problems have been addressed by the manufacturers after a flight vehicle had already been built, using trial and error techniques to reduce the vibratory loads to an acceptable level. However, within the last ten years, attempts have been made to address vibration problems during the helicopter design phase through the use of computer analyses. Once implemented, however, these designs have generally failed to demonstrate significant reductions in vibration levels. This has shown that helicopter analyses are not yet sophisticated enough to be used reliably to design low vibration rotor systems. This paper will discuss a research project designed to further the understanding of the sources of rotorcraft vibrations. This research is being performed at the NASA Langley Research Center Transonic Dynamics Tunnel (TDT).
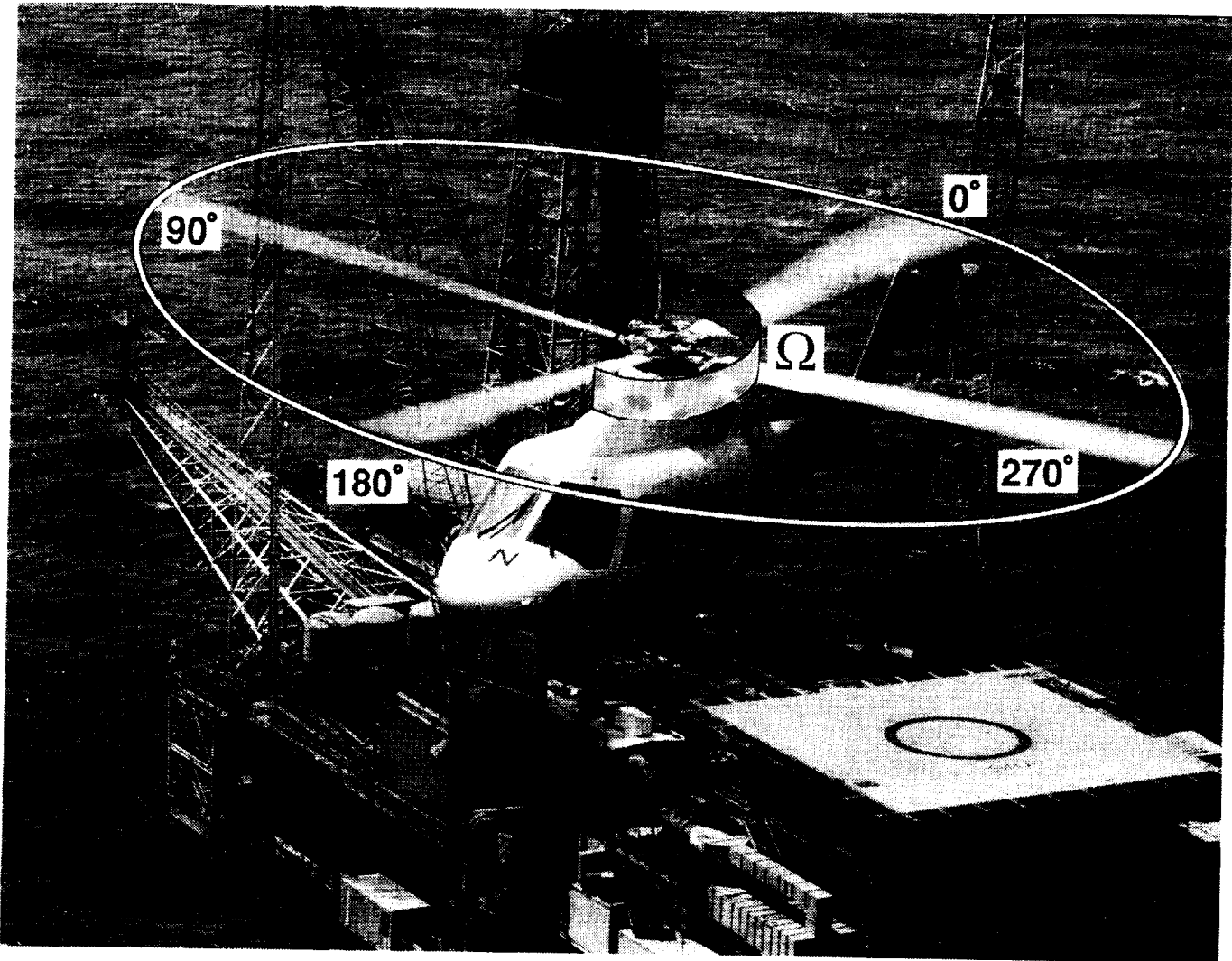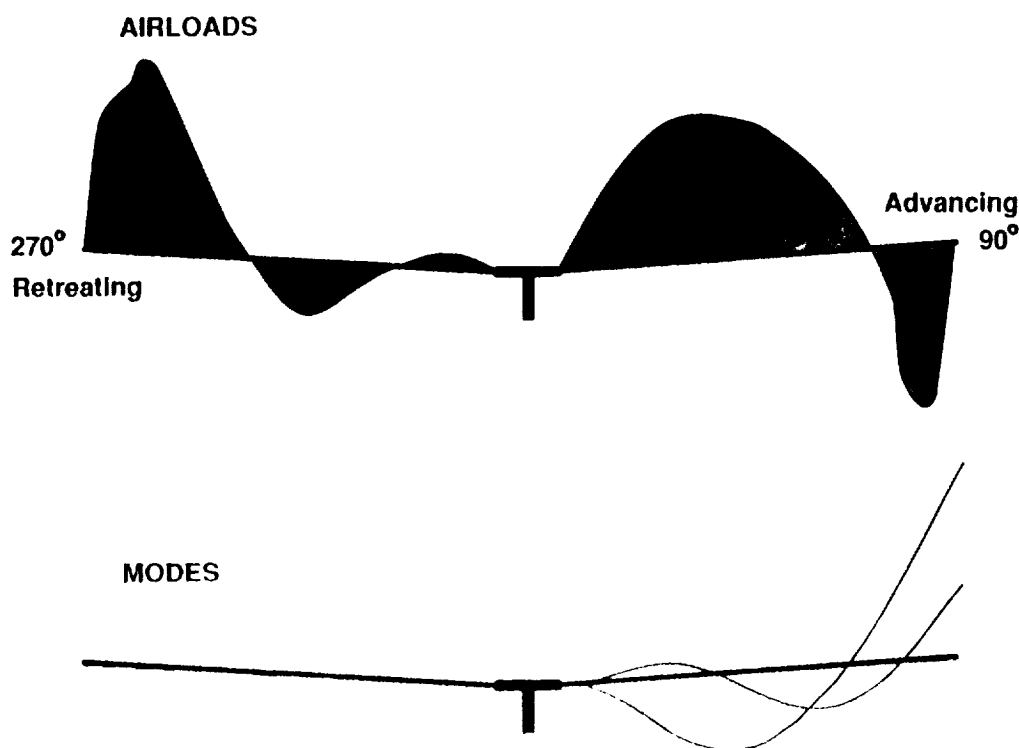
The photograph above, along with the following word chart, represent the terminology which will be used throughout this paper. The photograph shows a Sikorsky S-76 helicopter in flight. As indicated, the rotor rotates counterclockwise at a rotational velocity of Ω. Also shown on the photo is the generally accepted blade-azimuth orientation. As a blade passes over the tail of the aircraft, it is at $0°$ azimuth. The other angles are indexed from the tail and in the direction of rotation so that $90°$ azimuth is over the right side, $180°$ azimuth is over the nose, and $270°$ azimuth is over the left side of the aircraft. When a blade is between $0°$ and $180°$ azimuth it is called an advancing blade, since it is advancing into the free-stream velocity. Likewise, a blade in between $180°$ and $360°$ is called a retreating blade since it is retreating from the free-stream velocity. Advance ratio, μ, is a velocity term used for rotorcraft. It is the ratio between the free-stream velocity, V, and the rotor tip velocity denoted by ΩR, where R is the rotor radius. The other term listed is nP (or n per revolution) which represents a frequency relative to the rotor rotational frequency. In other words, the n is a multiplier which is applied to the rotor rotational velocity.

Rotorcraft Terminology

- Blade azimuth, Ψ

- Advancing blade -- between 0 and 180 deg

- Retreating blade -- between 180 and 360 deg

- Advance Ratio, μ $\mu = V / \Omega R$ (0.0 to 0.4)

- nP -- n times per revolution

Sources of Rotorcraft Vibrations

AIRLOADS

270° Retreating

Advancing 90°

MODES

The figure above, along with the following word chart, represent some fundamental rotor dynamics and discuss the major sources of rotorcraft vibrations. Primarily, the oscillatory shear applied to the hub by the rotor blade is the driving force behind vibratory loads. These shears are caused by a coupling of the airloads which are applied to the blade, and the blade's response to those airloads. This is shown graphically in the upper figure. The figure shows two in-plane views of a rotor in forward flight. The flight direction is into the page so that the blade on the right is at 90° azimuth, and the blade on the left is at 270° azimuth. The applied airloading is shown as well as the blade's modal response. As is apparent from the figure, the airloading environment of a rotor is highly oscillatory in nature. On the advancing side, the majority of the airloading is applied to the central section of the blade while the tip actually produces a negative load. On the retreating side, the majority of the airload has shifted out towards the tip of the blade while the inboard sections produce little or negative lift. The oscillatory airloading in turn excites the blade's modal response. The two effects combined produce a large oscillatory shear at the blade root which is transferred directly to the hub and into the helicopter body.

For a 4-bladed rotor as will be discussed in this paper, the primary vibratory loading of concern is the 4P (or 4 per revolution) load since each of the 4 blades apply their own root shear to the hub.

Rotor Dynamics

- Primary source of rotorcraft vibrations is oscillatory blade root shear
  - Airloads
  - Blade modes/frequencies

- For a 4-bladed rotor system, primary fixed-system load is 4 per rev

Vibration Reduction Methods

- **Change airloads**
  - **Active controls**
  - **Planform**
  - **Twist distribution**
  - **Pitch-flap coupling**

- **Change modes/frequencies**
  - **Stiffness**
  - *Mass*

The figure above discusses some of the basic techniques which could be used to reduce a helicopter's vibratory loads. Since the airloads and the blade modal response are the largest drivers of vibratory loads, it is natural to expect that changing these characteristics will affect the vibratory characteristics of the rotor system. There are several ways in which these changes could be effected. To change the airloads, a designer could employ active controls to adjust the pitch of each blade individually as it rotates. Other choices would involve passive means of changing the airloads such as planform changes, blade twist changes, or blade pitch-flap coupling changes. To change the blade modal response, the frequencies and/or the mode shapes could be adjusted by changes in the blade stiffness or mass distributions. In the figure, mass distribution has been italicized since it is the subject of a research program designed to experimentally investigate the cause and effects of rotorcraft vibrations. This research program is the subject of the remainder of this presentation.

90

Tailored Growth Black Hawk (GBH-T) Rotor Program

- **Objective**
  - **Investigate passive means of reducing fixed-system vibratory loads**
  - **Provide a data base for correlation with and development of analytical methods**

- **Approach**
  - **Build aeroelastically scaled rotor blade hardware with provisions for insertable masses along radius**
  - **Test on the ARES testbed in the TDT**

The project is called the Tailored Growth Black Hawk (GBH-T) Rotor program and is being performed at the TDT. The objective of the program is to investigate a passive means of reducing rotorcraft fixed-system vibratory loads through the use of blade non-structural mass. This allows for the development of a data base for use in correlation, validation, and development of more accurate analytical prediction methods. The approach taken was to have aeroelastically scaled rotor blade hardware fabricated which have provisions for insertable masses along the blade radius. These blades have been tested on the ARES helicopter testbed in the TDT.

ROTOR BLADE COMPONENTS

AIRFOIL GLOVE

INSERTABLE MASS
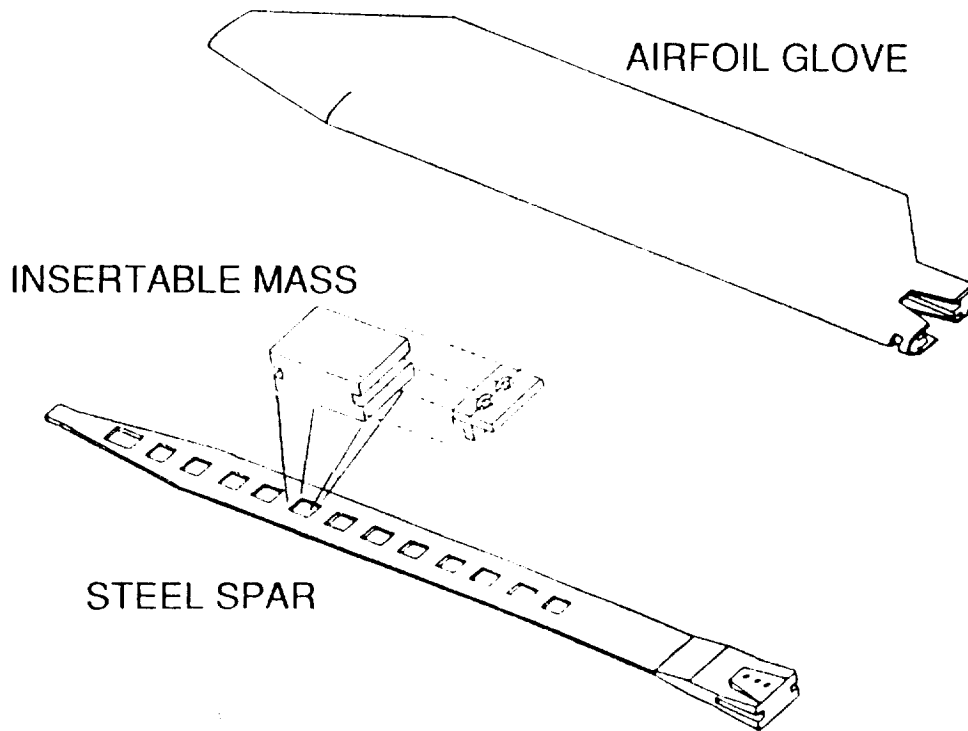
STEEL SPAR

The figure above shows the main components of the GBH-T rotor blades. The basic blade consists of the airfoil glove and the steel spar as shown. The airfoil glove is responsible for maintaining the aerodynamic shape and to provide the majority of the blade stiffness. The glove has an internal channel centered about the quarter-chord which runs the full length of the blade. This channel is made to accept and lock in place the steel spar. The steel spar has cutouts located every 5% of blade radius, (or length) beginning inboard at the 30% radial station and extending outboard to the 90% radial station. These cutouts provide a mounting area for the insertable non-structural masses. The masses were made from tungsten (0.27 lbs) and steel (0.11 lbs) to provide an additional parameter of study. Throughout testing, only one mass was inserted in the spar at a time providing a local change in the mass distribution.
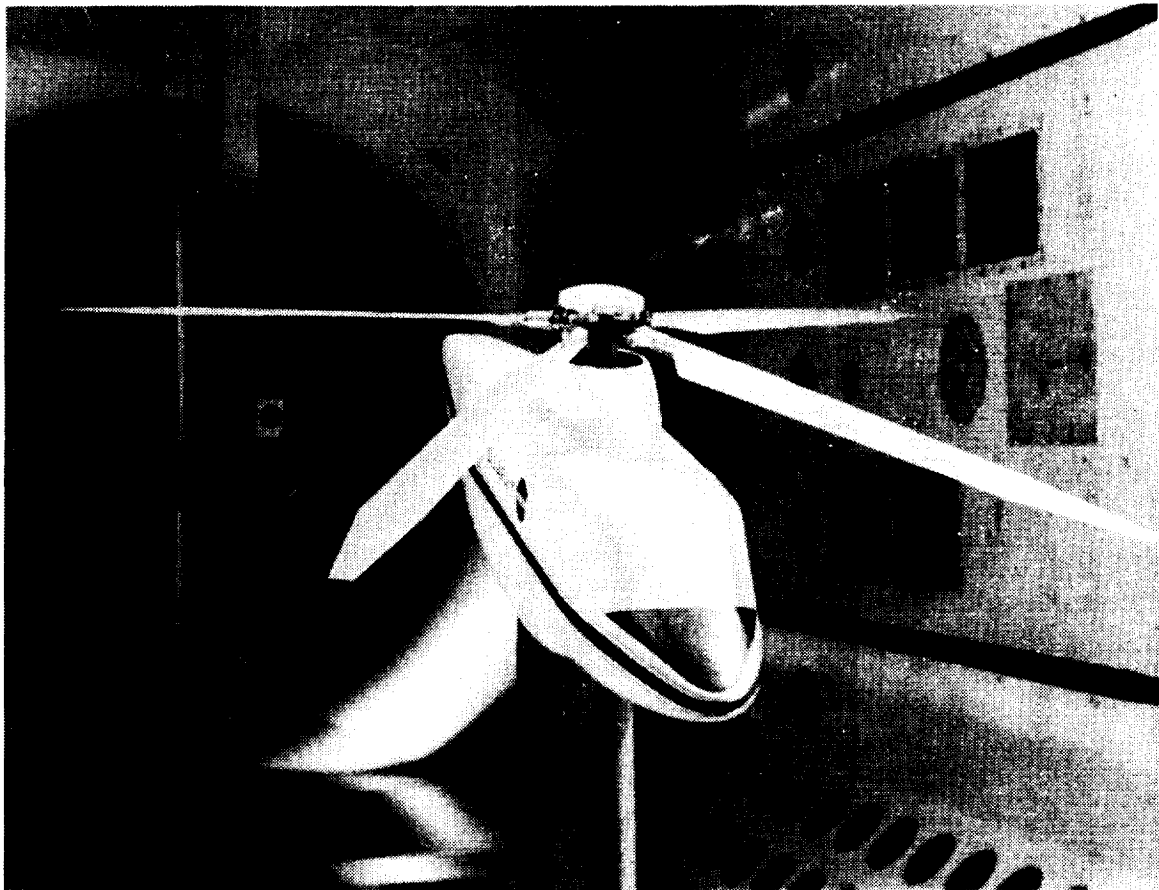
Testing of the GBH-T rotor blades was conducted on the ARES model in the TDT. The photograph shows the model as tested. Configurations tested include the baseline configuration in which none of the insertable masses were installed. Also tested were several configurations in which a single tungsten mass was installed. These configurations ranged from a mass installed at the 30% radial station to the 85% radial station. Finally, one configuration was tested in which a single steel mass was inserted at the 80% radial station.

The testing was comprised of sensitivity studies. Measurements provide vibration sensitivities due to the forward flight velocity, the radial mass placement, the rotor thrust condition, and the rotor trim condition.

WIND TUNNEL TEST

- Configurations tested

  - Baseline rotor (no insertable masses installed)

  - Single tungsten mass (0.00838 slugs / 0.27 lbs) from 30% radius to 85% radius

  - Single steel mass (0.00342 slugs / 0.11 lbs) at 80% radius

- Sensitivity studies

  - Flight velocity

  - Radial mass placement

  - Thrust condition

  - Trim condition

94

C-2

Fixed—System Loads vs. Velocity
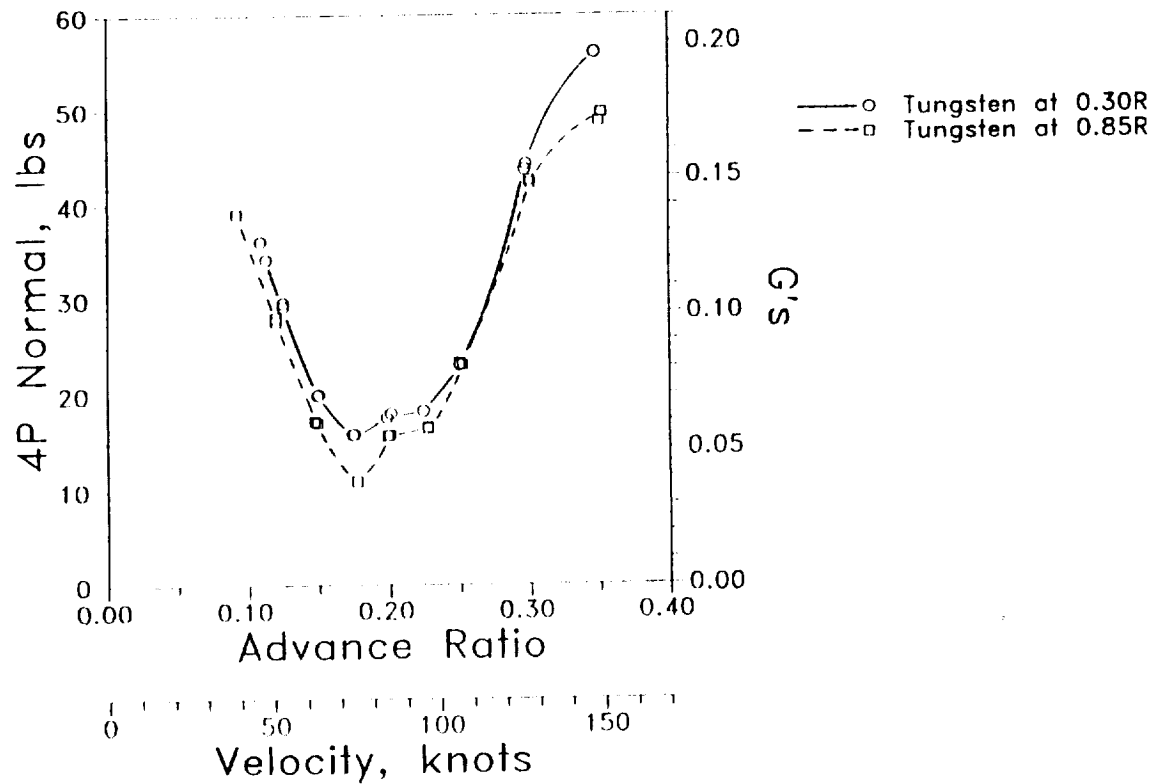
The figure shows results for two of the configurations throughout the forward flight speed range. Plotted is the 4 per revolution load in the fixed-system Normal direction (the direction along the rotor shaft or thrust axis) versus rotor advance ratio. Also shown is the equivalent full-scale flight velocity and the magnitude of the 4P vibration in g's. The data show that the configuration in which a tungsten mass was placed at the 85% radial station results in lower vibrations than the configuration in which a tungsten mass was placed at the 30% radial station. It is useful, however, to look at many configurations at one time. To do so requires a look at a cross-section of the data at individual forward flight velocities. Three sets of forward flight data (denoted by speed as low, mid, and high) will be examined more closely.

Fixed-System Loads vs. Mass Radial Location
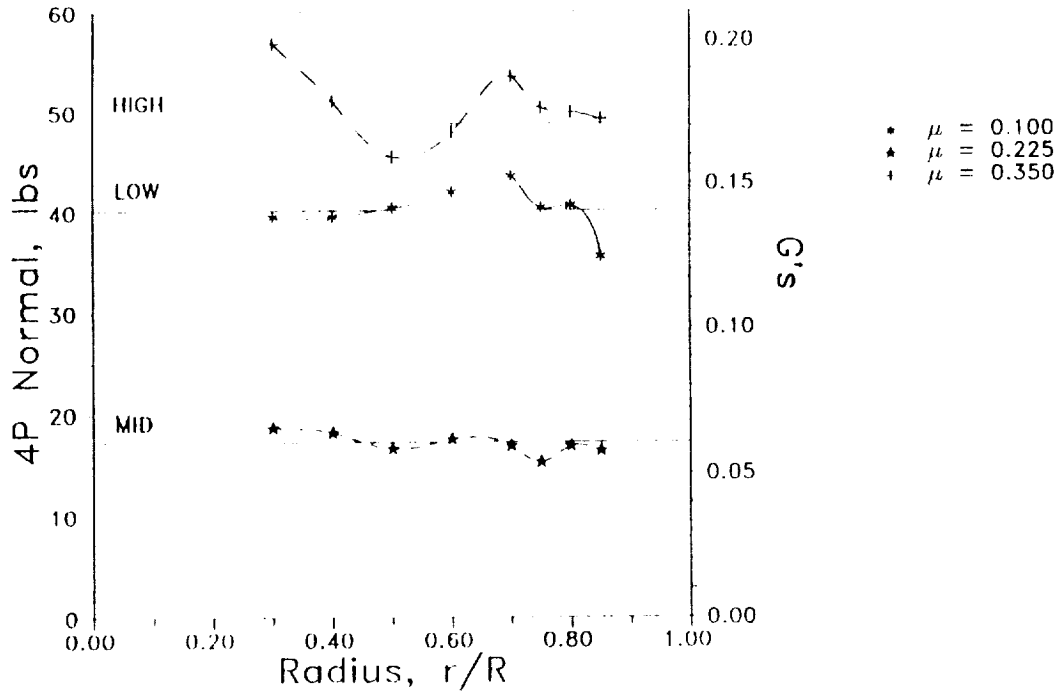
This figure shows the 4P Normal load plotted versus the radial location of an added tungsten mass. Results are shown for the three forward flight velocities denoted on the previous figure. The horizontal lines represent the vibratory load generated by the baseline configuration (the configuration without any insertable masses installed). As is shown, the mass placement has a substantial effect on the fixed-system loads at the low and high speeds. The mid-range speed shows little sensitivity to mass placement, however, the load levels are already quite low at this speed. The data also show that for the GBH-T rotor, different mass locations are required to minimize the vibrations between the low and high speeds.

SIGNIFICANCE

- **Only comprehensive study available**
- **Analysis validation / development**
    - **CAMRAD -- Government owned helicopter code**
- **Optimization efforts**
- **Industry**

The data base generated by the GBH-T research program is the only comprehensive study of its kind available in the public domain. The data base will be used for analysis validation, correlation, and development. Within the Government, it will be used to correlate with the Comprehensive Analytical Method for Rotorcraft Aerodynamics and Dynamics (CAMRAD), a government owned and developed rotorcraft analysis, and to compare with rotorcraft optimization efforts. It is also expected to be used within the rotorcraft industry for comparison with proprietary analyses.

97

SUMMARY

- Tailoring blade mass distribution is a passive means of reducing fixed-system loads

- TDT test has provided a data base for use with analysis development and validation

- Test indicates that mass distribution must be tailored to suit vibration requirements

In conclusion, the Tailored Growth Black Hawk (GBH-T) rotor program has shown that tailoring the blade mass distribution is an effective passive means of reducing rotorcraft fixed-system loads. The test has provided a data base to be used in the correlation, development, and validation of rotorcraft analytical methods. Finally, the results show that the GBH-T rotor would require tailoring specifically intended for reducing the vibrations for a particular flight velocity and that no one mass location can provide reduced vibrations throughout the flight envelope.

98

A PRELIMINARY STUDY TO DETERMINE THE EFFECTS OF TIP GEOMETRY

ON THE FLUTTER OF AFT SWEPT WINGS

Bryan E. Dansberry, José A. Rivera, Jr., and Moses G. Farmer
NASA Langley Research Center
Hampton, VA

99

OUTLINE:

* **Background Information**

* **Objective**

* **Approach**

* **Test Procedure**

* **Results**

* **Comments**

This talk will cover the points shown in the figure. First, background information concerning the study will be covered. That will lead into a definition of the main objective of the study and the approach taken. At this point, a technique typically used in the Transonic Dynamics Tunnel (TDT) to define a flutter boundary will be discussed. A presentation of the results will follow and, finally, summary comments concerning the study will be presented.

OBJECTIVE:

* **Add To The Parametric Data Base**

APPROACH:

* **Test 6 Flat-plate Models**

* **Two Aspect Ratios**

* **3 Tip-chord Orientations**
    - **Parallel To The Root Chord**
    - **Perpendicular To The Mid-chord**
    - **Perpendicular To The Root Chord**

The basic aerospace design practice which led to this study can be stated as: the continued efforts of engineers to maximize the aerodynamic and structural efficiency of new aircraft designs by employing new and novel aerodynamic and structural concepts will often lead to unconventional geometric configurations which may have serious aeroelastic deficiencies. Many of the new configurations which have recently been in the public eye have unusual tip geometries.

A search of reference material produced very little in the way of parametric data on the effect of tip geometry changes on flutter. The basic objective of this study, therefore, was to add to the parametric studies data base some information concerning the effect of tip-chord orientation on wing flutter. To achieve this end, six flat-plate models were tested in the TDT. The models were made from quarter-inch aluminum sheet and were instrumented with strain guage bridges so that flutter frequency could be defined as the flutter boundary was experimentally determined. Flutter characteristics of these models were defined in the Mach number range from 0.3 to 1.2.
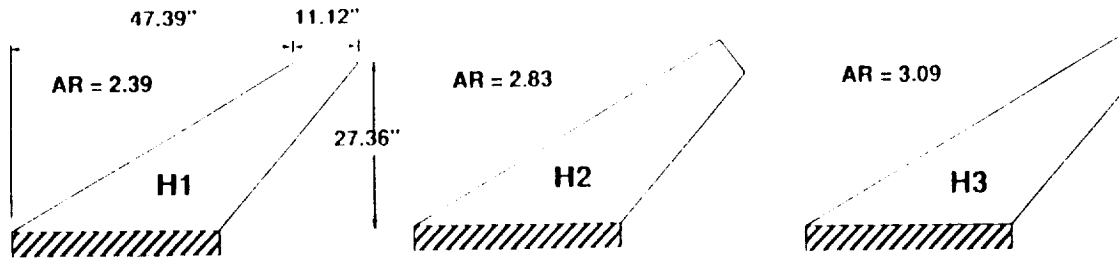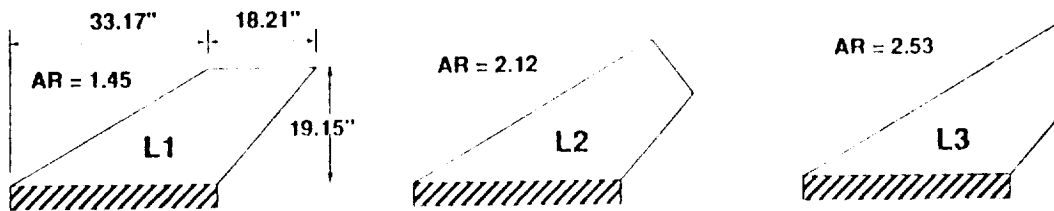
H-SERIES   L-SERIES
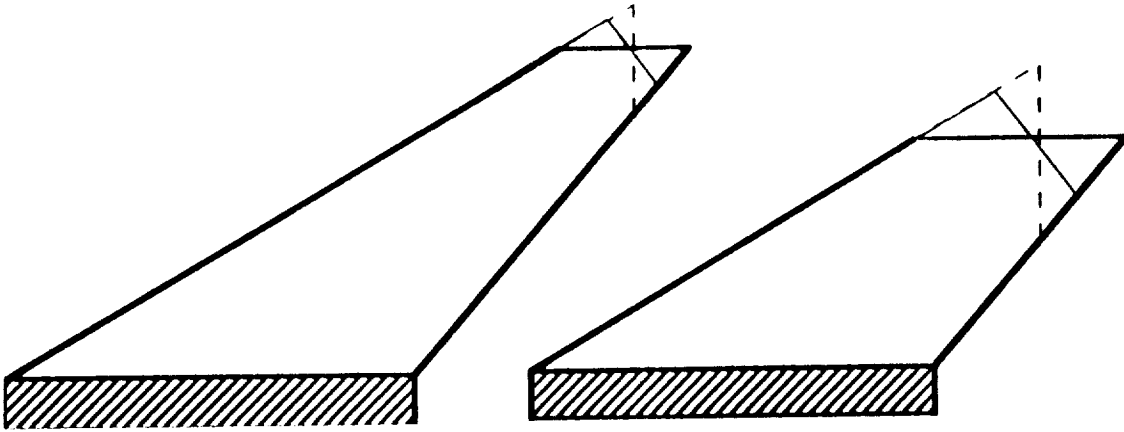
These six models were divided into two series of three models each. These series were identified as the H-series and the L-series for higher-aspect-ratio series and lower-aspect-ratio series, respectively. As can be seen in the above figure, the aspect ratio was the primary difference between the series. This figure also illustrates the primary variable within each series, tip chord orientation. Three orientations were tested in both series. The first was streamwise, or parallel to the root chord, the second was perpendicular to the model mid-chord line, and the third was perpendicular to the root chord or 90 degrees from streamwise.

H-SERIES MODELS

H SERIES GEOMETRIC CONSTANTS:
planform area = 627.5 sq. in.

L-SERIES MODELS

L SERIES GEOMETRIC CONSTANTS:
planform area = 507.1 sq. in.
root chord   = 34.75 in.
leading edge sweep = 60 deg.
trailing edge sweep = 41 deg.

Within each series, planform variables such as leading edge sweep, trailing edge sweep, and root chord length were held constant. Planform area was also a constant for each series. The planform area of the L-series was 20 percent less than that of the H-series. The rectangular area at the root of each wing, denoted by slashes in the figure, was the mounting tab. When mounted in the wind-tunnel test section, the tab was sandwiched between two angle irons to provide a fixed-root, cantilevered condition. The entire mounting apparatus was separated from the free-stream flow by a splitter plate.

103

First Five Measured Natural Frequencies
(Hz)

	H1	H2	H3	L1	L2	L3
f_1	4.4	4.1	4.1	8.0	8.1	7.8
f_2	16.7	17.1	17.4	23.0	25.0	27.8
f_3	28.8	27.2	26.4	51.0	44.1	40.5
f_4	40.0	42.0	42.8	54.2	62.5	61.1
f_5	62.4	63.6	61.2	87.1	99.6	97.4

The next two figures show the experimentally defined vibrational characteristics of the six models as determined by ground vibration tests performed prior to flutter testing. The major point to be made here is that although the geometric variable has been well isolated, no attempt was made to hold constant the vibrational characteristics of the models within either series. Therefore, the test results represent integrated aerodynamic and structural effects. The above figure shows the fundamental frequencies of the six models. Note that the characteristic frequencies of the high-aspect-ratio series models are fairly constant while the L-series shows larger deviations between models.
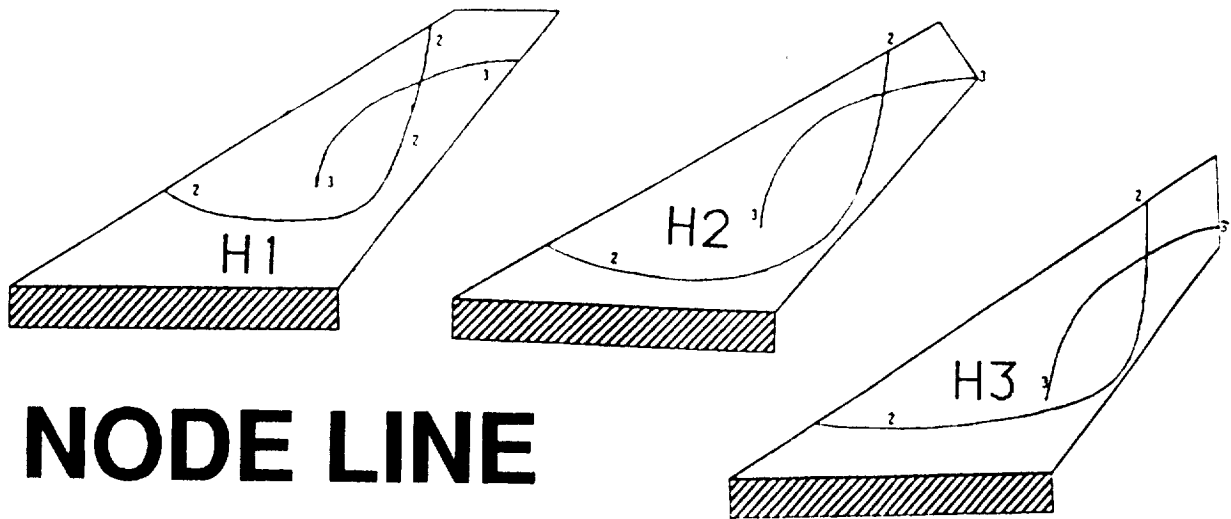
NODE LINE PLOTS
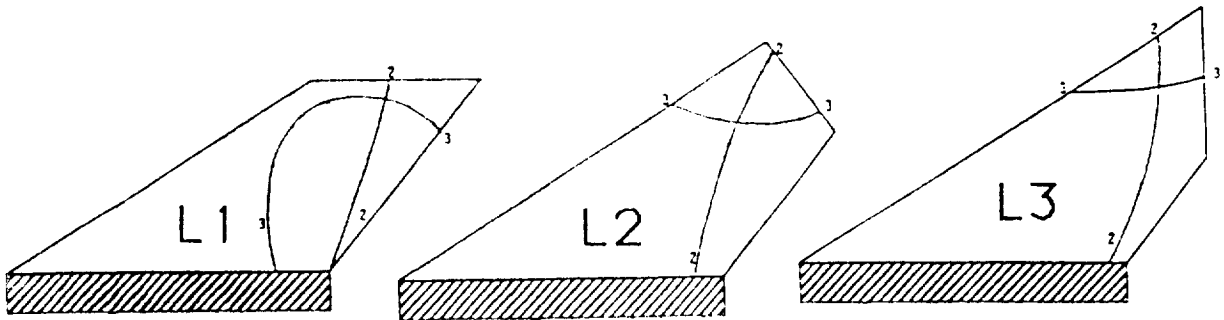
Reflecting the results shown in the previous figure, the node lines of the second and third models are of similar character for all three H-series models while the lower-aspect-ratio models show much greater deviations. This is likely due to the fact that the changes in tip geometry effect a larger portion of the total area of the L-series models.

The above figure shows a picture of model H1 mounted in the TDT. A splitter plate was located along the root chord of the models. The splitter plate served to separate the mounted hardware from the free-stream flow and also prevented the tunnel-wall boundary layer from affecting the results. Although it is difficult to see in this picture, aerodynamic trip strips were placed on both surfaces of the models to better simulate Reynolds number effects. These strips ran from root to tip on every model.

Test Procedure Used In TDT To Determine Typical Flutter Boundary.
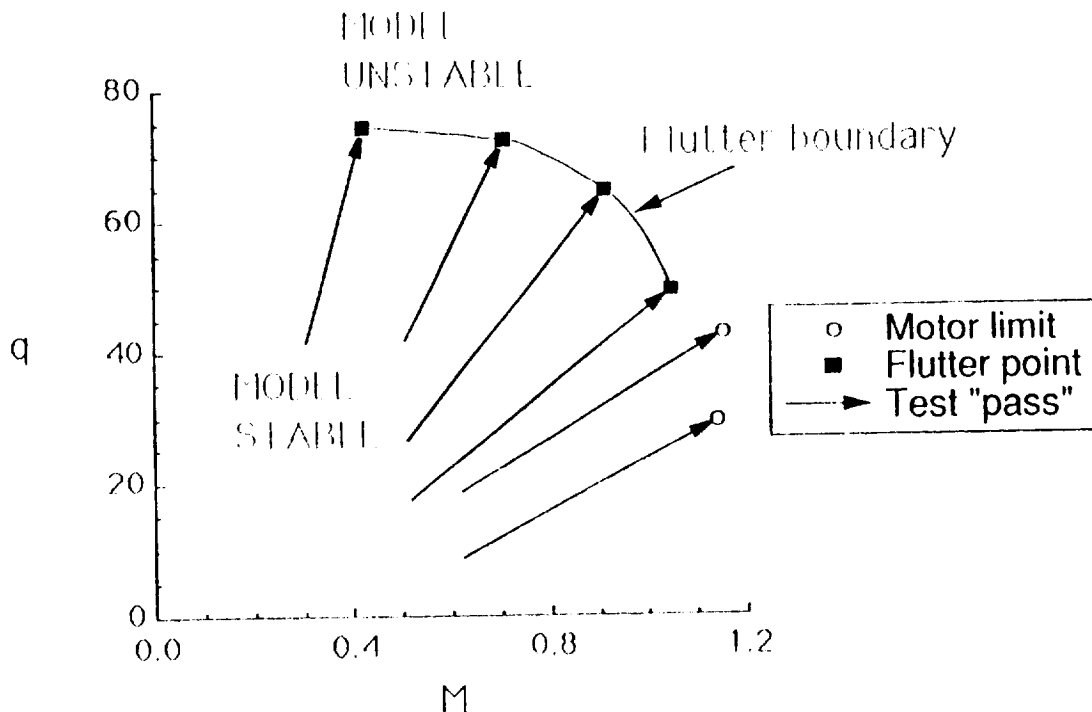
The method typically used in the TDT to define a flutter boundary is illustrated above. This figure shows a plot of the variation of dynamic pressure (q) at flutter onset versus Mach number for a model with a typical flutter boundary. The solid lines with arrows at the end represent lines of nearly constant total pressure. The TDT is a variable density tunnel, making it advantageous to initiate testing at a lower density (therefore a lower total pressure line) than where flutter is expected. As the test progresses the motor speed of the tunnel is slowly increased, enchancing flow conditions along a line of constant pressure until either the motor limit is reached (the open symbols) or a flutter condition is identified (the solid symbols). At this point motor speed is reduced, decreasing Mach and q to a safe level. Air is then bled into the tunnel increasing total pressure and density and the process is repeated along higher total pressure lines until the flutter boundary is satisfactorily defined.

107
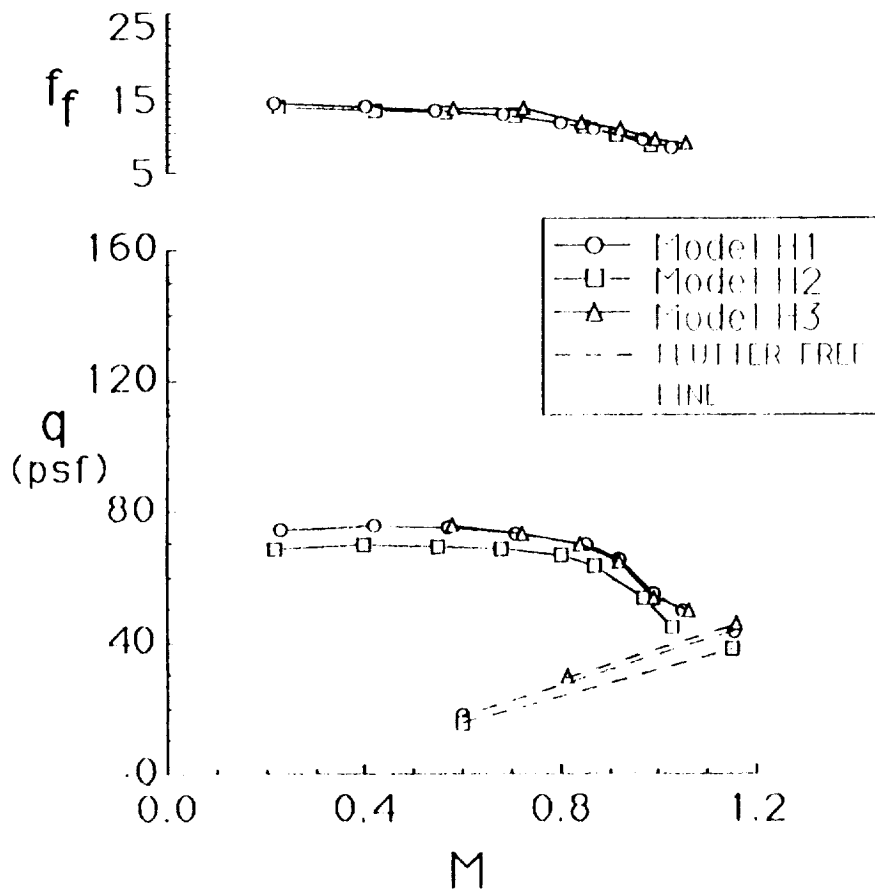
The above figure shows the flutter characteristics of the higher-aspect-ratio series of models. Again, the variation of flutter q with Mach number is shown. The variation of flutter frequency with Mach number is also displayed. For all six models, the flutter frequency at all conditions was between the first bending and first torsion frequencies. This indicates that the flutter mechanism for all models was a coupling of the bending and torsion modes, the most common mechanism of flutter.
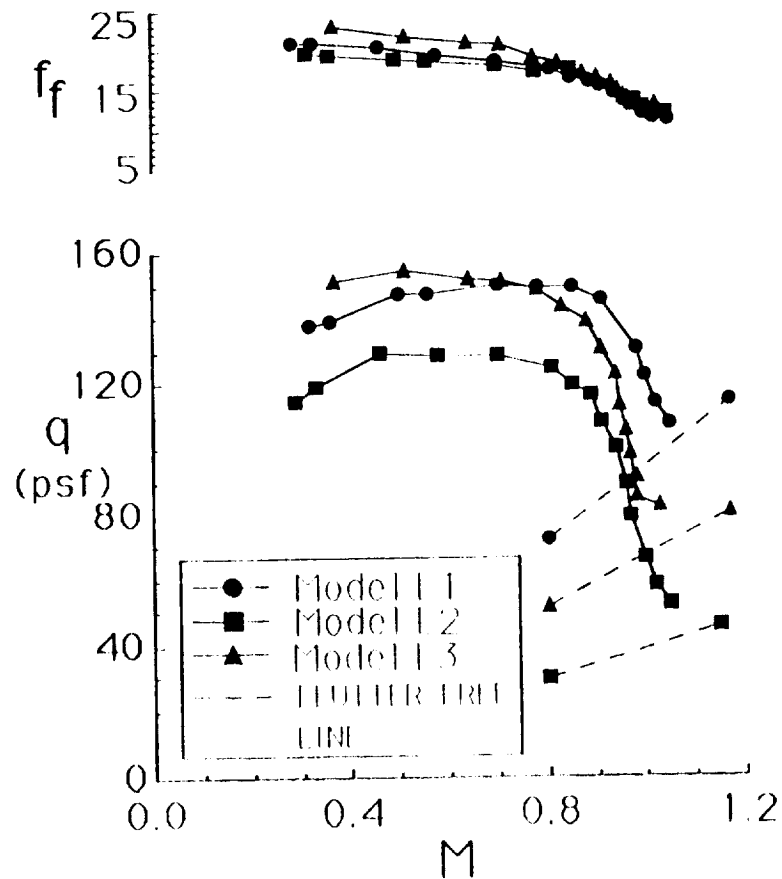
The above figure, with axes identical to the previous figure, shows the flutter characteristics of the lower-aspect-ratio series models. The dashed lines shown in the two previous figures indicate total pressure lines at which flutter was not found. These dashed lines are included to indicate that the flutter boundaries of these models do not continue their downward trend, but turn up as they enter the supersonic regime.

FLUTTER CHARACTERISTICS OF ALL MODELS IN AIR.
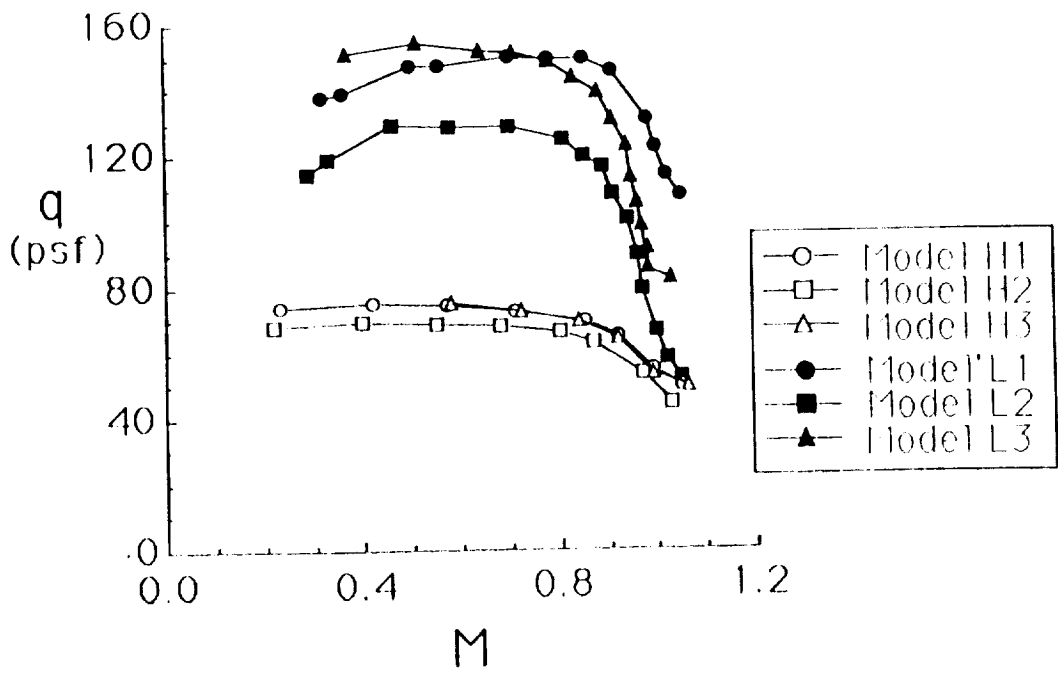
The above figure is a composite of data from the two previous figures. Only the six experimentally determined flutter boundaries are shown. Once again, the figure shows the variation of dynamic pressure at flutter onset with Mach number. The open symbols represent the higher-aspect-ratio (H-series) models and the dark symbols represent the lower-aspect-ratio (L-series) models. The circles represent models with "standard" streamwise wing tips, the squares represent models with tip chord oriented perpendicular to the mid-chord line, and the triangles represent models with a tip oriented perpendicular to the root chord.

The most obvious characteristic of the data is that the lower-aspect-ratio models all have a higher flutter q than the higher-aspect-ratio models. That is to be expected because a reduction in aspect ratio usually results in an increase in flutter q. It is somewhat surprising that all the L-series models have a very pronounced transonic dip which eliminates much of the gain in flutter q observed in the subsonic region.

Another feature of the data is that the bottom of the transonic dip was above M=1 in all cases. However, this is not unusual for highly swept wings.

(Continued on next page)

A third feature is the homogeneous nature of the H-series results as compared to the L-series. All three boundaries for the H-series are similar in shape and nearly lie on top of each other. The L-series models display a much greater sensitivity to changes in tip geometry. This is probably a reflection of the greater disparity in vibrational characteristics within the L-series of models.

Another point of interest is the trend measured for the two models represented by square symbols. These are the models whose tip chord was oriented perpendicular to the mid-chord line of the wing. These models both display lower flutter boundaries than the other models in their series. In other words, this tip orientation appears to adversely affect the flutter characteristics of the configurations tested in this study. Further investigation would be required prior to making more substantial conclusions concerning the wing tip shape.

SUMMARY:

* 6 Flat-Plate Models Tested

* Integrated Aerodynamic And Structural Effects Determined

* Results Showed:

    - L-series Show Greater Variation Of Results
    - Flutter q Varies Inversely With AR In Subsonic Region
    - Tip Orientation Perpendicular To Mid-chord Had
      Lowest Flutter q

To summarize, a study was performed in the TDT which provided some preliminary insight into the effects tip geometry changes can have on the flutter of swept and tapered wings. The results shown represent the integrated aerodynamic and structural effects of changing tip geometry for six flat-plate wing-models. The results indicated that in the subsonic region, a decrease in aspect ratio produces a large increase in flutter q. In the transonic region, however, this increase in q was largely negated by an unusually deep transonic dip for the lower-aspect-ratio wings. Also, the lower-aspect-ratio series of models displayed a greater sensitivity to the changes in tip geometry. Finally, the models with tip chords oriented perpendicular to the wing mid-chord line had the lowest flutter boundaries. Further work is required before any strong conclusions can be reached.

AEROELASTIC MODELS PROGRAM

Clinton V. Eckstrom
NASA Langley Research Center
Hampton, VA

OUTLINE

- **Background**

- **Objectives**

- **Approach**

- **Status**

- **Models**

- **Summary**

OUTLINE (**Slide 2**):

This slide presents a brief outline of the presentation. The presentation begins with a brief background on the Aeroelastic Models Program which includes a description of some of the aeroelastic challenges to be worked. The program objectives are then defined along with our approach to meeting these objectives and our current status. This is followed by a description of what models we are currently working with followed by a brief summary.
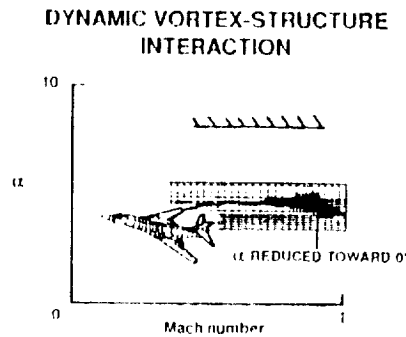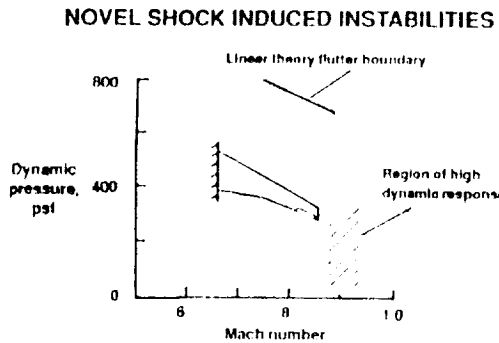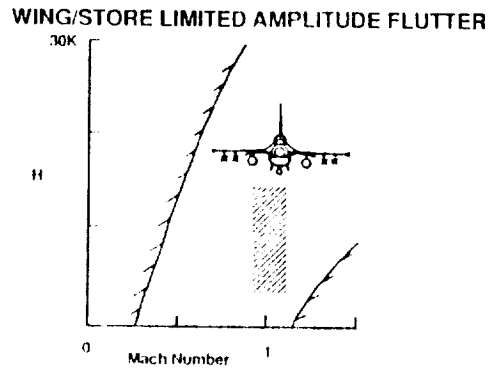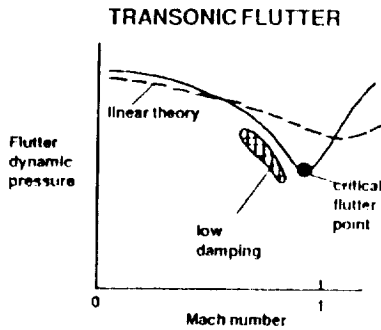
BACKGROUND

- Wind tunnel model measurements needed for Development / Validation of analysis programs

- "Aeroelastic Models Program" proposed

- Joint activity between CAB and UAB

- Program aimed at some specific aeroelastic challenges

BACKGROUND (**Slide 3**):

The development of CFD codes often requires experimental data to check and validate the analysis results. In some instances experimental results may be required to assure that the right types of flow phenomena are being modeled. This type of model test data is used in the Structural Dynamics Division by the Unsteady Aerodynamics Branch (UAB) for validation of codes such as the CAP-TSD code.

As a result of the need for code validation data an "Aeroelastic Models Program" was proposed by a committee set up by the Structural Dynamics Division Office. Bob Bennett of UAB chaired that committee. For this reason it is not unexpected that implementation of the program is a joint CAB and UAB activity. The proposed program is aimed at several specific aeroelastic challenges, four of which are presented on the next slide.

115

AEROELASTICITY CHALLENGES

TRANSONIC FLUTTER

WING/STORE LIMITED AMPLITUDE FLUTTER

NOVEL SHOCK INDUCED INSTABILITIES

DYNAMIC VORTEX-STRUCTURE INTERACTION

AEROELASTICITY CHALLENGES (**Slide 4**):

The first example aeroelastic challenge deals with transonic flutter. The plot, which presents a dynamic pressure flutter boundary as a function of Mach number, shows results for both experiment and analysis. The minimum or critical flutter point noted on the figure is at the bottom of the flutter dip at the transonic speed range. Analysis results normally do not accurately predict experimental results in this region. **Slide 5** shows a typical cantilevered model that might experience such a transonic dip in the experimentally determined flutter boundary.

The second example aeroelastic challenge deals with wing/store limited amplitude flutter. The plot, which presents flight altitude as a function of Mach number for a fighter aircraft, shows upper and lower speed boundaries and a cross hatched area in the transonic speed range where limit cycle wing/store instabilities can occur. **Slide 6** shows a fighter model with stores used for store flutter clearance testing.

The **third** example challenge deals with novel shock induced instabilities such as one experienced on a high aspect ratio transport type wing. The plot, which presents dynamic pressure as a function of Mach number, shows a region of wing high dynamic response at transonic speed, but at dynamic pressures well below the predicted flutter boundary. **Slide 7** shows the wing on which the instability was measured.

The **fourth** example challenge deals with a wing response encountered on the B-1 aircraft that is now attributed to a dynamic vortex-structure interaction. The plot, which presents angle of attack as a function of Mach number shows a trace of wing response measured during flight testing. At the initial flight angle of attack the wing response increases in amplitude until angle of attack is reduced toward zero degrees. **Slide 8** shows the B-1 flutter model being tested in the TDT.
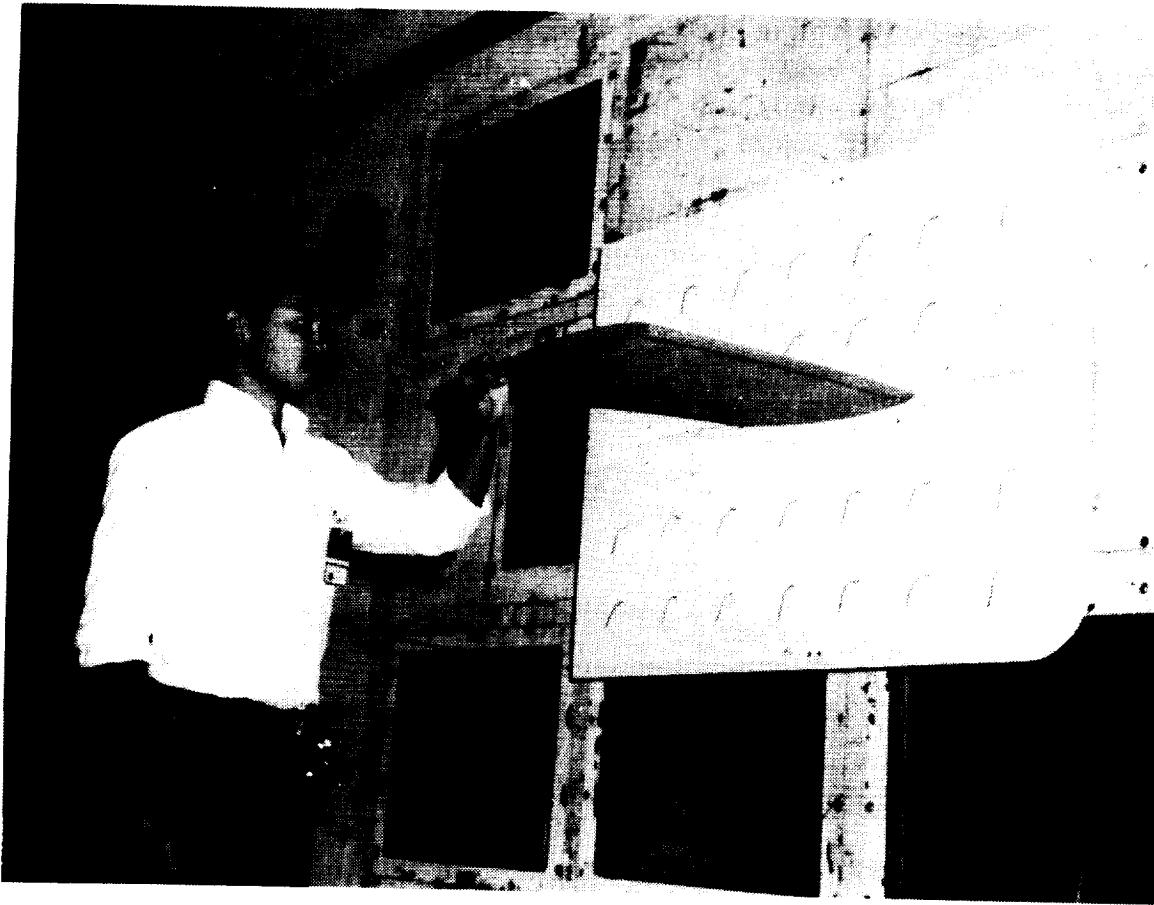
TYPICAL CANTILEVERED MODEL (Slide 5):

The flexible rectangular wing model shown is typical of those used to define flutter boundary characteristics. The model is cantilevered from a splitter plate mounted off the tunnel wall to eliminate wall boundary layer effects. These models are typically instrumented with a bending and a torsion strain gage bridge located near the wing root to monitor wing motion for determination of flutter onset.
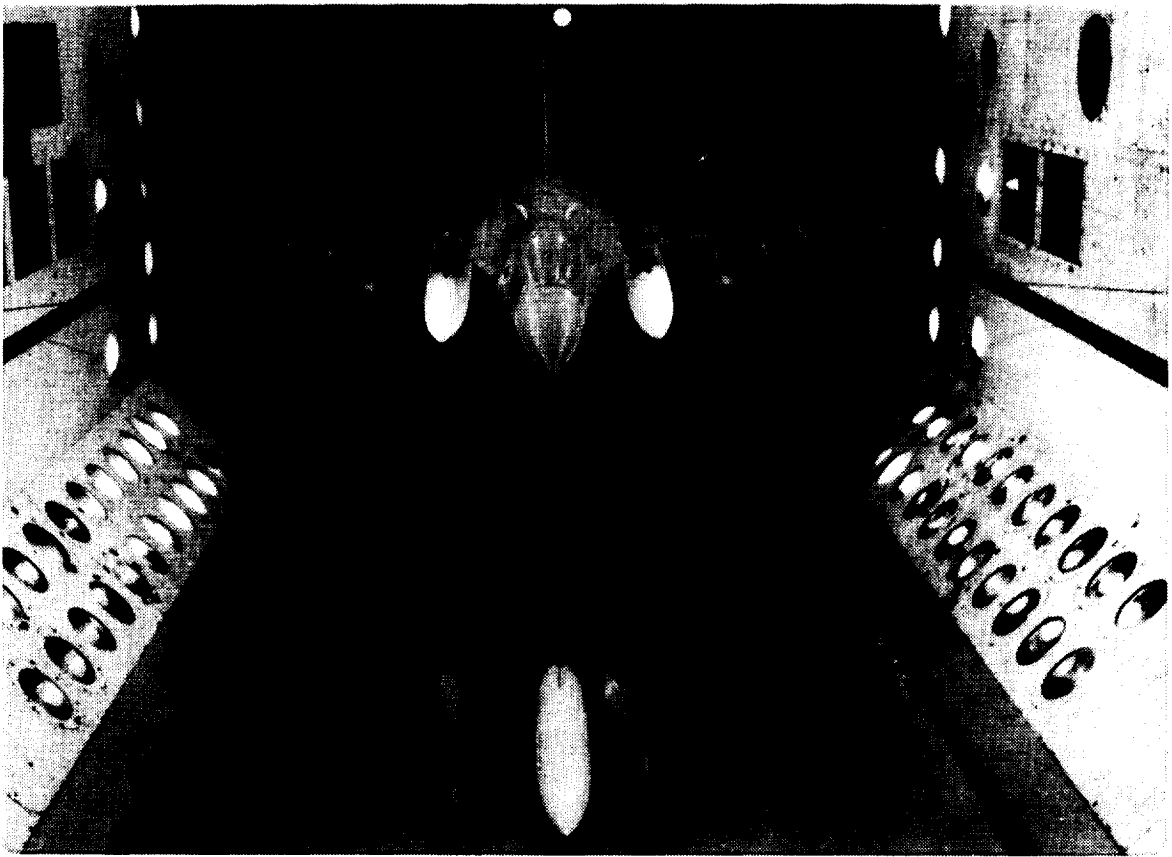
F-16   FIGHTER

F-16 FIGHTER WITH STORES (Slide 6):
     An F-16 fighter flutter model is shown in the Transonic Dynamics Tunnel with three different store types suspended from the wing. Also shown on the tunnel floor are several other store types that are used in various combinations with this fighter aircraft. From the variety of store shapes and sizes, and fin locations and sizes, it is not hard to imagine that some flow instabilities might occur to cause limit cycle oscillation.

DAST ARW-2 WING (**Slide 7**)

The DAST ARW-2 is a high aspect ratio (10.3) transport-type wing. During unsteady pressure measurement tests the unexpected region of high dynamic response was encountered at transonic conditions.

B-1 SHOCK-INDUCED INSTABILITY STUDIED IN TDT
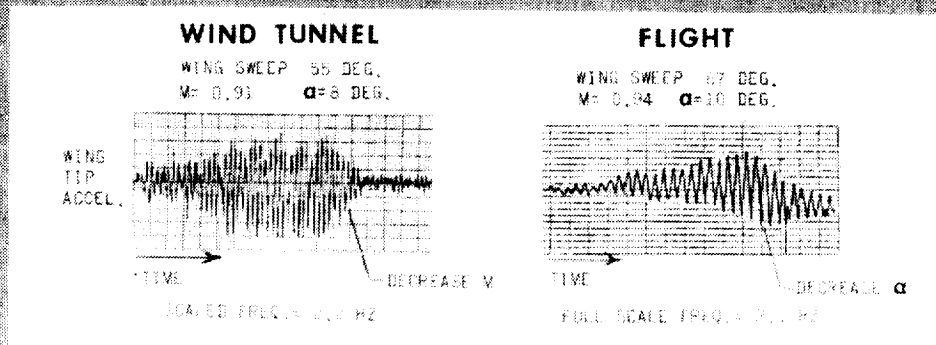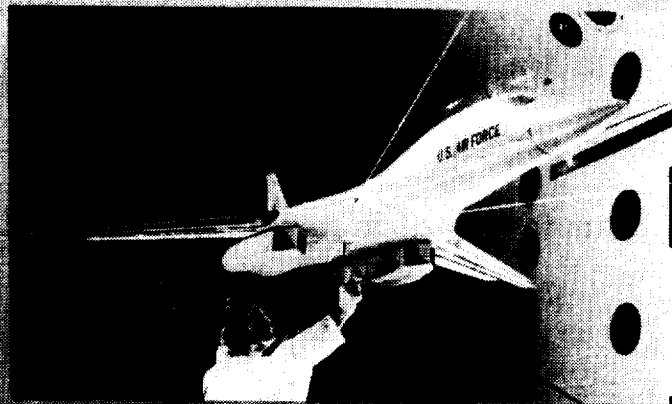
B-1 FLUTTER MODEL (Slide 8)

The B-1 flutter model was tested in the TDT to see if the instability encountered in flight could be reproduced during wind tunnel testing. The wing responses measured in the tunnel test and in flight are shown for comparison. At the time the wind tunnel test was conducted the instability was thought to be shock-induced as indicated by the figure title. It was later considered to more likely be a vortex interaction problem. The Aeroelastic Models Program proposes further study of this phenomena using a side wall mounted half-fuselage/wing B-1 model instrumented for measurement of unsteady pressures.

OBJECTIVES

- **Obtain data for code validation / development**

- **Understand physics of unsteady flow**

- **Obtain data for empirical design**

OBJECTIVES (**Slide 9**):

    As indicated earlier, the program's first objective is to acquire data useful for analytical code development and validation. In order to do this it may also be necessary to perform tests aimed primarily at developing an understanding of the unsteady flow phenomena of interest. For some aeroelastic problems it may be necessary to limit our objective to obtaining data for empirical design methods.

APPROACH

- **Design and Build Models**

- **Use Existing Models**

- **Conduct Tests in TDT**

- **Measure Model / Flow Characteristics**
    - **Flutter Boundaries**
    - **Dynamic Responses**
    - **Unsteady Surface Pressures**
    - **Flow Visualization**

APPROACH (Slide 10):

Our approach to the Aeroelastic Models Program is to design and build models for testing or to use existing models where possible. The testing will be conducted in the Transonic Dynamics Tunnel. Our plan is to make extensive measurements of both model and flow characteristics as listed.

123

STATUS

- **Test Program Defined**

- **New Initiative Proposed**

- **Test Group Formed**

- **Model Fabrication Initiated**

STATUS (**Slide 11**):

At present, the Aeroelastic Models Program test plan has been defined as shown on **slide 12** where the planned model types are listed. A new initiative has been proposed to fund and implement the program. A test group has been formed, which as indicated earlier, is a combined effort of CAB and UAB. The test group members are listed on **Slide 13** in alphabetical order. Fabrication activities on two models have been initiated.

PLANNED MODEL TYPES

- Rigid wings on flexible mount system

- Series of flexible wings with circular
  arc airfoils

- Wing canard model

- Fighter wing with stores

- Generic transport model

- Use some existing models with
  modifications

PLANNED MODEL TYPES (**Slide 12**):
 The overall program includes tests of: (1) a series of panel aspect ratio 2.0 rigid airfoils to be tested on a flexible mount system referred to as PAPA (Pitch and Plunge Apparatus), (2) a series of circular arc airfoils having the same aerodynamic shape but with different structural stiffness, (3) a clipped delta wing and canard model, (4) a generic fighter wing to be tested with various store types and combinations, (5) a generic transport model for evaluation of transonic flow conditions, and (6) the use of some existing models such as an instrumented semispan-half fuselage model of the B-1.

TEST GROUP

CAB	UAB
Bryan Dansberry	Robert Bennett
Clinton Eckstrom	David Seidel
Moses Farmer	
Jose Rivera	

TEST GROUP (**Slide** 13):

     The test group consists of members from both the Configuration Aeroelasticity Branch (CAB) and the Unsteady Aerodynamics Branch (UAB). Each test group member will have responsibility for a particular model test with all other members functioning as a part of the test team.

CURRENT MODELS

- **NACA 0012 rigid wing on flexible mount**

- **Flexible wings with circular arc airfoils**

- **Supercritical rigid wing on flexible mount**

- **Delta wing/canard unsteady pressure model**

CURRENT MODELS (**Slide 14**):

Our first model is a NACA 0012 rigid wing to be tested on a flexible mount system. It has been fabricated and is currently being instrumented.

The second model type consists of a series of flexible wings with circular arc airfoils one of which is currently being fabricated. These models will be used for an oscillating shock study as shown on **Slide 15**.

The third model is a supercritical airfoil on a flexible mount similar to the first model. Fabrication of this third model will begin as soon as the validity on the design and layout of the first model is proven by the wind tunnel test scheduled for June.

The fourth model is an existing wing/canard unsteady pressure model as shown on **Slide 16**.

127

CIRCULAR ARC AIRFOIL OSCILLATING SHOCK STUDY

- 18% thick airfoil

- Shock oscillation in
  narrow Mach range

- Shock oscillation 180°
  out-of-phase

- Large pressure
  fluctuations

- Coupling with
  structural modes

Time 1 — Strong Upper Shock — Wake — Weak Lower Shock


Time 2 (Half cycle later) — Weak Upper Shock — Wake — Strong Lower Shock
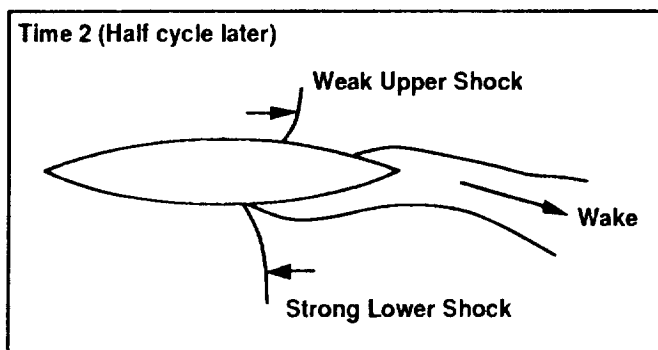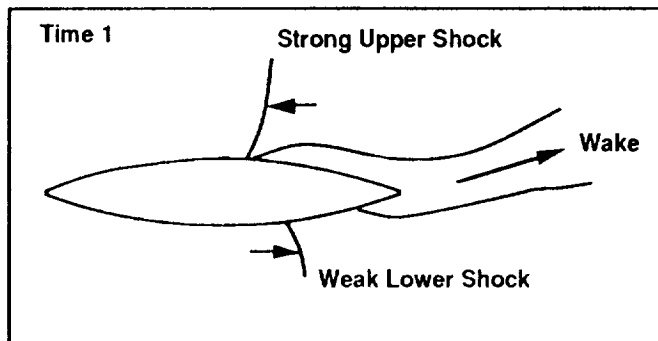
CIRCULAR ARC AIRFOIL OSCILLATING SHOCK STUDY (**Slide 15**):

Tests with rigid circular arc airfoil models have established that an oscillating shock system exists as shown in the sketch for 18% thick circular arc airfoils. Our goal is to determine if, and possibly how, this oscillating shock system might couple with model structural modes. The model currently being fabricated has only strain gage bridge and accelerometer instrumentation to measure model response. If significant structural response occurs, then later models of varying structural stiffness will include a row of pressure transducers to measure unsteady pressures at an outboard spanwise station.

128
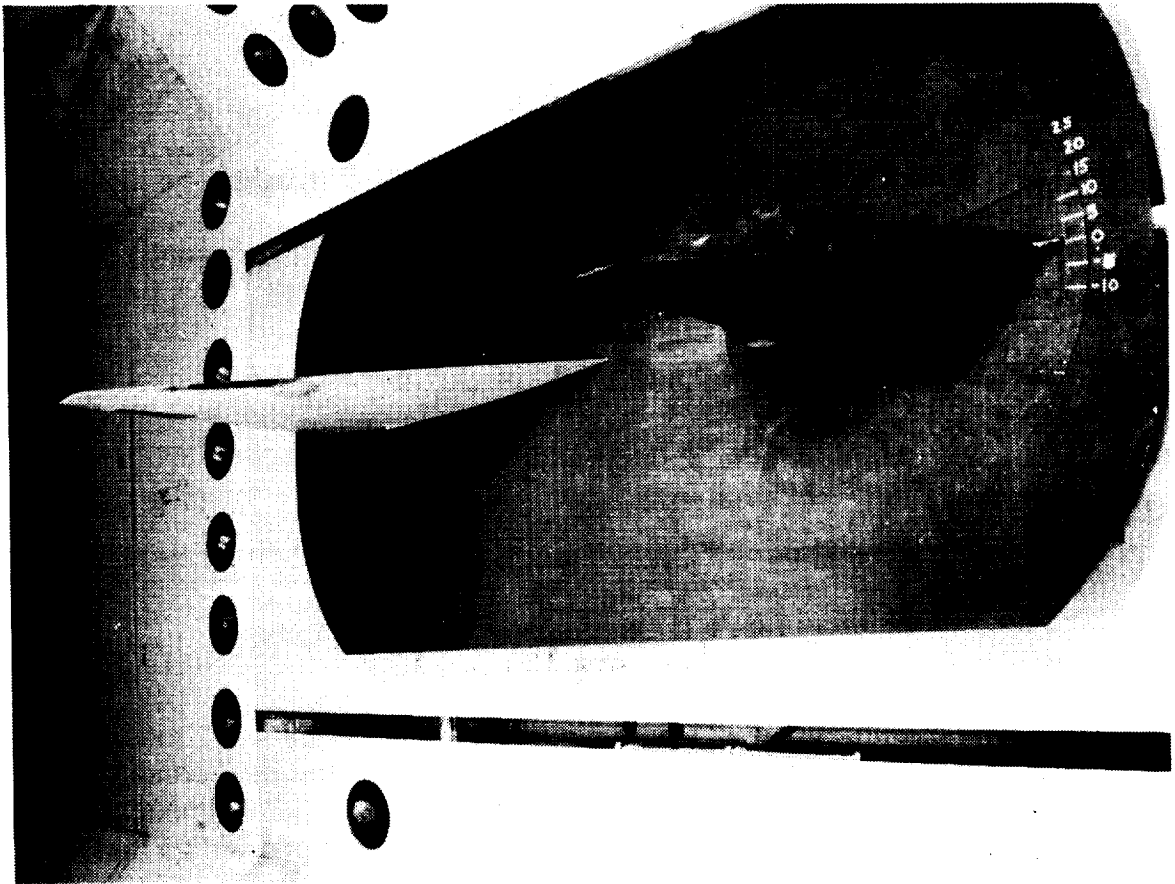
WING/CANARD MODEL (Slide 16):

For this model we need to rebuild the canard to take higher loads. Also both the canard and the wing need to be instrumented with new pressure transducers for measurement of unsteady pressures. The canard is difficult to see as it was painted a flat black the same as the splitter plate to facilitate use of a laser flow visualization system used for this test. The canard is mounted on the shaft of a large hydraulic actuator. The initial pitch angle can be set at varying angles up to 50 degrees and the model can then be oscillated in pitch up to +/-12.5 degrees. Both the wing and the canard have the same planform layout with a 50-degree leading edge sweep and a clipped tip region.

SUMMARY

- **Fabrication completed for NACA 0012 model**

- **First flexible Circular Arc Wing model is being fabricated**

- **Initial tests in TDT to start this June**

SUMMARY **(Slide 17)**:

In summary, fabrication has been completed for the NACA 0012 model. Tony Rivera covers details of this model and its planned testing in the next presentation. The first flexible circular arc airfoil model is being fabricated. It is of simple aluminum plate/balsa wood construction so it will be available very soon and will be tested at the first reasonable opportunity (Model was tested April 12-13, 1990). The first major scheduled test starts in June, 1990, so very quickly the Aeroelastic Models Program will be underway.

NACA 0012 PRESSURE MODEL AND TEST PLAN

José A. Rivera, Jr.
NASA Langley Research Center
Hampton, VA

NACA 0012 PRESSURE MODEL AND TEST PLAN

A description of the NACA 0012 pressure model, the instrumentation, and the plan for a test to be conducted in the Transonic Dynamics Tunnel (TDT), are the subject of this presentation.

In the past steady and unsteady pressures have been measured on rigid oscillating models, such as the rectangular supercritical wing shown in figure 1, and models with oscillating control surfaces as shown in figure 2. In addition, flutter boundaries have been determined for (complex and simple) flexible models. An example of a complex model with nacelles is shown in figure 3. Presently, with the Pitch and Plunge Apparatus (PAPA) figure 4, flutter boundaries can be determined for rigid models because the PAPA allows the degrees of freedom necessary for the instability. The PAPA is a flexible mount system on to which a rigid model can be mounted. The rod system allows the wing model to pitch and plunge. The new direction of this project is to combine a rigid model on a flexible mount with steady and unsteady pressure measurements at various test conditions (including transonic Mach numbers) including flutter. This is planned for June of 1990.

The objective of the wind-tunnel test is to gather both pressure (steady and unsteady) and flutter data for analytical code validation. In addition, the data gathered will add to the understanding of the physics behind the structural dynamic and the aerodynamic interaction associated with flutter and other dynamic instabilities.

To accomplish this a standard symmetric airfoil (NACA 0012) with steady and unsteady pressure measurement capability is mounted on a flexible mount system, or Pitch and Plunge Apparatus (PAPA), in the Langley TDT. Then pressures are

132

measured at various conditions including during flutter.

A photograph of the NACA 0012 pressure model is shown in figure 5. The model has an unswept rectangular planform with a NACA 0012 airfoil section. The wing semi-span measures 32 inches with a chord length of 16 inches.

Figure 6 is a list of instrumentation for the wind-tunnel test. A total of 80 pressure transducers are mounted within the wing model. Forty are located to measure pressures at the 60% span station, and forty to measure pressures at the 95% span station near the wing tip. The location of each pressure transducer along a chord is shown in figure 7.

Figure 8 shows a photograph of the model divided into its three major sections, and photographs showing details of the instrument installation. The upper left photograph shows a pressure transducer, a transducer/sleeve assembly, and the internal face into which this assembly is installed. The pressure transducers are installed within sleeves to facilitate handling. After installation and appropriate sealing, the transducer will sense the pressure at the orifice along the surface of the wing model.

The wing model also has 4 accelerometers situated to identify non-rigid motion of the wing model. The upper right photograph of figure 8 shows an accelerometer and the pocket (close to the trailing edge and wing tip) into which it is installed.

Figure 9 is a photograph of the PAPA rod system mounted in the TDT test section. Flow is essentially towards the reader. The PAPA has 2 strain gage bridges oriented to measure bending and torsional moments from which wing model plunge position and pitch angle can be obtained. In addition the PAPA is instrumented with

133

accelerometers to determine pitch and plunge motion.

The PAPA splitter plate (figure 10) is instrumented with 20 pressure transducers divided in groups of 5 located above, below, in front of and behind the wing model to measure splitter plate pressures. In addition a boundary layer rake is situated above and behind the wing model. This rake includes 10 pressure transducers.

Data obtained during the test will include steady and unsteady pressure measurements at various conditions with the flexible PAPA, and with the PAPA rigidized. In addition, the conventional and stall flutter boundaries will be determined. Pressure measurements will be obtained during and leading up to flutter.

The schedule being worked towards is shown in figure 11. At present (March 1990), pressure transducers are being installed in the wing model, and software is being developed for the wind tunnel test. Instrumentation checkout and ground vibration test will lead up to the wind-tunnel test in June 1990.

In summary, a wing model has been described which will be used for a wind-tunnel test in order to combine a rigid model/flexible mount with unsteady pressure measurements. Also the flutter boundaries for this arrangement will be determined. The test will provide pressure and flutter data for analytical code validation, and to understand the physics behind the structural dynamic and the aerodynamic interactions associated with flutter and other dynamic instabilities. These tests will begin in June 1990.

TRANSONIC PRESSURE DISTRIBUTIONS MEASURED
ON A RECTANGULAR SUPERCRITICAL WING
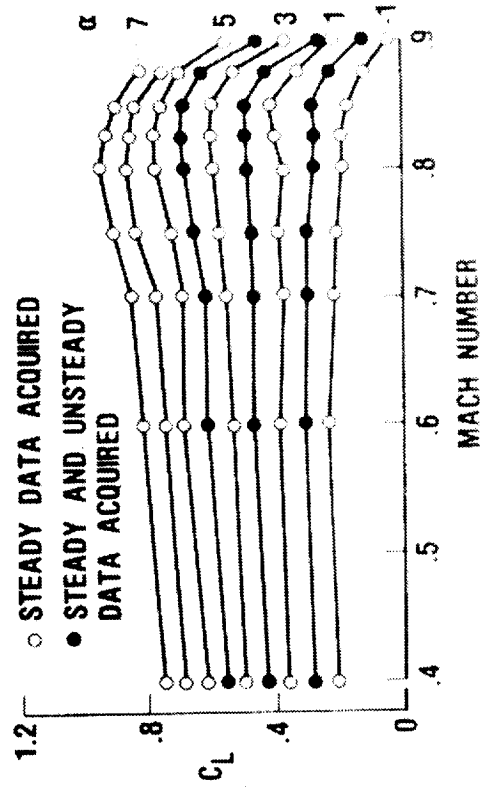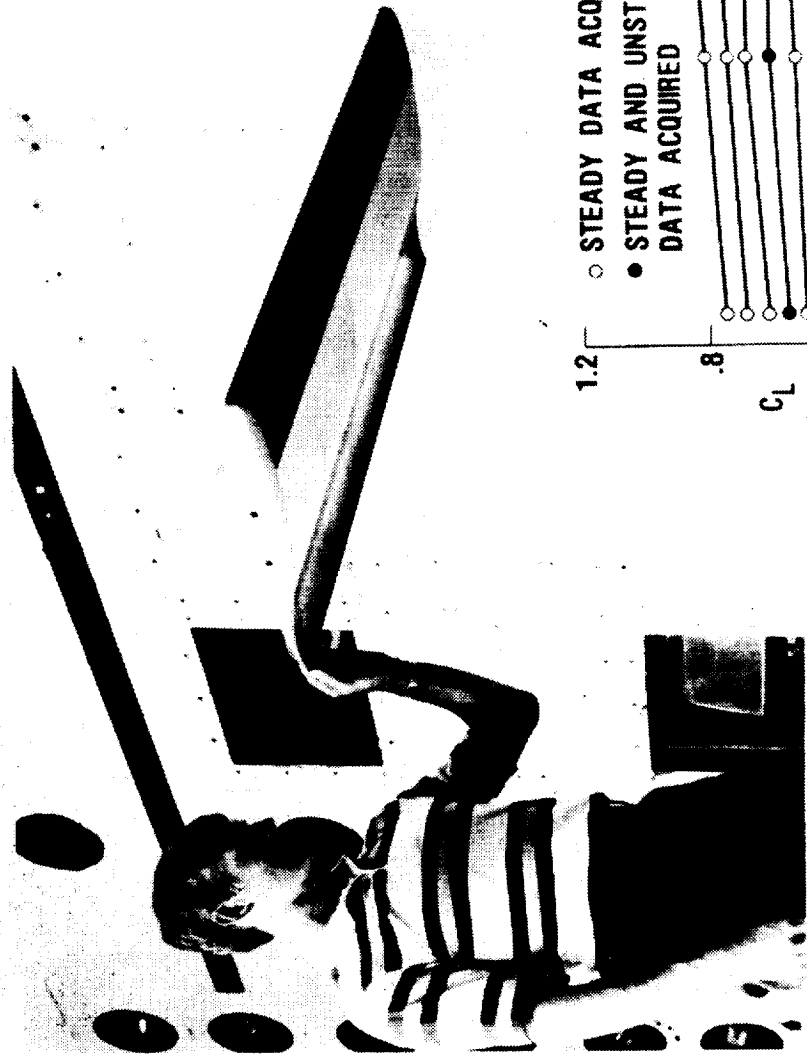### OSCILLATING IN PITCH

Figure 1 - The rectangular supercritical wing mounted in the TDT.

135

TRANSONIC AIRLOADS MEASURED ON SUPERCRITICAL WING WITH OSCILLATING CONTROLS
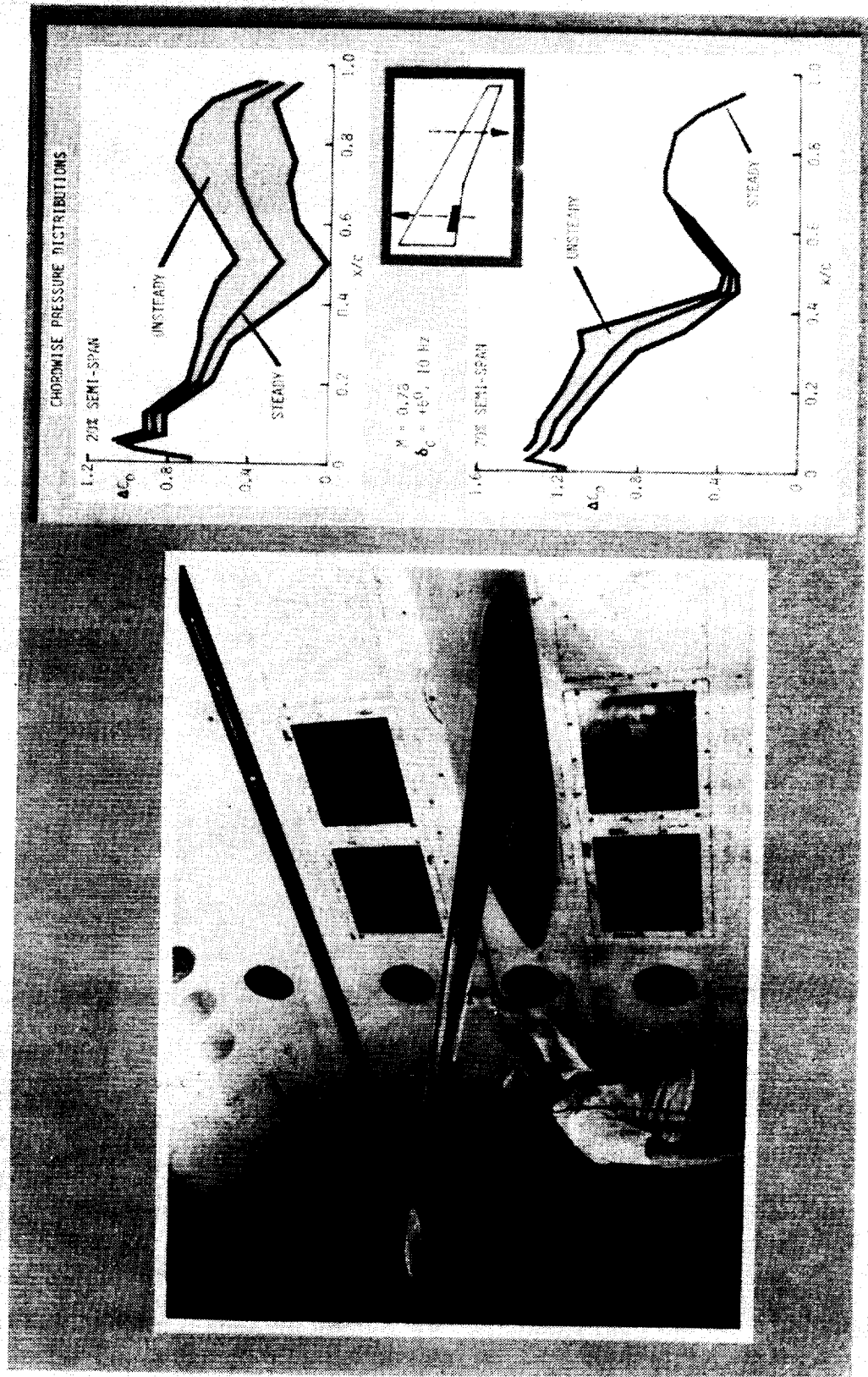
Figure 2 - A model with oscillating control surfaces that was tested in the TDT.

NASA
L-79-5291
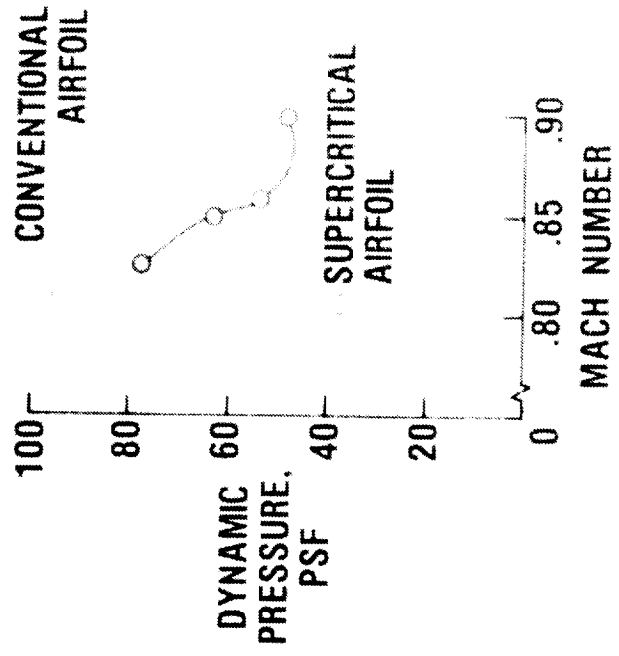
Figure 3 - An example of a complex flutter model and test results.

PAPA -- A NEW WIND TUNNEL MOUNT SYSTEM FOR FLUTTER RESEARCH
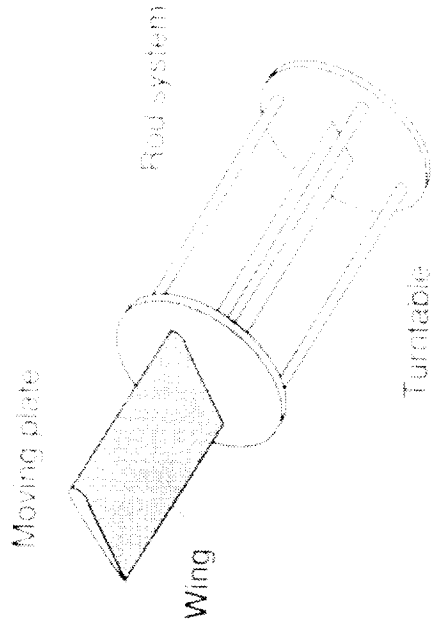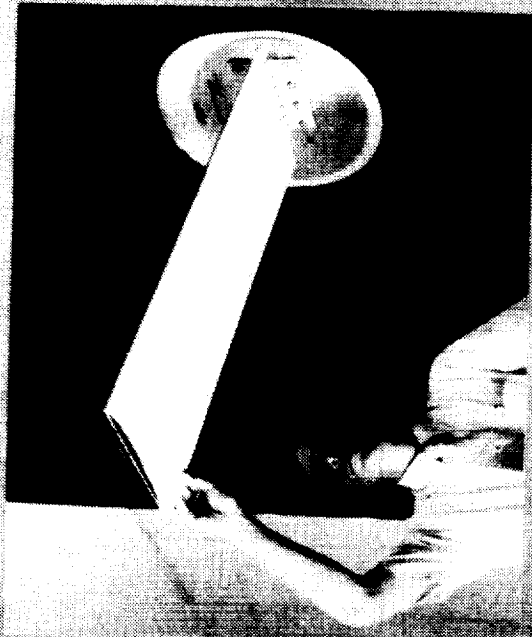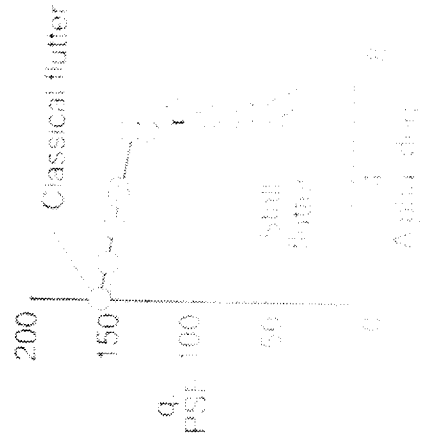
Figure 4 - The PAPA mount system and early test results.
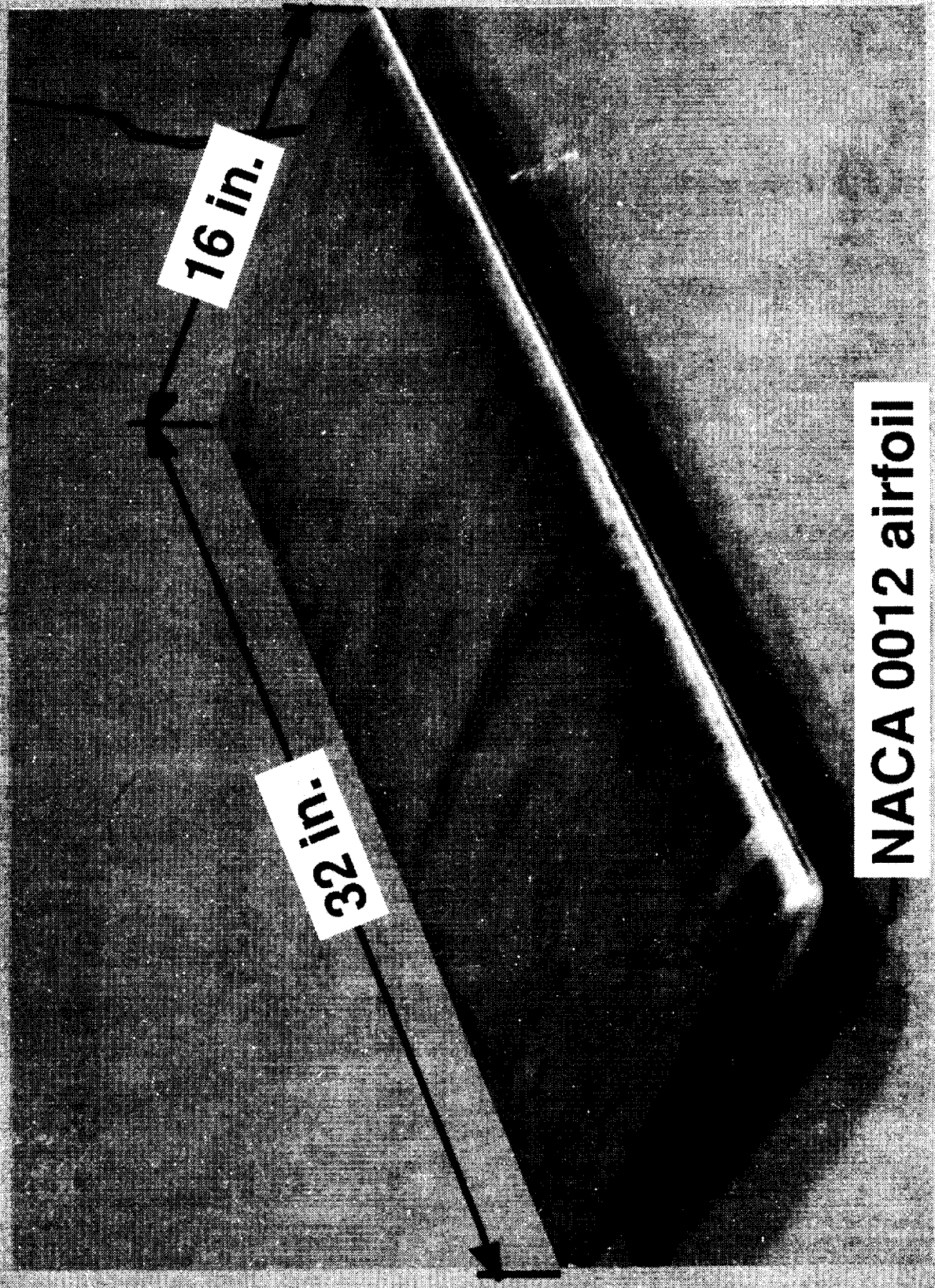
Figure 5 - The NACA 0012 airfoil pressure model.

INSTRUMENTATION LIST

- **Wing Model**

  Pressure Transducers (80)

  Accelerometers (4)

- **Pitch and Plunge Apparatus**

  Strain Gages (2)

  Accelerometers (2)

- **Splitter Plate**

  Pressure Transducers (20 + 10)

Figure 6 - A list of the NACA 0012 airfoil model instrumentation.

ORIFICE LOCATIONS

Pressure transducer
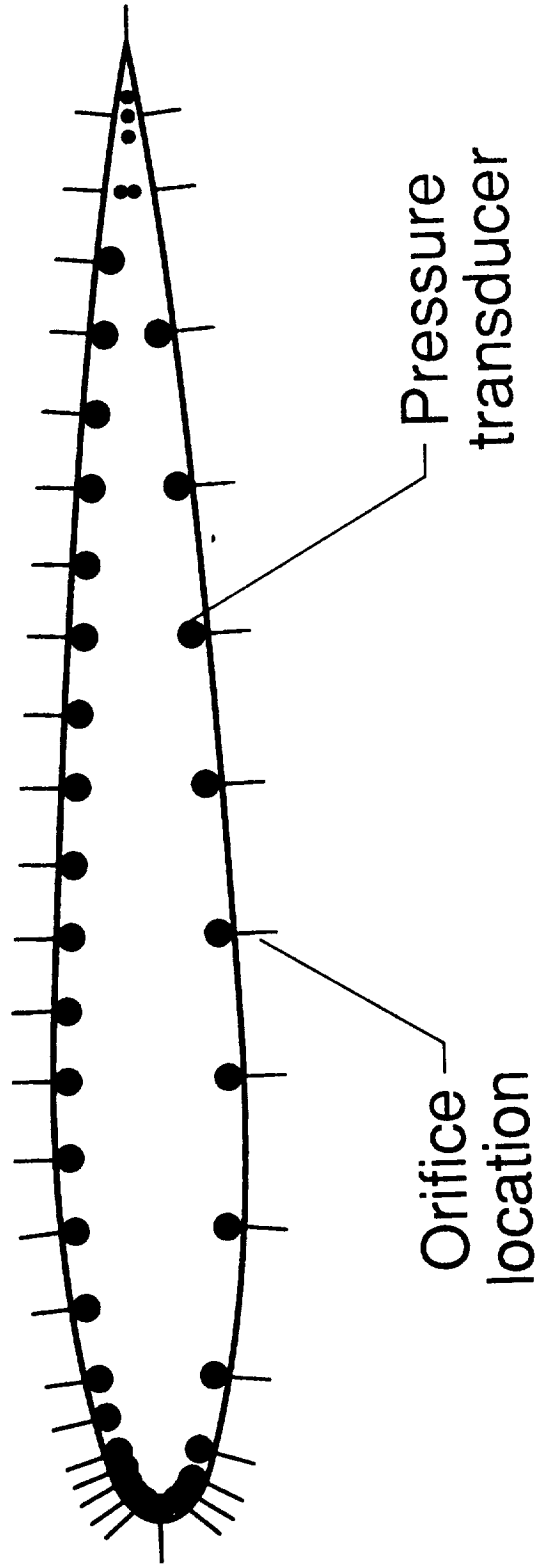
Orifice location

Figure 7 - Pressure orifice locations for the NACA 0012 airfoil model.

MODEL DETAIL
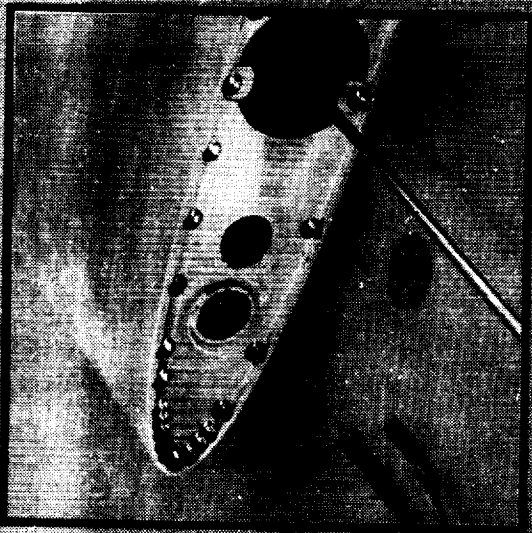
Figure 8 - Photographs showing details of the NACA 0012 airfoil model.

PAPA ROD SYSTEM

Bending and torsion strain gages

Pitch and pitch & plunge accelerometers

FLOW
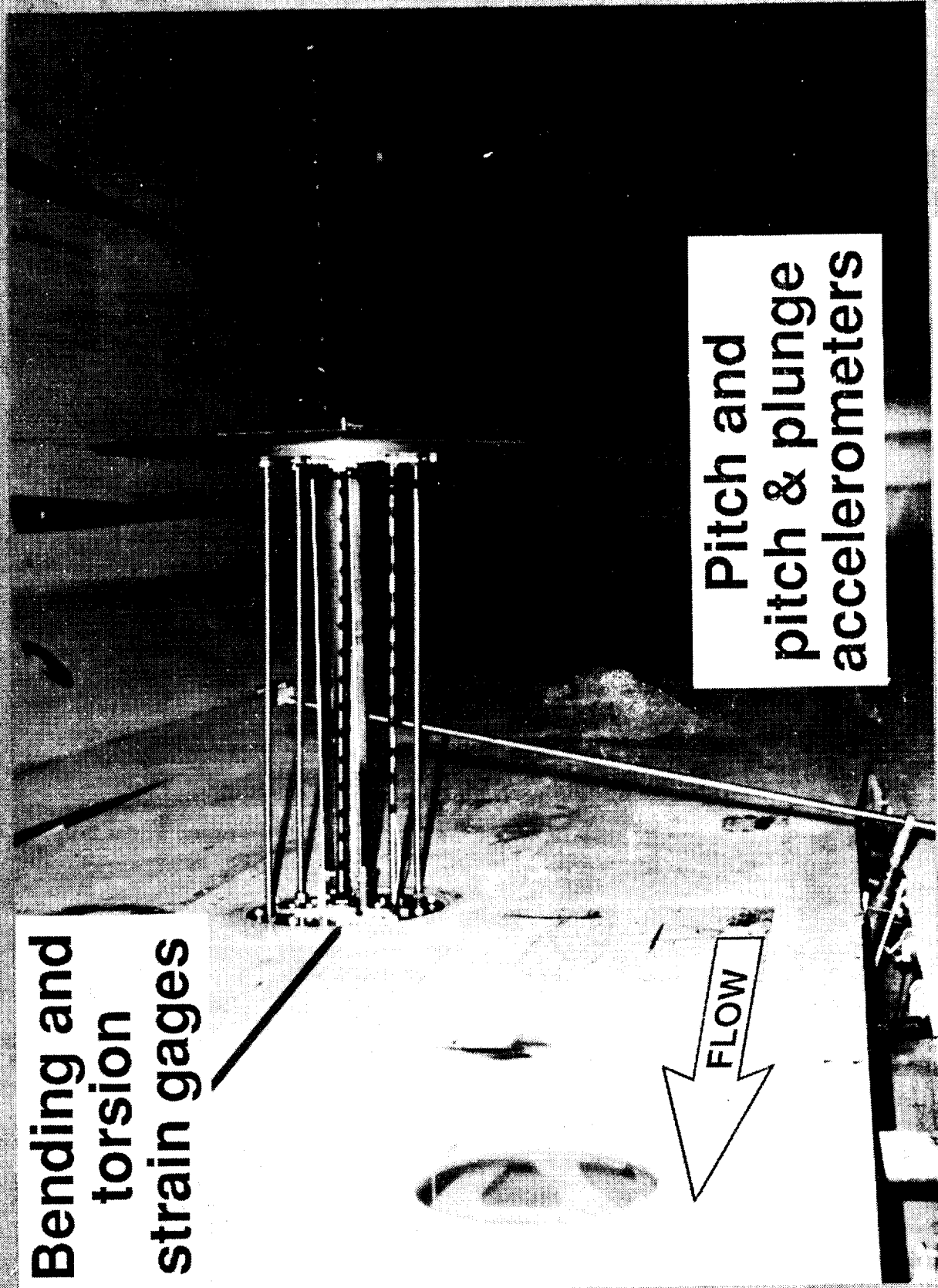
Figure 9 - Photograph showing some details of the PAPA mount system.

PAPA SPLITTER PLATE
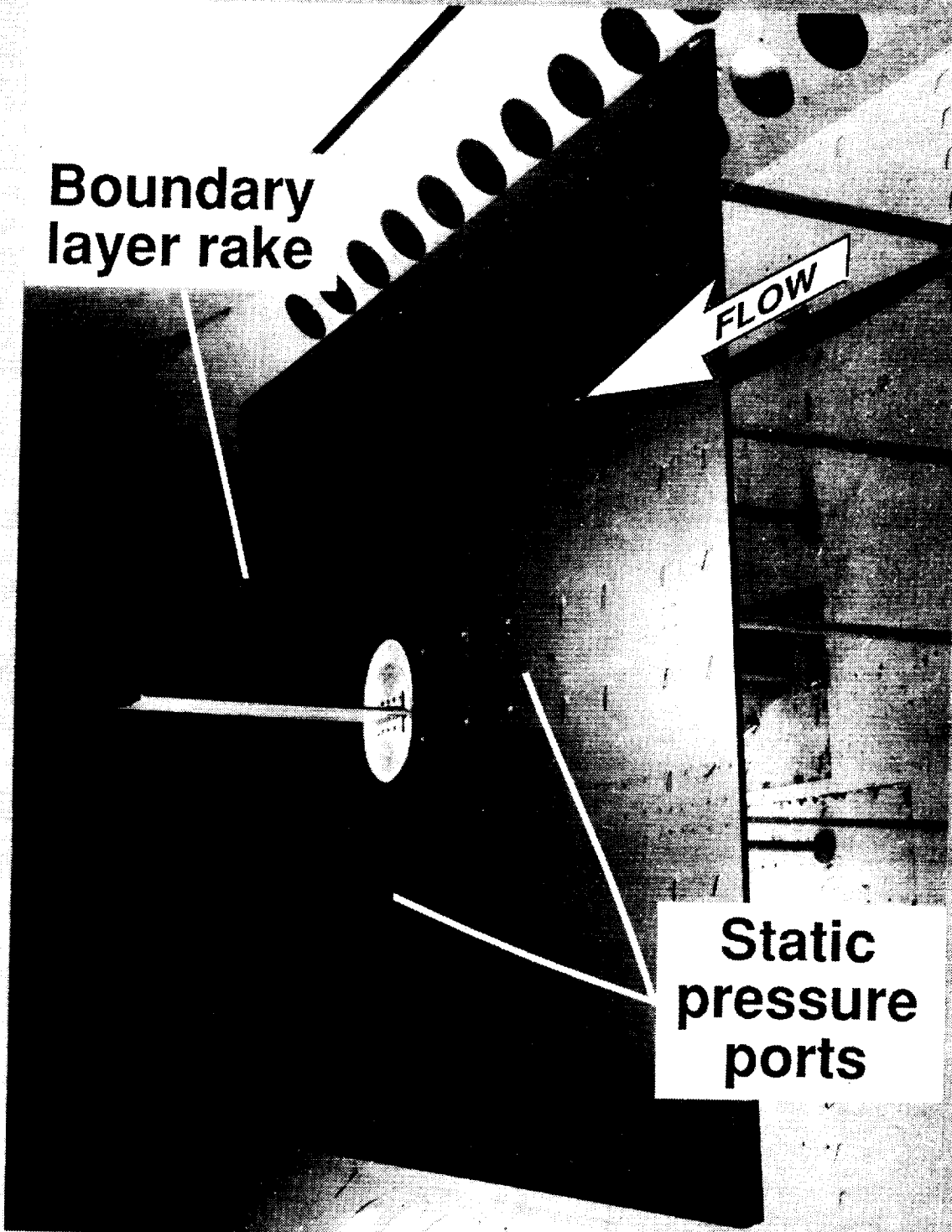
Figure 10 - PAPA splitter plate and flutter model mounted in the TDT.

SCHEDULE

- **Design Initiated**   June '89 ✔

- **Fabrication Started**   December '89 ✔

- **Model Delivered**   March '90 ✔

- **Transducer Installation Initiated**   March '90 ✔

- **Wind Tunnel Test**   June '90

Figure 11 - Project schedule for NACA 0012 airfoil model test.

INVESTIGATION OF THE USE OF EXTENSION-TWIST

COUPLING IN COMPOSITE ROTOR BLADES

Renee C. Lake
USAARTA-AVSCOM, ASTD
NASA Langley Research Center
Hampton, VA
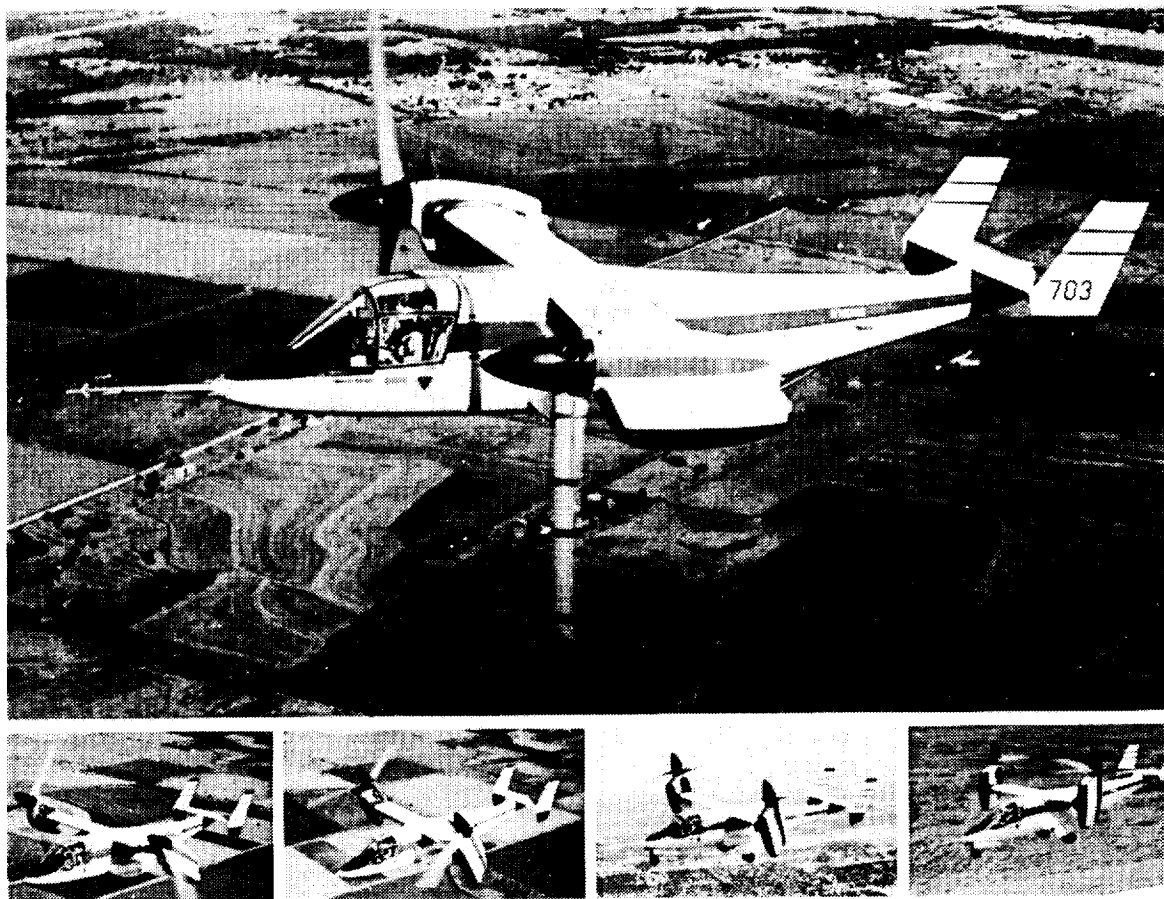
Tiltrotor aircraft, such as the XV-15 shown in the accompanying photograph, are designed to operate in both helicopter and airplane modes of flight. This operational flexibility results in several conflicting design requirements. One such design requirement, which has significant effects on aerodynamic performance, is the built-in twist of the rotor blade. Typically, the twist is not optimum for either flight mode. Performance could be improved if it were possible to vary blade twist between the airplane and helicopter modes. Tiltrotor aircraft typically vary rotor speed by 20 percent between flight modes, (100% rpm in helicopter mode, 80% rpm in airplane mode), which induces a change in the centrifugal force. This change in centrifugal force accompanying the change in rotor speed can be exploited to passively change twist in composite rotor blades which employ extension-twist structural coupling.

Linear Twist Performance Relative
to XV-15 Twist Performance

Power
Required
Relative
to XV-15
Twist,
%

Linear Twist, deg
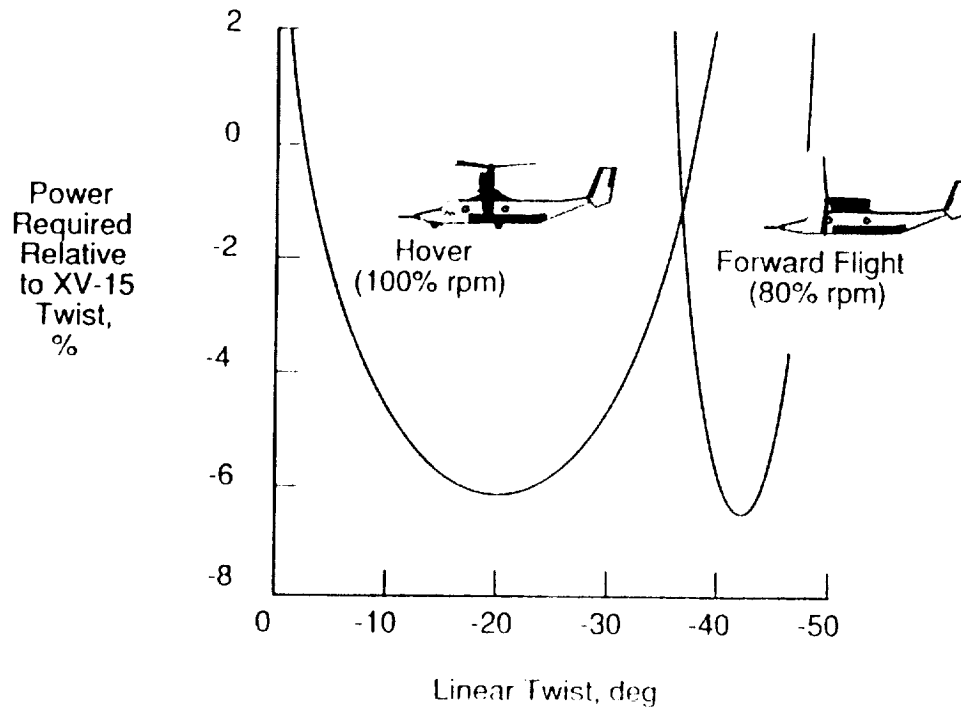
Recently, the aerodynamic performance of the XV-15 with its existing metal rotor system was determined for hover in the helicopter mode and forward flight in the airplane mode. A companion study was initiated to determine the optimum linear twist and associated performance improvement for each flight mode. The performance associated with the extension-twist-coupled rotor blades was compared to the performance associated with the existing metal rotor blades. The results (shown in the figure) indicate that the optimum linear twist corresponds to -20° in hover and -42° in forward flight. The associated aerodynamic performance improvements to the conventional twist design were about six percent in both flight modes. These figures represent substantial improvements in performance using passive twist control via extension-twist-coupled rotor blade designs.

PASSIVE TWIST CONTROL MECHANISM

Rotation Direction

- Blade twist distribution is altered by a change in axial force

Tailored Composite Structure

Change in Twist

Centrifugal Force
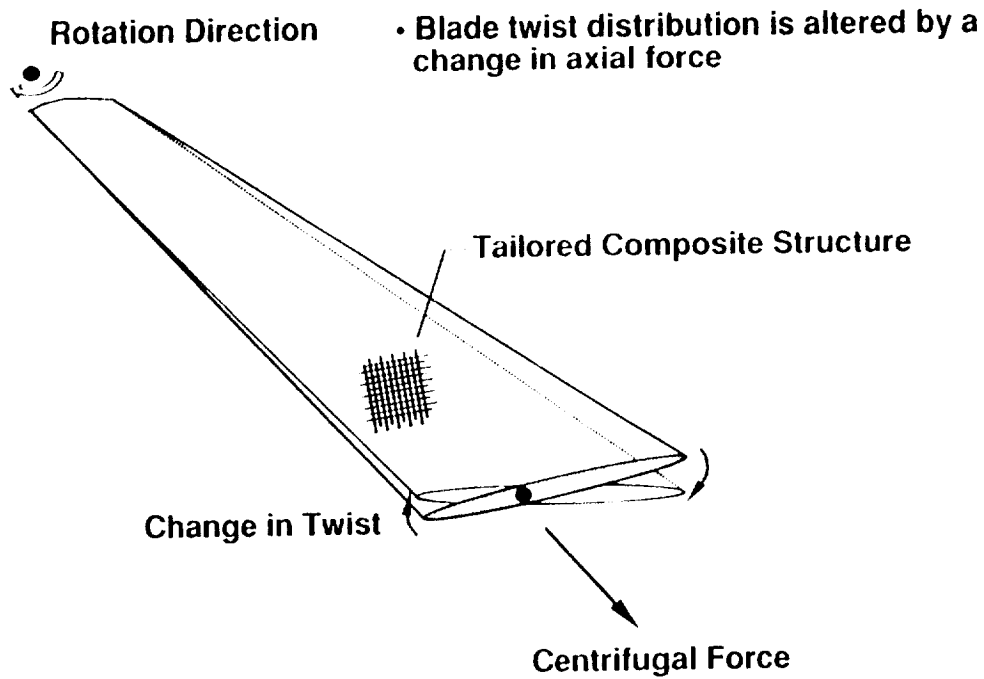
With the advent of composite materials technology, the development of a passive twist control mechanism can be effected through the implementation of elastic tailoring in the design of the rotor blade spar. Specifically, the use of an extension-twist-coupled layup allows the blade structure to twist in response to an extension, such as that created through a change in centrifugal force, and vice-versa. Thus, the use of such a layup allows the rotor blade to passively change twist as a function of rotor speed.

Problem Statement

Accurate, reliable computational methods for predicting the structural dynamic characteristics of composite rotor blades are essential to the development of advanced, cost-effective rotor systems.

Objective

Investigate, both analytically and experimentally, the dynamic characteristics of composite rotor blades exhibiting extension-twist coupling.

With this concept in mind, the above problem statement has been identified for this research investigation. That is, to accurately and reliably predict the structural dynamic characteristics of elastically-coupled composite rotor blades. The objective of this research is to investigate the dynamic characteristics of composite rotor blades through the effective implementation of experimental and analytical investigations.

Approach

- Conduct static/dynamic experiments of composite rotor blade structures

- Develop and evaluate companion FEM models of composite rotor blade structures using MSC/NASTRAN

  - Composite tube studies
    - ground vibration tests (frequency, mode shape, etc.)

  - Composite rotor blade studies
    - ground vibration tests
    - hover test (twist vs. rpm)

- Application to tiltrotor blade

The approach designed to meet this objective is summarized in the figure. To establish an experimental database, static and dynamic experiments have been performed on fabricated composite rotor blade structures, providing a verifiable means of comparing with analytical investigations. In addition, companion finite-element models of these structures have been developed and analyzed in MSC/NASTRAN. This has been performed for each of two tasks within an in-house research program: composite benchmark models and composite model rotor blades. The first task involves the investigation of composite tubular specimens, which are simplistic representations of rotor blades and which provide the foundation for the development of a database on elastically-coupled composite structures. The second task involves the development of a model-scale helicopter rotor blade. This study will provide a more in-depth understanding of the structural dynamic characteristics of elastically-coupled rotor blades. In addition to the ground vibration tests which have been performed in each of the two studies, a hover test has been conducted for the composite model rotor blade, where the blade twist was measured as a function of rotor speed. Following the completion of these two tasks, the application of extension-twist coupling in the design of a tiltrotor blade, which is a more highly-twisted version of a helicopter rotor blade, will be investigated.

While the scope of the in-house research effort includes both static and dynamic studies, this paper will focus on results obtained as part of the dynamics studies.

151
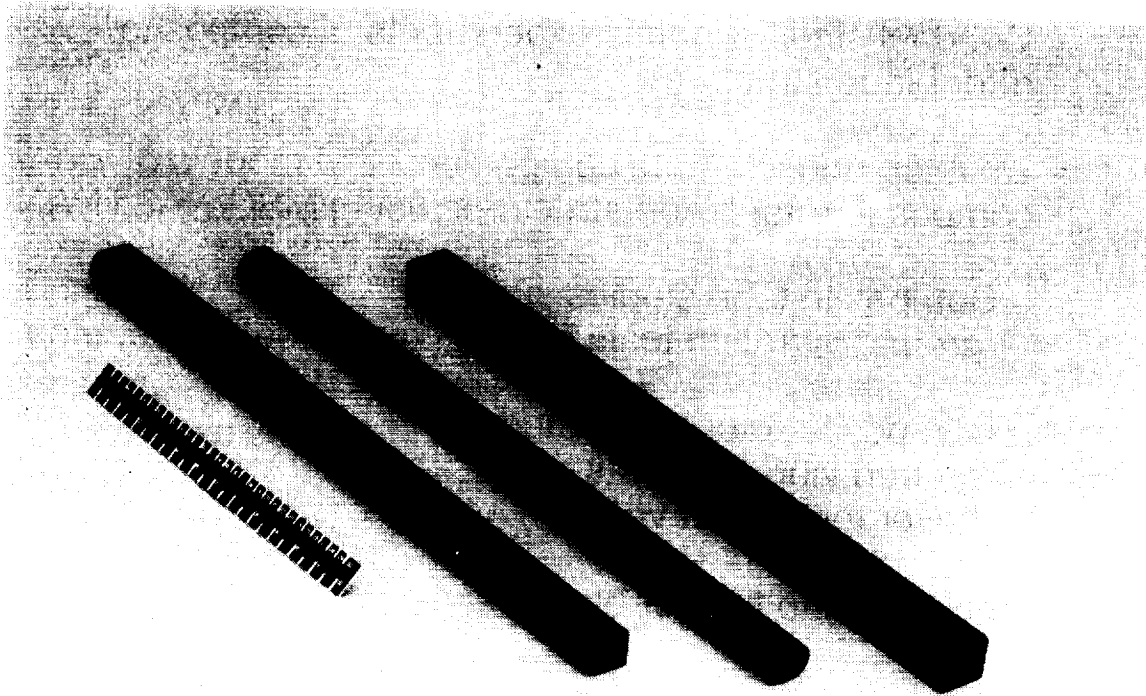
The experimental/analytical investigation of the extension-twist-coupled composite tubular specimens was performed for three cross-sectional designs: square, D-shape, and elliptical. These three designs are shown as a photograph above and as a drawing in the following figure.As these cross-sections are non-circular, they are prone to cross-sectional warping deformations. Additionally, the presence of extension-twist coupling in a laminate acts to "magnify" the warping effect, therefore a significant effect on the structural dynamic behavior may occur. The specimens were 24 inches in length and were fabricated from 4 plies of 0°/90° T-650/42 graphite fiber with ERLX 1925-2 epoxy resin plain weave "prepreg" fabric. The fabric plies were rotated 20° off-axis to achieve the desired extension-twist elastic coupling.

Warping-Prone Composite Specimens

Sections A-A

Ellipse — 0.95 in. × 1.45 in.

D-shape — 0.95 in. × 1.45 in., 0.475 in. radius

Square — 1.20 in.

4 x .007"/ply = .028" (typ)

A (Three cross sections)

20°

24 in.

Cross-Section Dependent
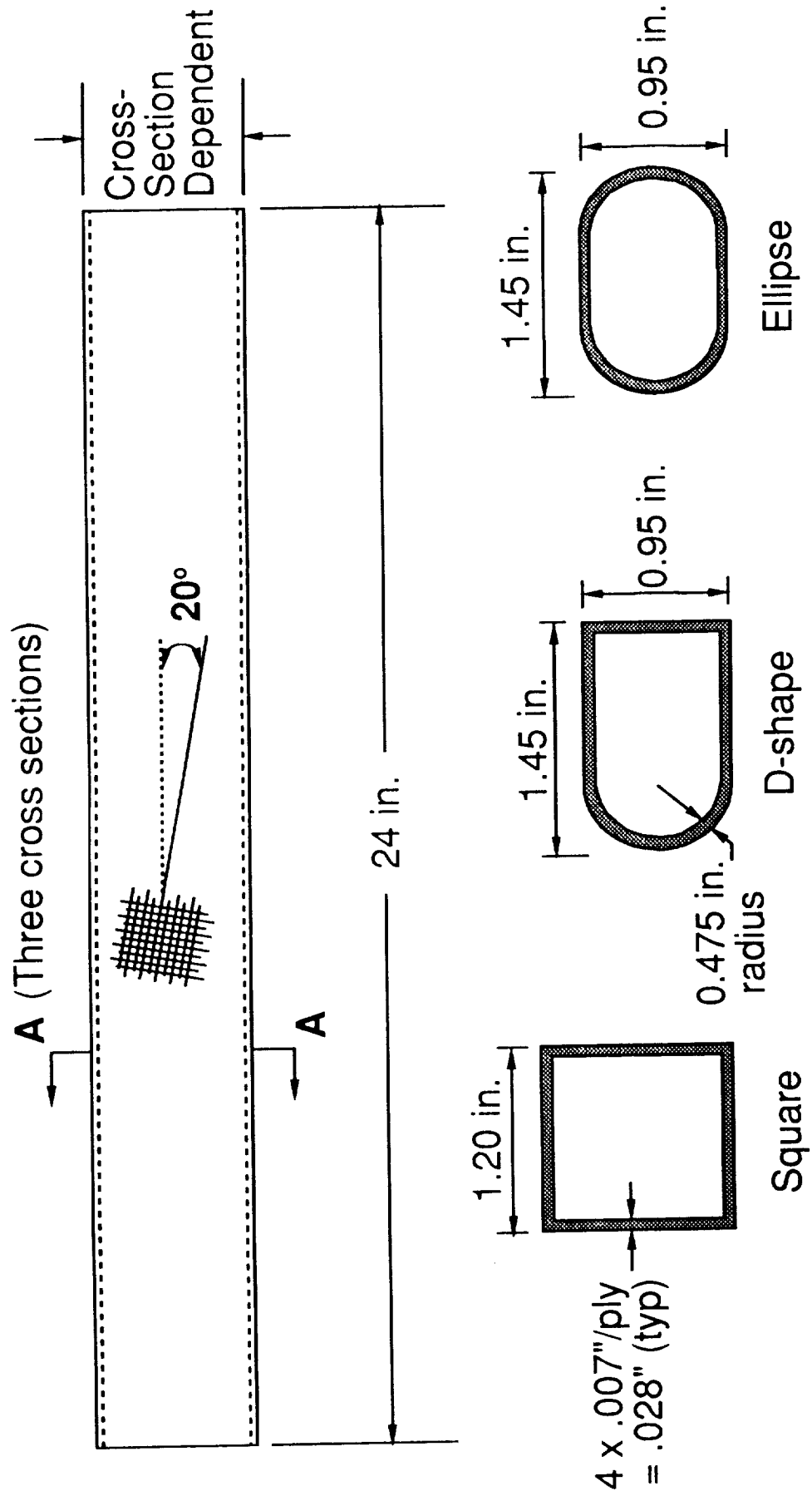
NASTRAN Finite-Element Model

Extension-Twist-Coupled D-shape Tube
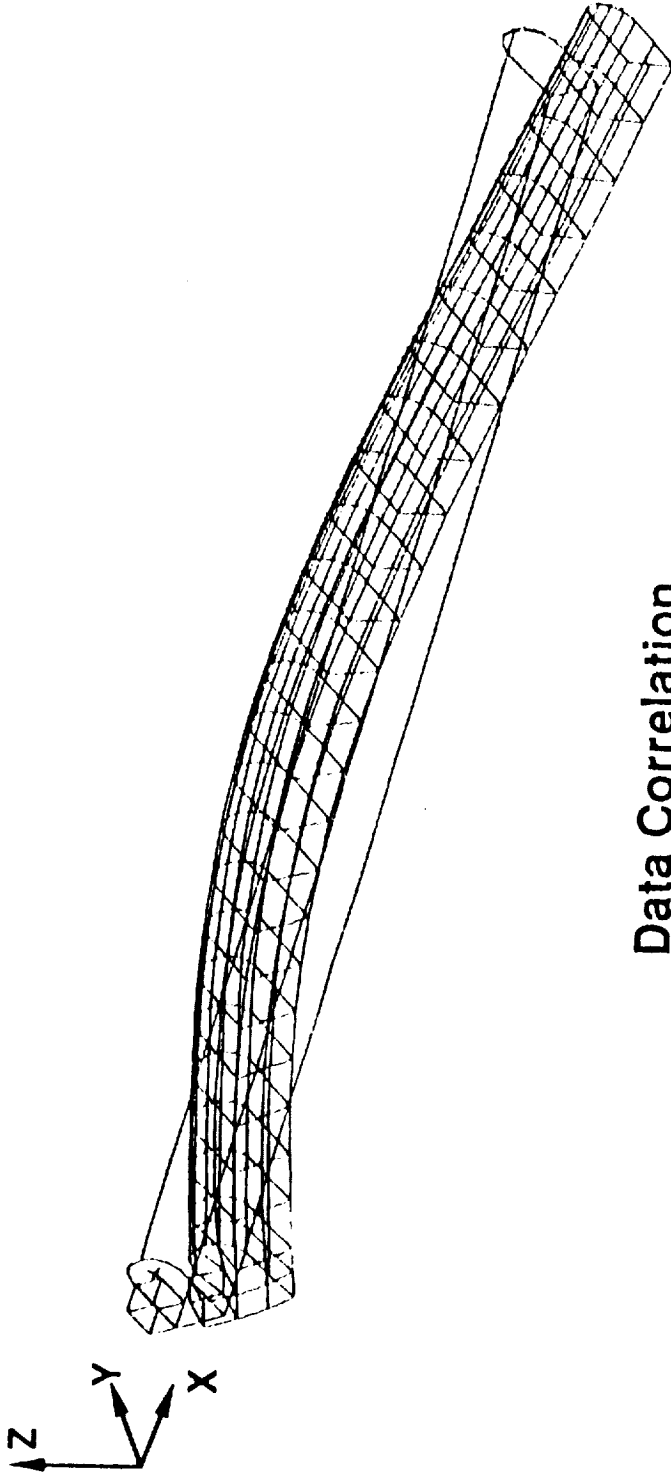
Data Correlation

Mode shape	Experimental (Hz)	Tube FEM (Hz)
* First vertical bending	394.4	402.0
First lateral bending	575.1	596.2
Second vertical bending	904.2	1048.7
First vertical shear	1175.9	1254.9
Second lateral bending	1576.7	1647.7

* indicates displayed mode shape

154

Extension-Twist-Coupled D-shape Tube
Free-free condition
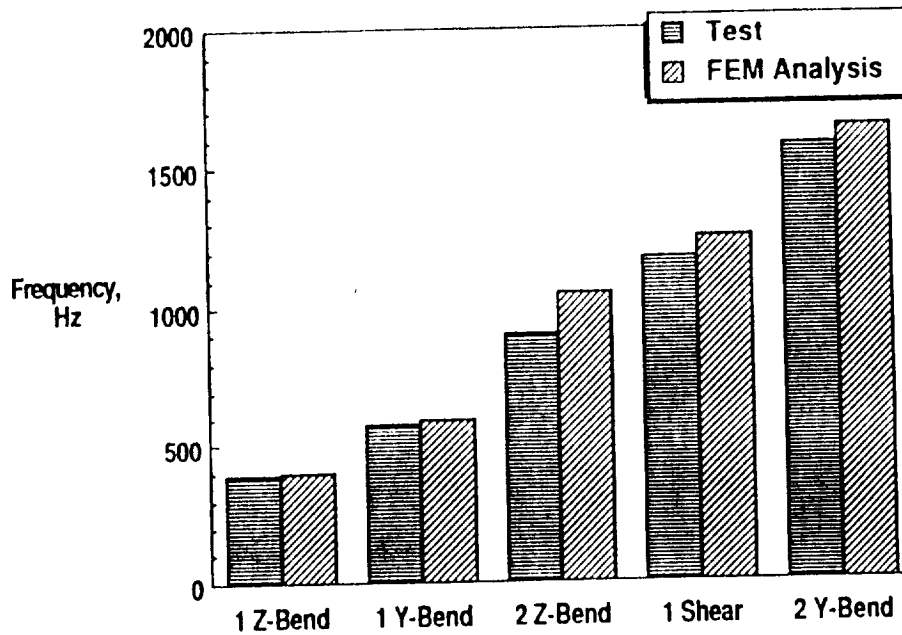
A free-free ground vibration test was conducted to determine the modal properties (frequency, mode shape and damping) for each specimen type. The excitation was provided using a roving impact hammer, while the response was measured using three single-axis accelerometers which were mounted in a tri-axial configuration on an aluminum block affixed to one end of each specimen.

The results of the test/analysis comparison for the D-shape tube are shown in the preceding figure. The mode shape and frequency data are plotted in tabular fashion for both experimental and analytical data. The finite-element model of the tube, which was constructed of 300 flat plate elements, is shown plotted in a deformed (first vertical bending mode) versus an undeformed outline for the tube. A single solid element was used to represent the accelerometer mounting block affixed to the test specimen. Five global or "non-shell" modes, which are the primary mode types of interest, were determined in the 0-2000 Hz frequency range: first vertical bending, first lateral bending, second vertical bending, first vertical shear, and second lateral bending. (The first vertical shear mode was identified by the relative shearing of leading and trailing edges in the vertical plane with no net torsion present in the mode.)

As a means of facilitating test/analysis correlation, the modal frequencies are plotted versus mode shape for both test and analysis in a bar chart fashion. The overall agreement for the D-shape tube results is good, ranging from 2% difference (first vertical bending case) to 13.8% difference (second vertical bending case). The average difference is approximately 6.5%.

NASTRAN Finite-Element Model

Extension-Twist-Coupled Elliptical Tube
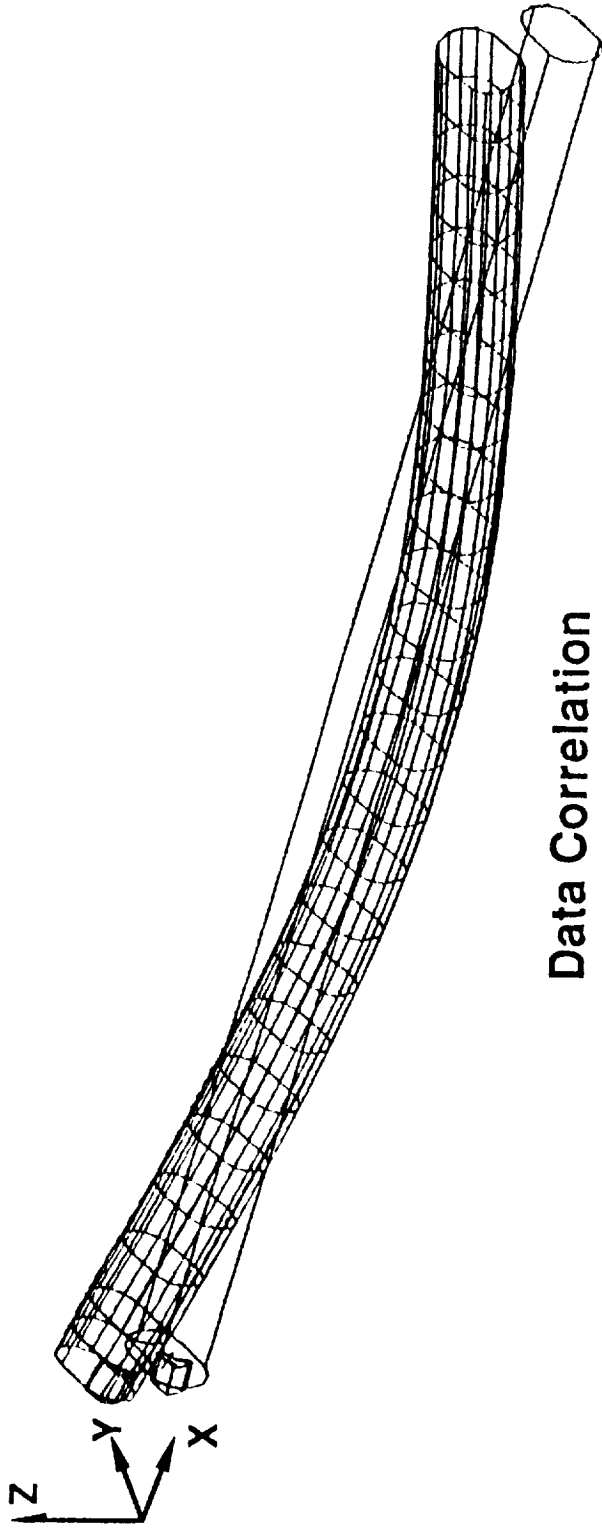
Data Correlation

Mode shape	Experimental (Hz)	Tube FEM (Hz)
* First vertical bending	378.7	383.3
First lateral bending	457.7	504.6
Second vertical bending	1023.6	1063.5
Second lateral bending	1233.5	1344.9
First torsion	1514.7	1615.4

* indicates displayed mode shape

156

Extension-Twist-Coupled Elliptical Tube
Free-free condition
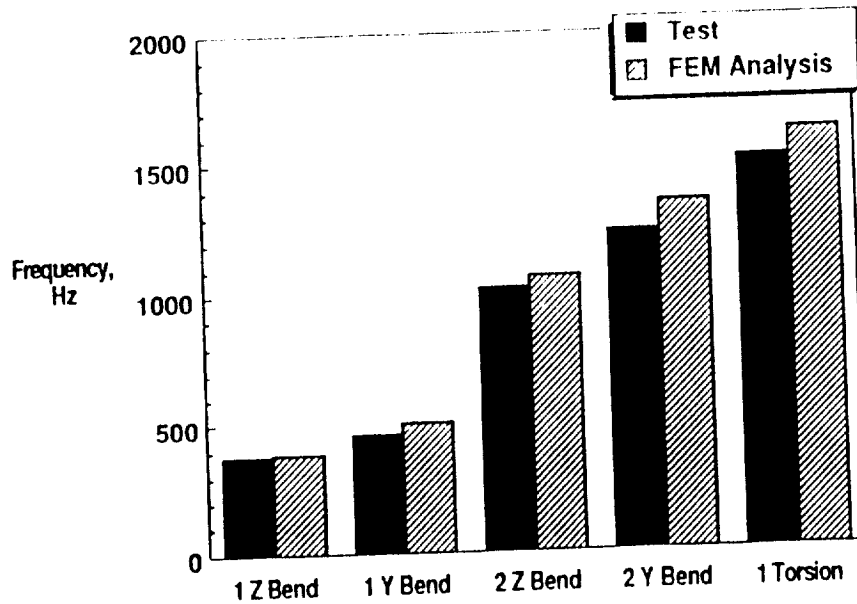
The test and analysis results for the elliptical tube are shown in the figure on the preceding page and the figure above, plotted in a fashion similar to that of the D-shape tube. The finite-element model for this specimen was constructed from 350 flat plate elements. A total of four solid elements were used to represent the accelerometer mounting block in this instance, due to the curved geometry of the mounting surface. Because of the improved coherence and phase characteristics of the measured data in the upper frequencies, the frequency range of interest for this specimen was extended to span 0-2500 Hz. Again, five global modes were identified for the elliptical tube within this range: first vertical bending, first lateral bending, second vertical bending, second lateral bending, and first torsion. Results from the comparison of test and analysis data show very good agreement, ranging from 1% difference (first vertical bending) to 9.3% difference (first lateral bending). Overall, the average difference in test and analysis data was approximately 5.7% for the five modes.

157

NASTRAN Finite-Element Model
Extension-Twist-Coupled Square Tube
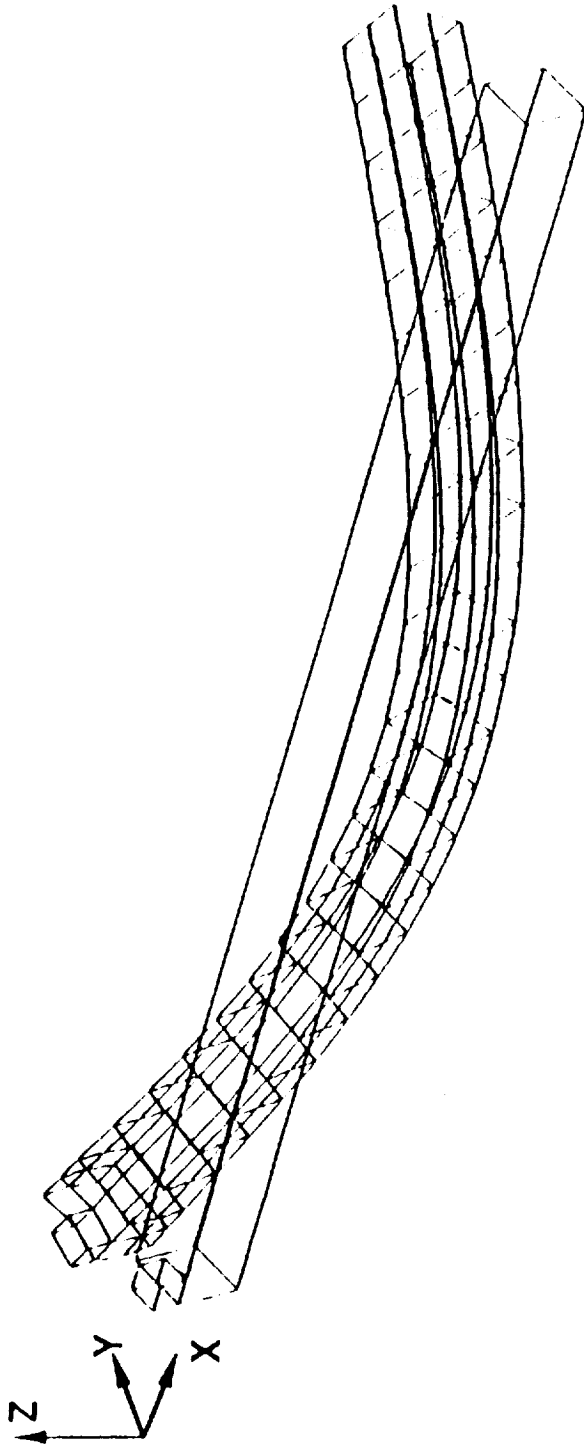
Data Correlation

Mode shape	Experimental (Hz)	Tube FEM (Hz)
* First vertical bending	464.1	499.8
First lateral bending	486.3	516.0
Second vertical bending	1260.9	1345.3
Second lateral bending	1412.2	1559.6

* indicates displayed mode shape

Extension-Twist-Coupled Square Tube
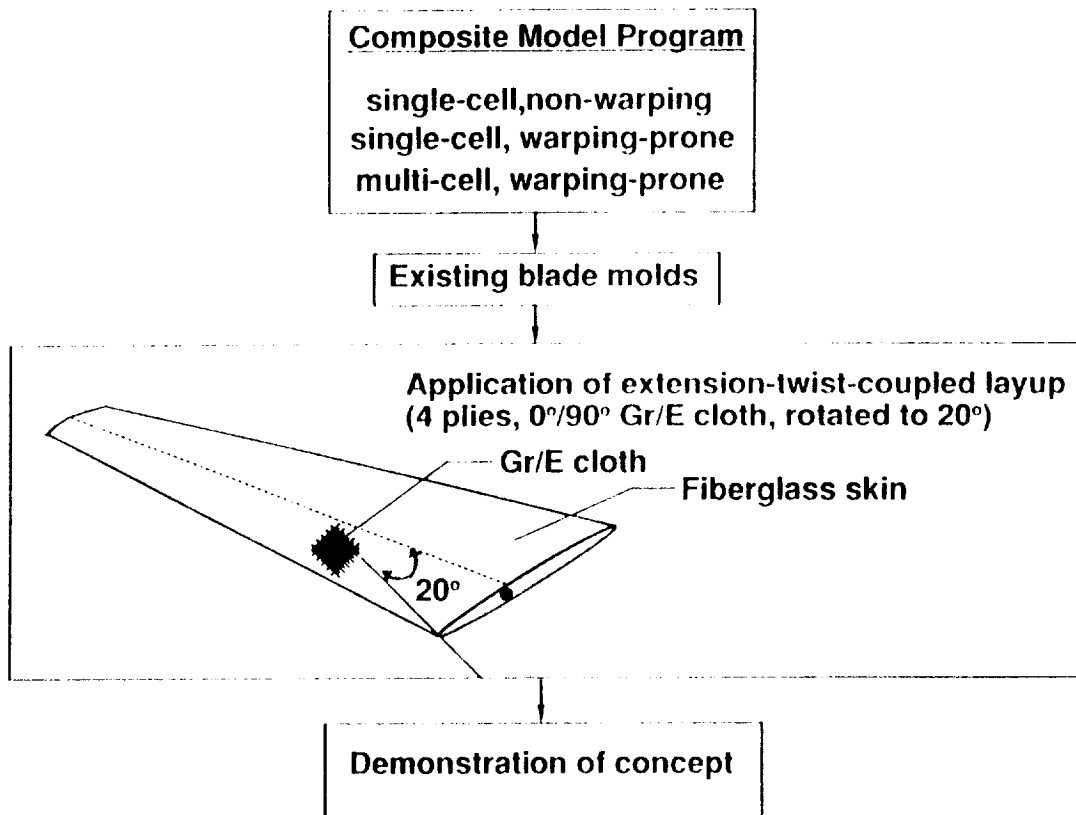## Free-free condition
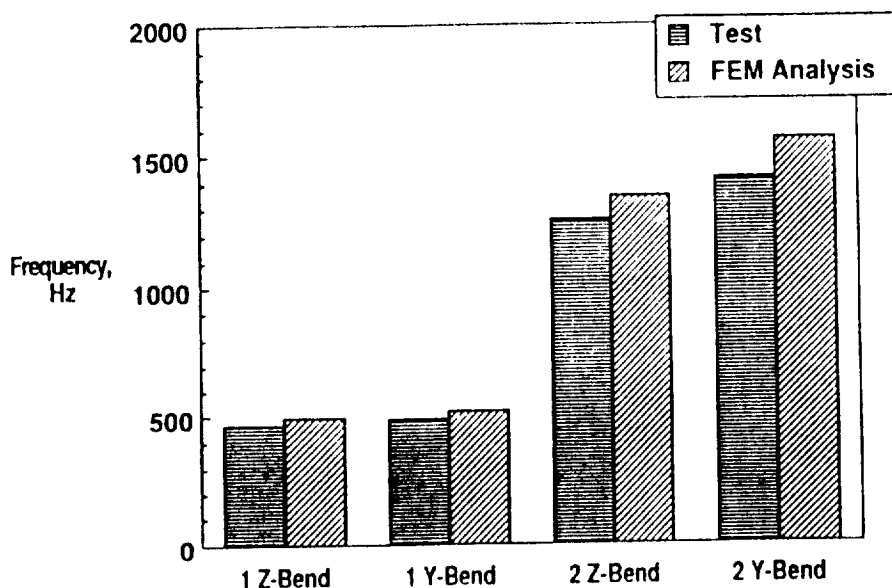
In the final specimen case, the results from the vibration test of the square tube are compared with those obtained from the corresponding finite-element analysis and are shown in the preceding figure and the above figure. The finite-element model of the square specimen, which is shown in the first vertical bending mode, was constructed from 200 flat plate elements. The accelerometer mounting block was represented using a single solid element, similar to that in the D-shape specimen finite-element model. Four global modes were identified in the 0-2000 Hz frequency range: first "vertical" bending, first "lateral" bending, second "vertical" bending, and second "lateral" bending. The terms "vertical" and "lateral" are used here to indicate the general plane of deformation for the bending modes, although the "true" bending planes are slightly canted from absolute vertical and lateral axes. The magnitude of this inclination is on the order of 22° for the first vertical and first lateral bending modes, and approximately 6° and 2° for the second vertical and second lateral bending modes, respectively. It must also be noted that some torsional deformation is present in each of the second bending modes, thereby producing a "coupled" mode. Although the agreement of this data was within 9.5% overall (second lateral bending), the average difference was approximately 7.2%, with the best-case (first lateral bending) showing 5.8% difference between test and analysis data.

Collectively, these results suggest that the structural dynamic characteristics of composite structures employing extension-twist coupling can be determined within practical engineering accuracy. The investigation of these tubular specimens leads to an enhanced understanding of the structural dynamic characteristics of elastically-coupled structures and provides a basis for the development of practical composite rotor blade designs incorporating extension-twist structural coupling.

Development of Model Rotor Blade

Composite Model Program

single-cell,non-warping
single-cell, warping-prone
multi-cell, warping-prone

Existing blade molds

Application of extension-twist-coupled layup
(4 plies, 0°/90° Gr/E cloth, rotated to 20°)

Gr/E cloth

Fiberglass skin

20°

Demonstration of concept

With the results of this phase of the research task in place, the development of a model rotor blade was initiated. The above figure summarizes the basic steps that have been taken towards this goal, with the fundamental development proceeding from single-cell, non-warping tubular specimens (circular cross-sections), to the single-cell, warping-prone tubular specimens (non-circular cross-sections) as presented. This, in turn, led to the next step of the program, which was the development of a model rotor blade (multi-cell, warping-prone design). A complete set of model rotor blades was fabricated using an existing set of blade molds for a NACA 0012 cross-sectional design. The layup design of the rotor blade spar incorporated four plies of 0°/90° Fiberite graphite/epoxy fabric, rotated to 20° off-axis, such that the desired extension-twist coupling effect could be achieved. The culmination of this phase of the research task was then effected through a demonstration of concept with the planned hover test, in which the actual blade twist was measured as a function of rotor speed.
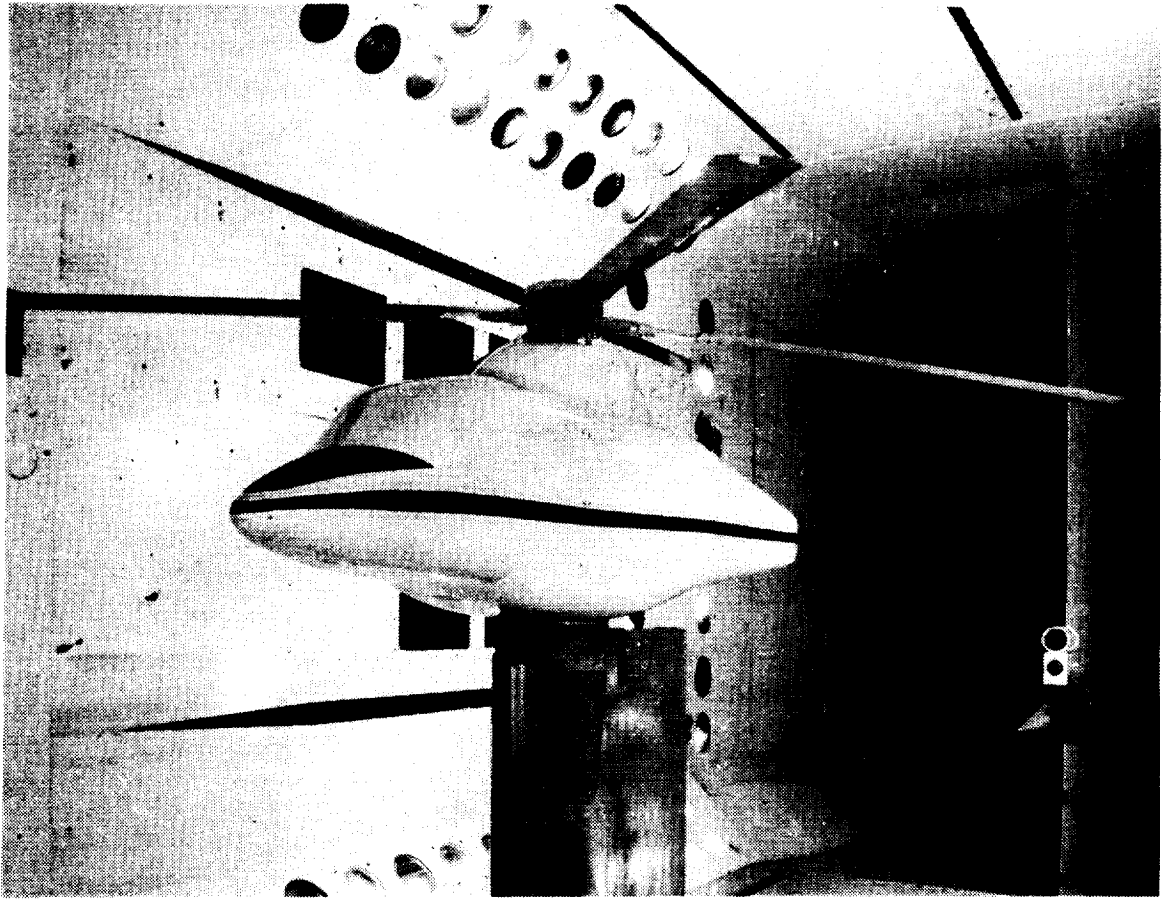
The set of fabricated blades are shown in the following photograph, as mounted on the ARES (Aeroelastic Rotorcraft Experimental System) test stand during the hover test in the Transonic Dynamics Tunnel (TDT). The darker part of the blade structure corresponds to the elastically-coupled graphite/epoxy blade spar, while the trailing edge, which is essentially honeycomb filler wrapped by the single layer of fiberglass skin, appears as the lighter portion of the structure.

Extension-Twist-Coupled Model Blade FEM

- 8.25° pre-twist
- 326 grid points
- 290 CQUAD4 plate elements
- 60 CHEXA/CPENTA solid elements
- 59 CBEAM beam elements
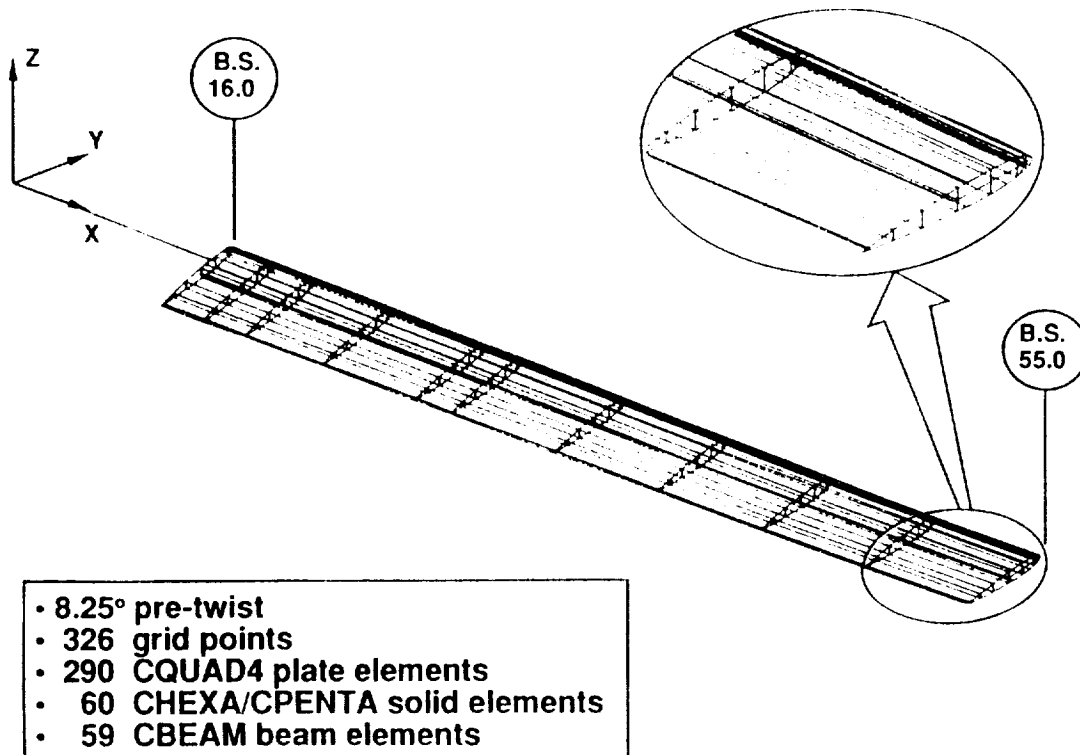
The MSC/NASTRAN finite-element model of the model rotor blade is shown in the following figure. The blade incorporates about 8.25° of pre-twist over its 42.5 inch length. The finite-element model is composed of 326 grid points, 290 flat plate elements, and 60 solid elements contained in the model (representing the balsa filler and honeycomb components of the structure). In addition, a total of 59 beam elements were used to represent the two internal ballast weight tubes within the blade as well as the transition blade area, rotor cuff, and hub arm.

NASTRAN Finite-Element Model
Extension-Twist-Coupled Rotor Blade
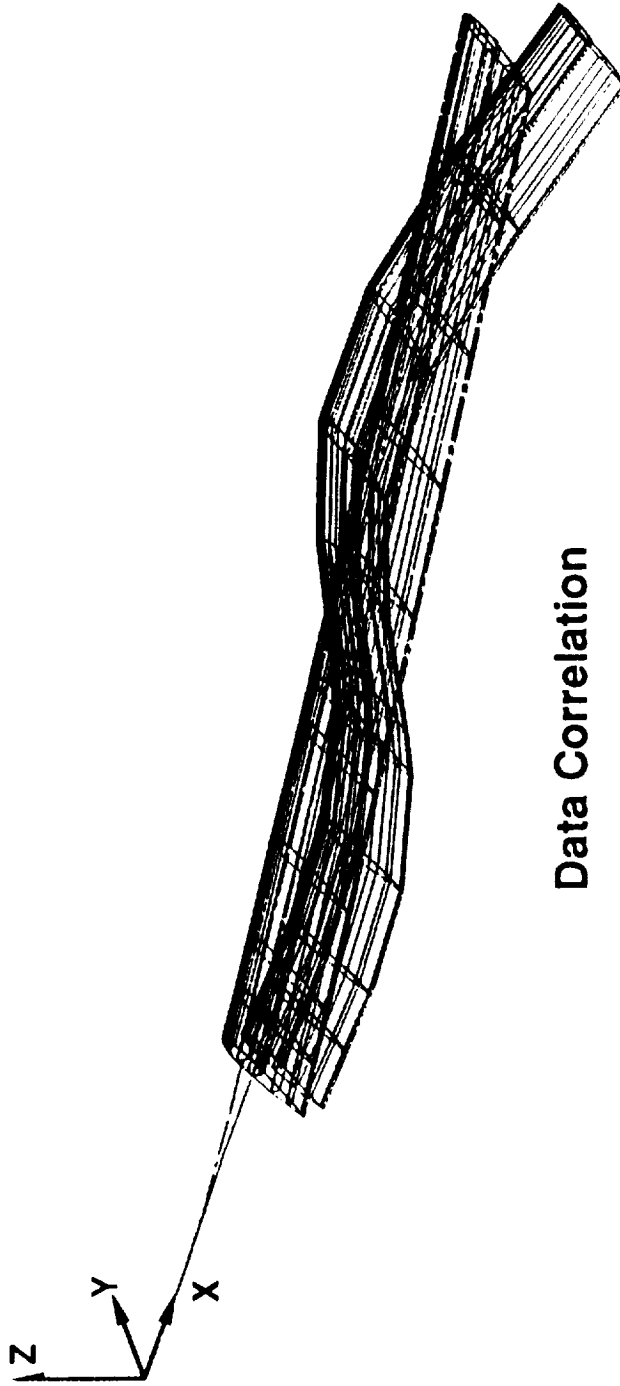
Data Correlation

Mode shape	Experimental (Hz)	Blade FEM (Hz)
First flap bending	6.0	6.75
First lag bending	24.0	26.22
*Second flap bending	40.0	39.32
Third flap bending	98.0	103.75
First torsion	116.0	132.80
Second lag bending	141.0	154.80
Fourth flap bending	180.0	203.00
Second torsion	338.0	305.30

* indicates displayed mode shape

163

Extension-Twist-Coupled Rotor Blade
cantilevered, unballasted
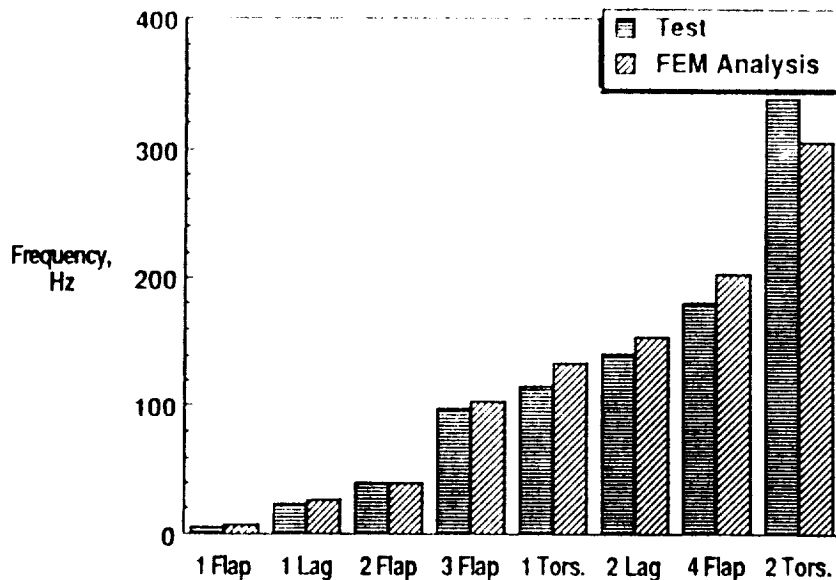
The results of the ground vibration test are compared with those obtained from the finite-element analysis for the cantilevered, unballasted configuration of the blade. There were eight mode shapes identified in the 0-350 Hz range: first flap (vertical) bending, first lead-lag (lateral) bending, second flap bending, third flap bending, first torsion, second lead-lag bending, fourth flap bending, and second torsion. The deformed mode shape displayed in the preceding figure is that of second flap bending. The test and analysis data correlated well, ranging from 2% difference in the second flap bending mode, to 12.7% difference in the first torsion mode. The average difference in test and analysis data was approximately 8.8%.

EXTENSION-TWIST-COUPLED BLADE TEST IN HOVER

Strain gage locations

8.25° twist
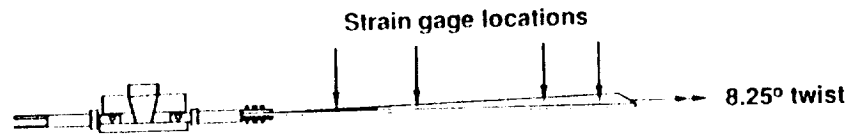
MEASUREMENTS

- Twist as a function of rpm
- Flap-wise, chord-wise loads

STATUS

- Hover test initiated 9/89
- Testing completed 2/90
- Data reduction initiated

TEST PARAMETERS

- ballasted, unballasted blade configurations
- atmospheric and near-vacuum conditions
- 0-800 rpm range sweep
- collective pitch sweep

An overview of the hover test is presented in the following figure, indicating test and measurement parameters. The blades were mounted on an articulated hub, with a total of four strain gage locations per instrumented blade. These gages were used to determine measurements of blade twist as a function of rotor speed and were calibrated such that twist readings were output real-time during the course of the test. The flapwise and chordwise bending moments were also monitored and recorded in addition to the usual balance information. The blades were tested in both ballasted (ballast weight tubes filled), and unballasted (ballast weight tubes empty) configurations in atmospheric conditions. The ballasted configuration was additionally tested in a near-vacuum condition. This was done to divorce any contributions of aerodynamic-induced twist effects from the twist due to the elastic-coupling effects. Data was obtained for a 0-800 rpm range sweep, with corresponding sweeps in collective pitch, ranging from the minimum pitch necessary to obtain a zero coning condition, to a maximum of 17°. Hover tests were initiated in September 1989 in the hover test facility behind the TDT, with an initial unballasted, atmospheric test configuration. Testing was suspended soon after completion of the first configuration due to minor structural damage to two of the blades. The damage was associated with an adhesive bond failure between the weight tubes and the clear tube designed to close-off the weight tubes. Following the repair of the set of blades, testing resumed in the TDT and was completed in February 1990. Data reduction has been recently initiated for all test configurations, therefore a complete set of the results from processed data is forthcoming.

Summary

- Dynamic testing and analysis of composite specimens is essential to the establishment of structural dynamics database

- Correlation of test/analysis provides basis for improvements in finite-element techniques and modeling methodologies

- Derivative blade designs result in improved dynamic and aerodynamic characteristics to meet future Army performance requirements

In summary, the dynamic testing and analysis of the composite tubular specimens has further enhanced the establishment of a structural dynamics database for elastically-coupled composite structures. In addition, the correlation of test and analysis data provides a basis for improvements in finite-element modeling techniques. This can be seen from the results of the warping-prone tubular specimen study, which exhibited good correlation between test and analysis (generally within 10%, with the exception of the 13.8% difference in the D-shape tube second vertical bending case), and additionally with the results of the model rotor blade study (within 12.7% difference overall). Advanced rotor blade designs which may be derived as a result of this research investigation will result in improved dynamic and aerodynamic characteristics.

166

IMPROVED FINITE ELEMENT METHODS FOR ROTORCRAFT STRUCTURES

Howard E. Hinnant
USAARTA-AVSCOM, ASTD
NASA Langley Research Center
Hampton, VA

Outline

- Background

  Problem Statement

  Objective

  Approach

- Overview of FEAT

- Discussion of p-version elements

- Current Status / Future Plans

- Summary

168

Problem

- Current day rotorcraft dynamic
  analyses are not accurate enough
- Analyses are not easy enough to use

Dynamic finite element analyses available today do not accurately predict the dynamic characteristics of rotorcraft. In particular, there continues to be a lot of trouble predicting some of the higher frequencies. The problem may be in the finite element codes or in the way engineers use the codes to approximate the physical structure. A leading cause of the misuse of a code is that the codes are often not very easy to use. There is a lot of tedious, repetitive work in building a good finite element model.
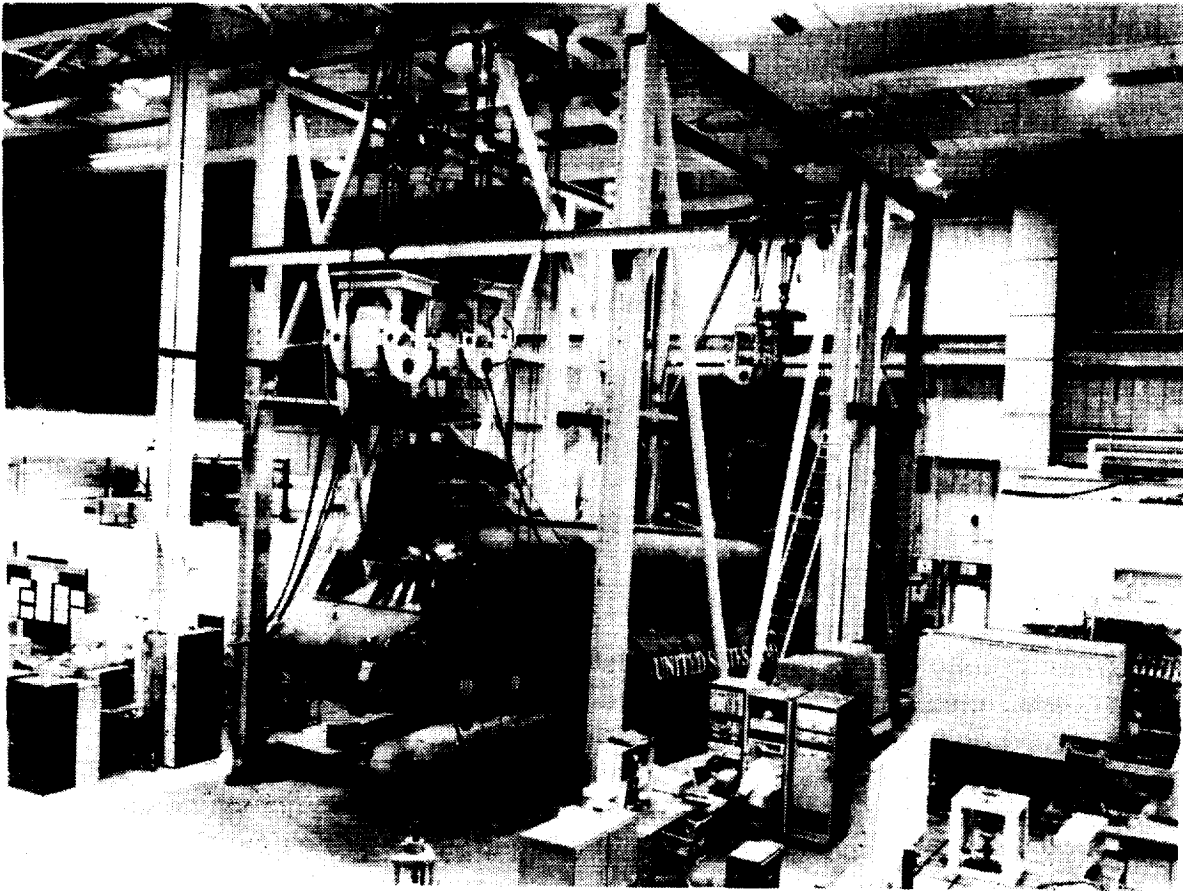
The above photograph shows a Boeing CH-47D helicopter airframe mounted in a ground shake test rig. The finite element model associated with this helicopter is shown in the following figure. The complexity of such structures leads to many approximations both in code development and in code use.

STATIC MODELING
CH-47D NASTRAN STRUCTURAL MODEL
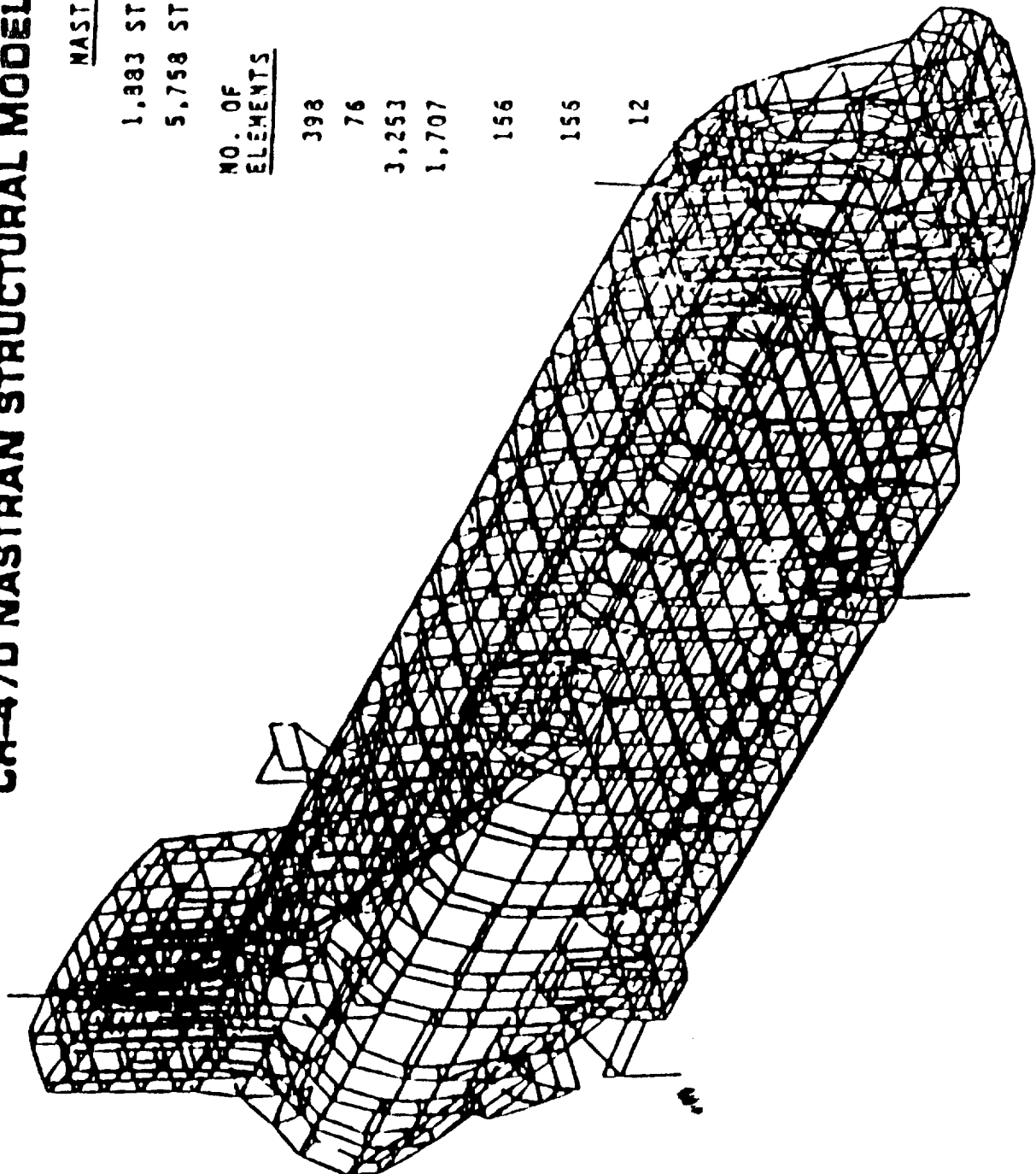
NASTRAN MODEL

1,383 STRUCTURAL NODES
5,758 STRUCTURAL ELEMENTS

NO. OF ELEMENTS	TYPE
398	C3AR - BEAM
76	CELAS2 - SPRING
3,253	CONROD - AXIAL
1,707	CSHEAR - QUADRILATERAL SHEAR
156	CTRMEM - TRIANGULAR MEMBRANE
155	CQUAD1 - QUADRILATERAL SHELL
12	CTRIA1 - TRIANGULAR SHELL

NASA LANGLEY RESEARCH CENTER

BOEING VERTOL COMPANY

171

Objective

- Develop technology needed for more accurate and easier to use analyses

The objective of this research is to develop finite element technology which can be used to improve the analysis capability of the rotorcraft industry. Improvements are needed to both the accuracy of finite element codes and in the user interface of these codes. An improved user interface should encourage the building of better finite element models.

Approach

- Develop a research finite element code for testing new ideas and techniques
- Fabricate and test a simple physical model
- Validate code with test results
- When satisfied with accuracy, increase complexity of physical model and analysis in order to more closely approximate a real-life structure

The approach taken with this research effort is to develop in-house a research finite element code for testing new computational and modeling techniques. A small, simple structure will be fabricated for testing. The code will be validated with the test results. If the validation is not accurate, then the code or the finite element model will be modified as necessary to improve the accuracy. When accuracy is satisfied, the complexity of both the finite element analysis and of the physical structure will be increased, and the process will be repeated. The cycle will continue in this way until experience and confidence indicate the ability to analyze full scale rotorcraft structures (see flow chart on the following page).

Approach
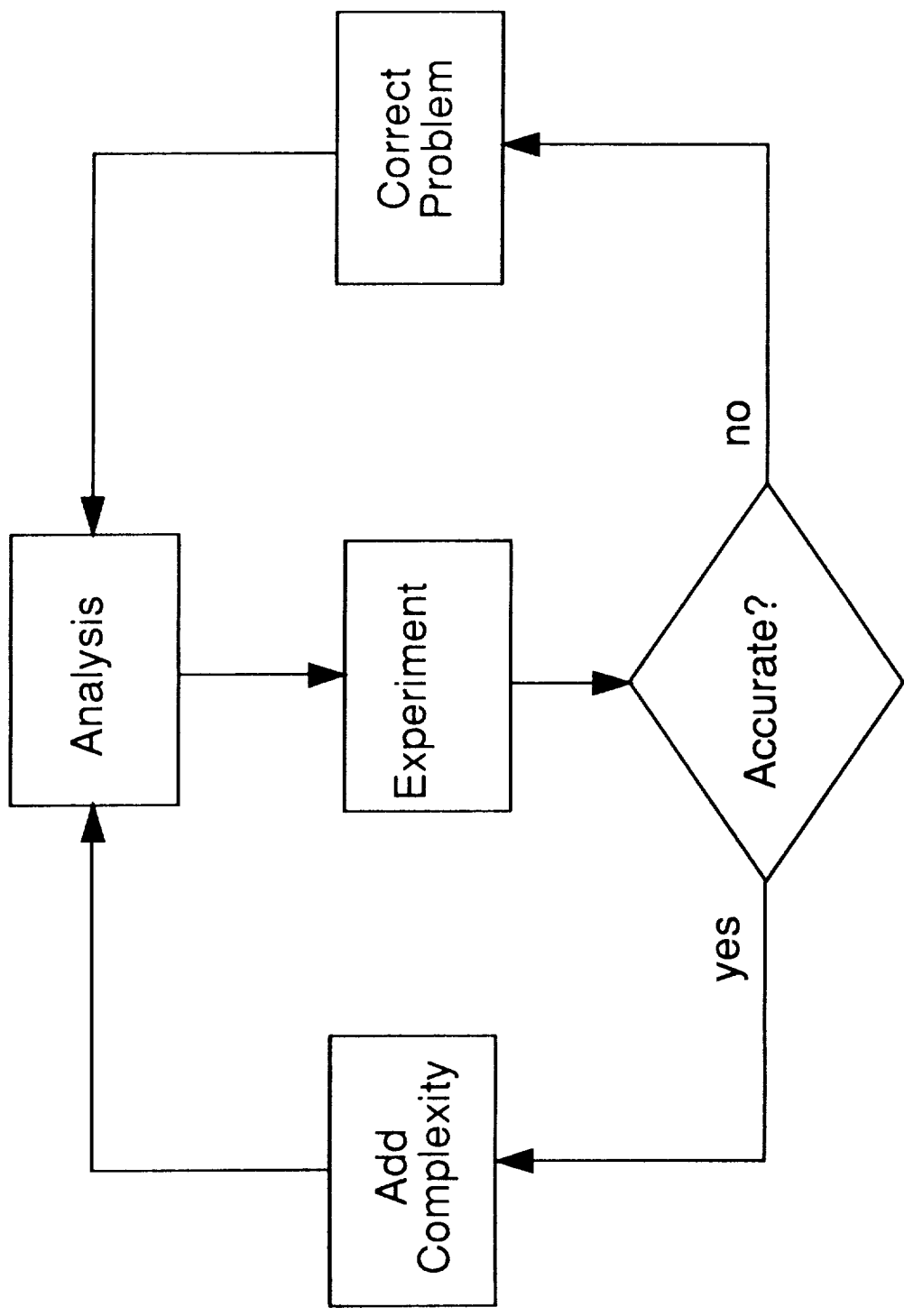
FEAT

Finite Element Advanced Technology

Features include

- Tapered p-version beam element

- General constraints - degrees of freedom can be made functions of other degrees of freedom

- Coordinate system definitions can be based on other coordinate systems

- Database managed by SQL (Structured Query Language) - A standard relational database format used for all types of data

The name of the research code developed is FEAT, which stands for Finite Element Advanced Technology. Features of FEAT include: A tapered p-version beam element. The beam's cross-sectional dimensions are allowed to taper from one end to the other. This allows much easier and more accurate representations of tapered structural members. Discussion of the p-version aspects of the element will follow later.

Any degree of freedom can be set to a constant or can be a linear function of other degrees of freedom. The constraint equations are defined with respect to local coordinate systems in which the degrees of freedom were defined. This constraint is analogous to the NASTRAN MPC constraint.

Coordinate systems can be defined with respect to previously defined coordinate systems, allowing the user to build complex chains of coordinate system definitions.

The input data for the program is stored in a Structured Query Language (SQL) database. SQL was developed by IBM specifically for manipulating relational databases and was adopted as an ANSI standard about four years ago. It is rapidly being accepted and endorsed by commercial database developers. Using a standard database in a finite element code has several advantages. A user, without the aid of FEAT, can query the database about his model. For example: "What elements are connected to grid point 738?" Another advantage is that FEAT is already capable of running in a multi-user network environment. SQL will handle multiple accesses to a database across the network. Still another advantage is that a lot of code development in FEAT was avoided because SQL handles many of the data manipulation tasks.

FEAT

## Finite Element Advanced Technology

Features (continued)

- All data structures allocated at run time. An analysis only takes up as much memory as it requires

- Global matrices use "skyline" storage technique. This saves vast amounts of storage and computational requirements.

- Matrix resequencing at the degree of freedom level is done with Reverse Cuthill-McKee

- Runs on a PC under OS/2

All data structures in FEAT are allocated dynamically at run time. There is no program statement in FEAT that gives a limit on the size of a job that the program can handle. Instead FEAT queries the SQL database for the size of the job, and then allocates only enough memory to handle the job. This allows the program to coexist with other programs in a multi-tasking environment in a very efficient manner. An added benefit is that the code is much easier to read and maintain when using dynamic data allocation.

The global matrices use the skyline storage technique. This technique takes advantage of the bandedness of structural problems by not explicitly storing many of the zeroes which appear in the global matrices. This not only saves vast amounts of storage, but also greatly reduces the computational requirements.

To further reduce the storage and computational requirements, the degrees of freedom are recorded using the Reverse Cuthill-McKee algorithm to reduce the skyline to a near minimum. FEAT currently runs on a PC under the OS/2 operating program. A port to VMS or Unix should be relatively easy.

Comparison Of
h-Version & p-Version
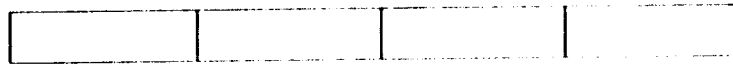
$$\boxed{|||}$$ h-version

$$v = q_0 + q_1 \, x \quad \text{on each element}$$

$$\boxed{}$$ p-version

$$v = q_0 + q_1 \, x + \ldots + q_p \, x^p \quad \text{on each element}$$

H-version elements, such as in NASTRAN and EAL, have fixed order polynomials which describe the displacement on each element. On this slide, I have shown linear polynomials. However, h-version elements can have any order polynomial describe the displacement. What makes it an h-version element is that the order of the polynomial is fixed when the element is developed. The p-version element has a path order polynomial on each element, where p is input by the user of the program. With h-version elements, one normally divides the domain up into a relatively fine mesh, but have a higher order polynomial approximate the displacement on each element.

h-Version Solution Of cos(x)
3 Degrees Of Freedom
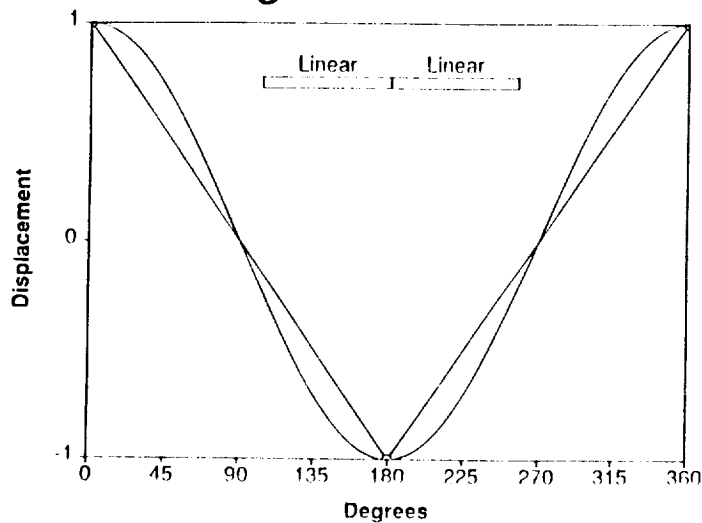
h-version Solution Of cos(x)
6 Degrees Of Freedom
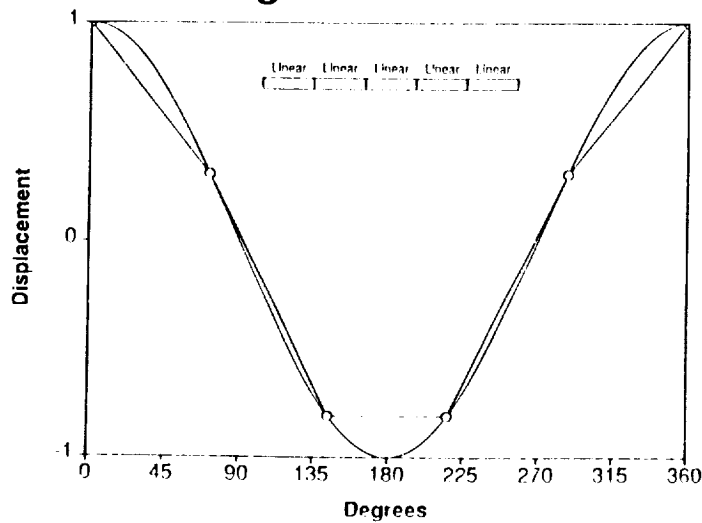
To demonstrate the difference between h-version and p-version elements, the figures above show two h-version solutions to a problem where the exact answer is known to be a cosine curve. The top figure is a two element approximation containing three degrees of freedom. The bottom figure shows the mesh refined to five elements for a total of six degrees of freedom. In general, as one adds more and more elements, the finite element solution will approach the exact solution over the entire domain.

178

p-Version Solution Of cos(x)
3 Degrees Of Freedom
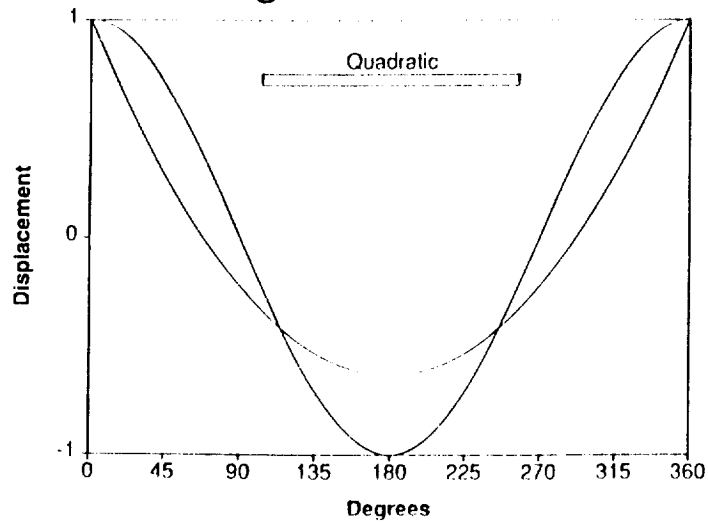
p-Version Solution Of cos(x)
6 Degrees Of Freedom
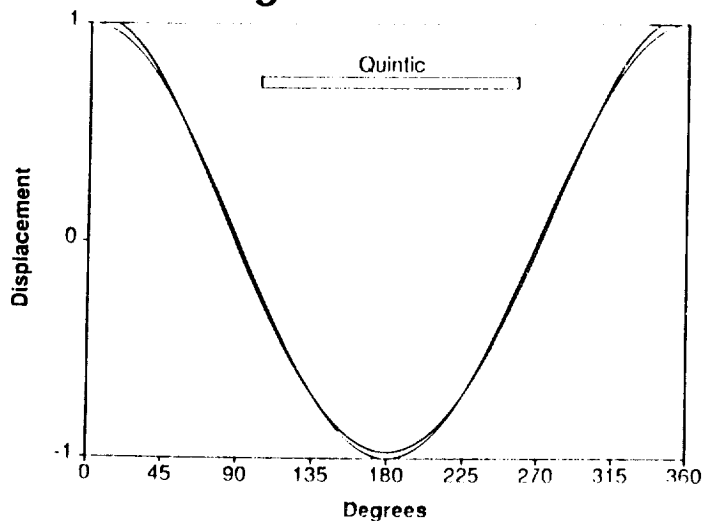
The two figures above show p-version solutions for the same problem discussed on the preceding page. These p-version solutions have the same number of degrees of freedom as the previous h-version solutions. In the bottom figure, one element using a 2nd degree polynomial has been raised to the 5th degree. The fact that convergence is achieved by raising the order of the polynomials, instead of refining the mesh, is what makes this a p-version solution.

Comparison Of Changes Needed In Input Data For h- & p-Version Models

Original h-version   h-extended   Original p-version   p-extended
data deck   data deck   data deck   data deck
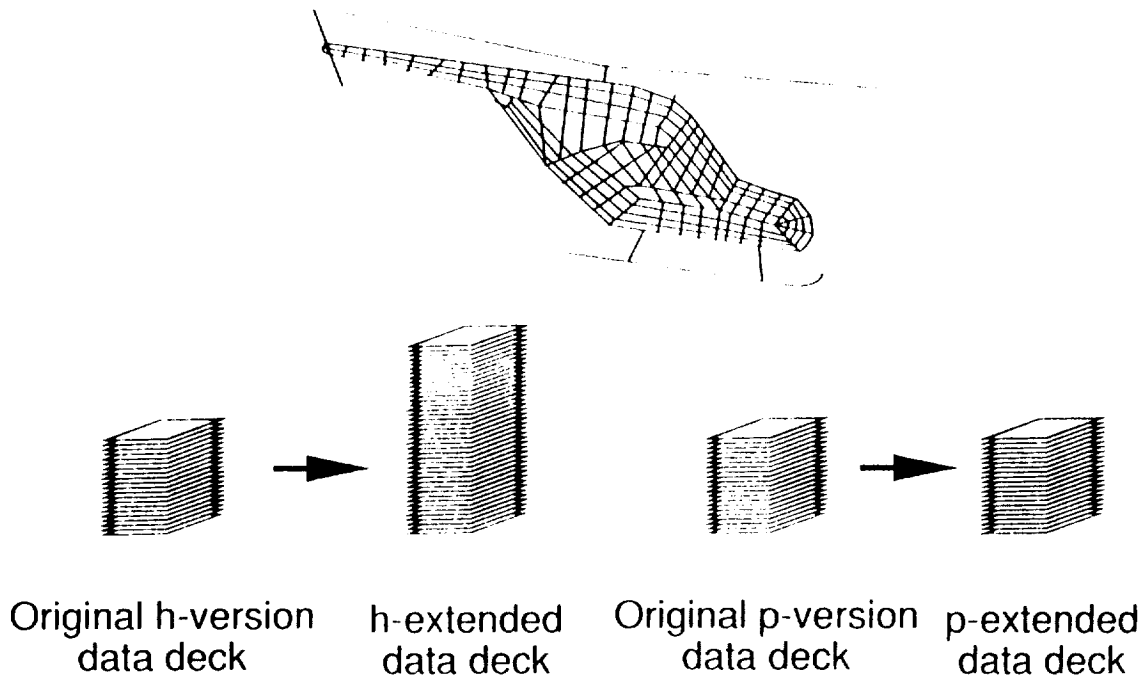
       Obtaining convergence by making your existing elements more accurate, instead of by adding more elements, has important implications for the finite element user. If one is trying to model a helicopter, it may take 10 man-months to generate the finite element model. If someone comes up and says: "That's great, but it is converged?", with an h-version code, you have no choice but to refine your mesh. This will probably double the size of your input deck and take another 5 to 10 man -months to generate. However, if you are using a p-version code, the modifications to the input data deck will take at most a man-afternoon. The size of the input data deck stays the same, only a few numbers in the data deck will change. This is the BIG advantage of p-version elements. It will be shown later that p-version elements are computationally more efficient than h-version elements, but the savings in computer time is nothing compared to the savings in engineering man-hours.

Conservation of Complexity

- Having p-version does not add complexity.

- It shifts complexity from the user to the finite element developer.

h-version   p-version

User   Developer   User   Developer
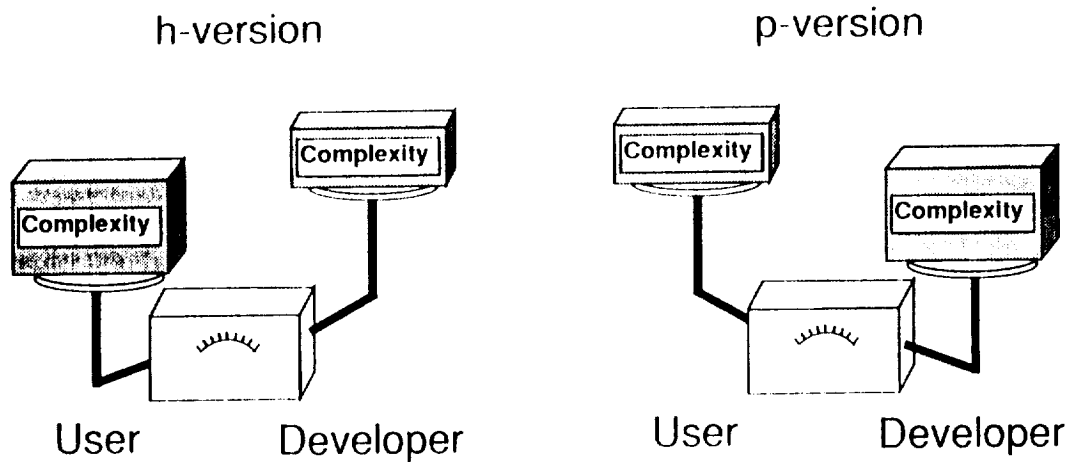
Some people complain about the complexity that p-version elements add to a finite element code. If one stands back and looks at the whole picture, that is, the user as well as the code developer, you can see that p-version elements don't add complexity, but merely shifts complexity from the user to the code developer. In my opinion, this is where the burden belongs.

Venn Diagram of
Finite Element Tools
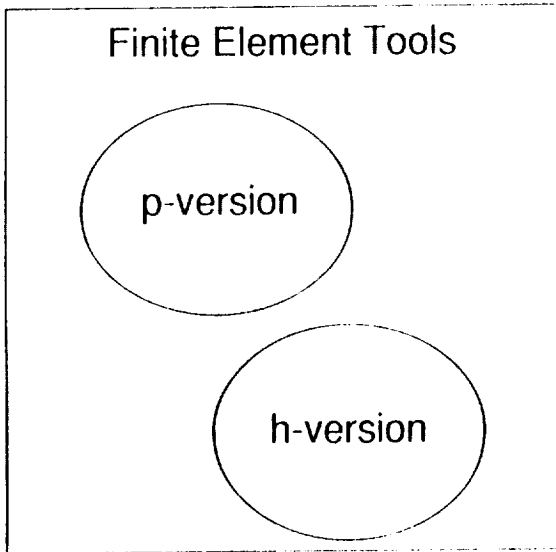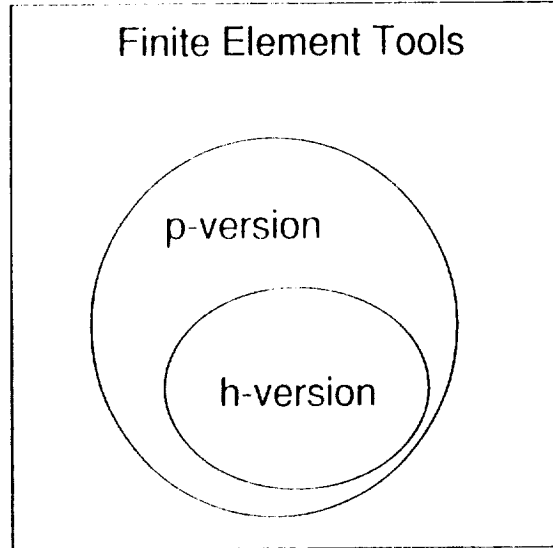
Finite Element Tools	Finite Element Tools
WRONG!	**RIGHT!**

Another misconception people have about p-version elements versus h-version elements is that they are two separate and non-overlapping entities. You have to choose to go with one way or the other. This is not completely true. H-version elements are actually a sub-set of p-version element. If you are using a p-version code, and you determine that you need an h-version elements, you simply say to yourself, "I will not change the order of the polynomials on that element. But I might subdivide that element." In other words you can use p-version elements as if they were h-version elements but not vice-versa.

Comparison Of h- And p-Version Convergence

Percent Error vs Number of Degrees of Freedom.
Fifth bending frequency
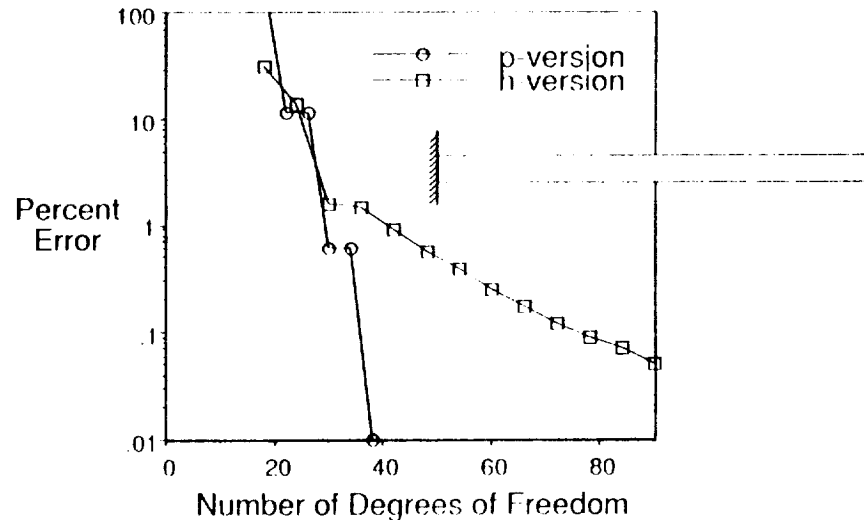
This figure shows actual results from FEAT. Plotted here is the percent error in the fifth bending frequency of a cantilevered beam versus the number of degrees of freedom in the finite element models. A p-version model is shown with the circle symbols, and an h-version model is shown with the squares. Note that the p-version model achieves a much lower error with fewer degrees of freedom. This translates to less computational effort for a given accuracy.

Current Status / Future Plans

- While development continues, FEAT is currently useable as a research tool.

- Contains only beam elements and concentrated masses. Plate elements will be included late this year or in early 91.

- A simple structural model has been fabricated and will be tested within one month. Correlation with FEAT will follow.

- Complexity will be added to the structural model at about the same time as plate elements are added to FEAT.

While development continues, FEAT is currently useable as a research tool. It contains only beam elements and concentrated masses at the moment, but a p-version plate element should be installed late this year or early next year. The first simple structural model has been fabricated and should be tested shortly. Complexity will be added to the physical model when plate elements are added to FEAT.

Summary

- Need to improve the dynamic analysis capability.

- FEAT is a research finite element code which will be used to experiment with new methodologies and modeling practices.

- p-version elements greatly reduce the complexity of the convergence study.

In summary, there is a need to improve the finite element technology on which the rotorcraft industry depends. FEAT is a research finite element code which will be used to try out new computational techniques and modeling practices. And finally, p-version elements greatly reduce the complexity of a convergence study.

TRANSONIC DYNAMICS TUNNEL

Bryce M. Kepley
NASA Langley Research Center
Hampton, VA

The Transonic Dynamics Tunnel (TDT) is a unique wind tunnel of the Langley Research Center that is located in the East Area of Langley Air Force Base, Hampton, Virginia. An aerial view of the TDT is shown in figure 1. The purpose of this facility is to determine the aeroelastic characteristics of high speed aircraft, rotorcraft, and most other aerospace vehicles produced in the U.S. Additionally, considerable efforts have been devoted to ground-wind loads tests for launch vehicles, especially the space shuttle. Since the wind tunnel supports a broad range of activities, such as basic research, industry and Department of Defense projects, there is a high demand for test time that normally perpetuates a schedule backlog of 1-1/2 years based on 2-shift operations. This backlog has recently diminished because of restrictions associated with a heavy gas test medium that will be discussed later.

The facility was originally constructed in the late 1930's as the 19-foot Pressure tunnel utilizing air as the test medium; however, it was modified in the late 1950's to become the TDT. Since that time, the test medium has been air or heavy gas (R-12) operating at atmospheric or subatmospheric pressure. Until the recently imposed limitations on operations, the test mode was heavy gas for approximately 80 to 90 percent of the time. Other subsequent modifications include a dedicated data acquisition system, a new cooling tower, and increased tunnel drive power which provided an increased density capability. These enhancements since the original construction amount to $27.7 million. The total replacement cost is estimated to be approximately $76.0 million.

Description

The TDT, as shown in figure 2, is a closed-loop wind tunnel. Continuous flow can be provided by a 30,000 horsepower motor which drives a 47-fiberglass blade, single-stage compressor. Total wind-tunnel volume is 1×10^6 ft3 with approximately 25 percent being contained in the plenum/test section which can be isolated with two large valves, a gate valve upstream, and a butterfly valve downstream. The cross-section view, figure 3, shows the 16 x 16 ft test section with the adjacent control room. Close proximity of the control room to the model is necessary to provide constant visual observation of the model, since aeroelastic testing is of a high-risk nature. Although the control room is physically within the plenum, it remains an atmospheric environment at all times. Figure 3 also shows "by-pass valve" which represents four 36-inch pipes, each with a fast operating valve connecting the plenum to the back leg of the tunnel. Operation of these valves during a wind-tunnel test rapidly reduces the test section dynamic pressure and Mach number to help prevent model failure due to aeroelastic instabilities.

Four primary model-support systems are used in the TDT wind tunnel. The model-support systems are a sidewall turntable mount (used primarily for semi-span aircraft models), a centerline sting mount, a free-flying cable mount, and a floor turntable mount. The sidewall and sting mounts provide the capability of remote angle-of-attack adjustment with "wind on" conditions. The floor mount may also be rotated remotely.

187

Capabilities

The Mach number range of the TDT is zero to 1.2. The highest Mach number and dynamic pressure combinations are only attainable in heavy gas. The heavy gas (R-12) test medium is a very critical aspect to the successful operation of the TDT. Since R-12 is approximately four times denser than air, it allows for easier scaling of the mass-density ratio, which may not otherwise be attainable. It is desirable for the ratio of the distributed mass of the vehicle to the mass of the surrounding flight medium, or mass-density ratio, to be the same for the model and the actual vehicle for developmental flutter clearance testing. Heavy gas provides the capability of testing heavier models which are easier to construct and build. This was the primary justification for the 50 percent operating-density increase in the mid 1980's. Other advantages of an R-12 test medium include lower scaled-model frequencies, higher Reynolds number, and lower drive motor horsepower requirements.

Heavy Gas System

The heavy gas test medium, R-12, is delivered in bulk quantities and stored at the TDT in the liquid state. Storage capacity is approximately 187 tons. The wind tunnel capacity is 147 tons when fully charged in the gaseous state. The gaseous state is attained through vaporization. When a test is completed or access to the model is desired for a configuration change, the R-12 gas is pumped from the wind tunnel and passed through a reclamation system to convert it back to a liquid for storage and subsequent pressure of 600 psi. The gas leaving this point is a 78/22 percent air/R-12 mixture. It is passed through a secondary recovery stage which is a three level +40, -40, and -80°F refrigeration system. Although the system is approximately 98 percent efficient, based on processing 5000 tons annually, the total loss of R-12 is significant. Other losses are from leaks at flanges, valves and valve stems, and compressor shaft seals. R-12 is also trapped in pockets in the plenum/test section area which cannot effectively be removed.

Recognizing the environmental responsibilities associated with R-12 and the need to be in concert with the Montreal Protocol, a number of activities were initiated in 1989 to reduce the loss of R-12. A study which was finalized as a preliminary engineering report was completed. Restrictions were imposed on the use of R-12 as a test medium thereby limiting tests to those related to national security and having high priority. These restrictions and associated uncertainties have reduced the schedule backlog for tunnel usage.

Heavy Gas System Modifications

A Construction of Facility (CofF) project was immediately approved to modify the heavy gas reclamation system. Project design is underway. Basically the existing refrigeration system will be replaced with a low temperature condenser (LTC) system which will use LN_2 as the coolant, thereby providing temperatures to -200°F. Leaks will be reduced by modifying flanges, replacing valves, and installing a scavenging system to capture gasses where leaks are probable. Pockets that trap heavy gas will

188

be filled with foamglass or will have ports installed to provide drainage. Adequate instrumentation will also permit an improvement in operating procedures. Normally a CofF project of this magnitude requires 2 to 4 years to be approved. This project is unique since it will have been approved and design completed in less than one year from concept. Moreover, construction is expected to be completed in late 1991; an additional year. The estimated project cost is $6.5 million.

Summary

Although environmental concerns were the original project justification, economic factors have since become an important consideration. An excise tax, which will reach $4.00 per pound before the turn of the century was applied to R-12 in 1990. The project goal is to reduce the heavy gas losses in the TDT to less than one ton per year.

The TDT has operated in the heavy gas mode for three decades; moreover, a successful completion of modifications to the heavy gas reclamation system should provide another three decades of heavy gas operation with the TDT continuing to be the lead facility in the area of aeroelastic research.
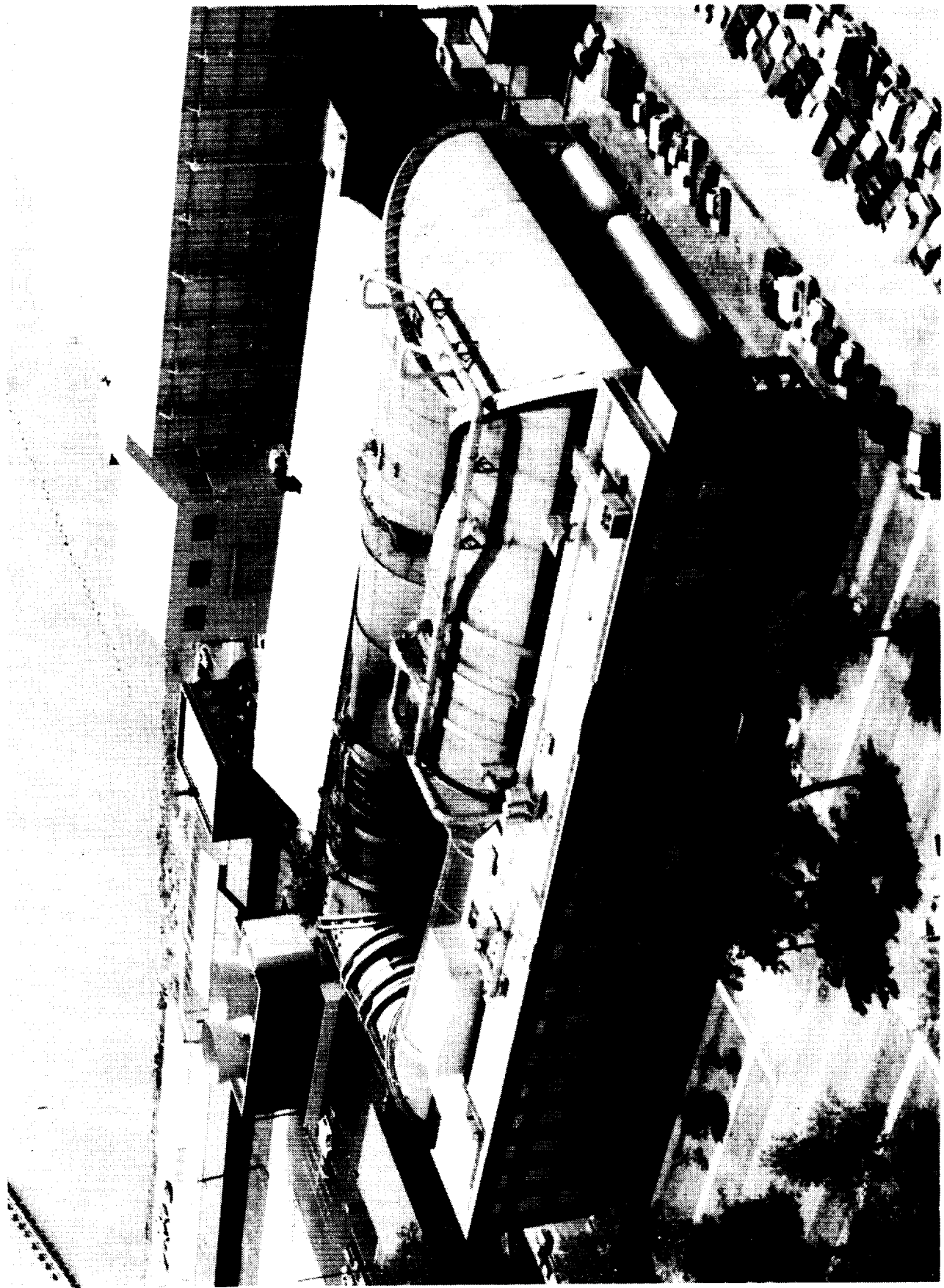
Figure 1 - Aerial view of the TDT facility.

Figure 2 - Planform View of the TDT.

FAN BLADES(47)

REMOTELY
ADJUSTABLE VANES

FIXED
VANES

MOTOR NACELLE

30,000 HP
MOTOR

ELECTRICAL
EQUIPMENT
BUILDING

2 ROW VERTICAL
TUBE COOLER

VANES

VANES

BYPASS
VALVE

TEST CHAMBER

GATE
VALVE

BUTTERFLY VALVE

FLOW

60'
DIA.

CONTROL
ROOM

3rd

2nd

LABORATORY BUILDING

EQUIPMENT BUILDING

Scale, ft

0   50

C-3

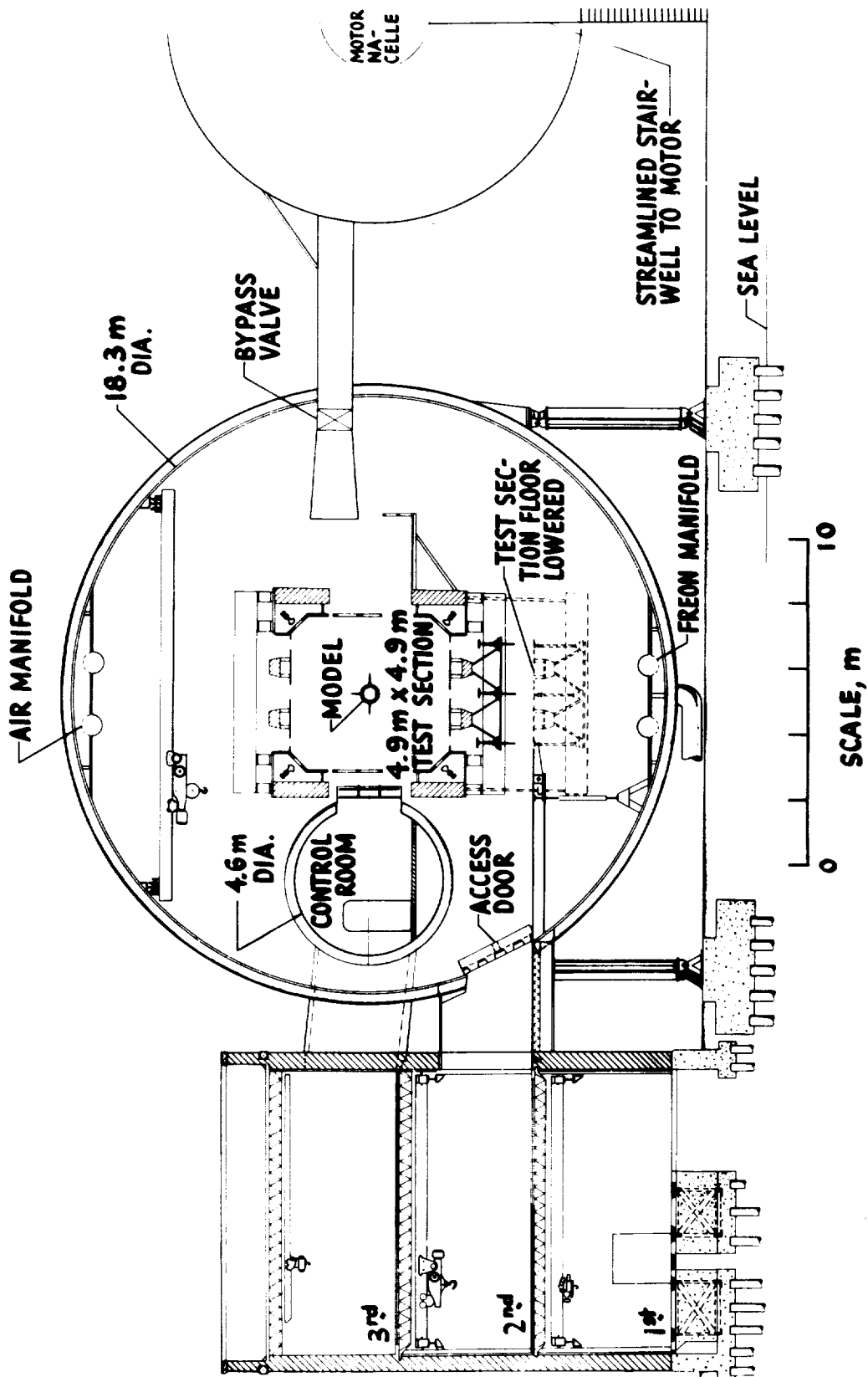Figure 3 - Cross-section View of the TDT.

REPORT DOCUMENTATION PAGE

Public reporting burden for this collection of information is estimated to average 1 hour per response, including the time for reviewing instructions, searching existing data sources, gathering and maintaining the data needed, and completing and reviewing the collection of information. Send comments regarding this burden estimate or any other aspect of this collection of information, including suggestions for reducing this burden, to Washington Headquarters Services, Directorate for Information Operations and Reports, 1215 Jefferson Davis Highway, Suite 1204, Arlington, VA 22202-4302, and to the Office of Management and Budget, Paperwork Reduction Project (0704-0188), Washington, DC 20503.

1. AGENCY USE ONLY (Leave blank)	2. REPORT DATE	3. REPORT TYPE AND DATES COVERED
	October 1991	Technical Memorandum

4. TITLE AND SUBTITLE
Technical Activities of the Configuration Aeroelasticity Branch

5. FUNDING NUMBERS
505-63-50

6. AUTHOR(S)
Stanley R. Cole, Editor

7. PERFORMING ORGANIZATION NAME(S) AND ADDRESS(ES)
NASA Langley Research Center
Hampton, Virginia 23665-5225

8. PERFORMING ORGANIZATION REPORT NUMBER

9. SPONSORING / MONITORING AGENCY NAME(S) AND ADDRESS(ES)
National Aeronautics and Space Administration
Washington, DC 20546-0001

10. SPONSORING / MONITORING AGENCY REPORT NUMBER
NASA TM-104146

11. SUPPLEMENTARY NOTES
This compilation is a summary of a technical review of the Configuration Aeroelasticity Branch of the Structural Dynamics Division.

12a. DISTRIBUTION / AVAILABILITY STATEMENT
Unclassified-Unlimited

Subject Category 39

12b. DISTRIBUTION CODE

13. ABSTRACT (Maximum 200 words)

A number of recent technical activities of the Configuration Aeroelasticity Branch of the NASA Langley Research Center are discussed in detail. The information on the research branch is complied as twelve separate topics. The first of these topics is a summary of the purpose of the branch, including a full description of the branch and its associated projects and program efforts. The following ten papers cover specific projects conducted or underway in the branch. The final paper describes the primary facility operation by the branch, the Langley Transonic Dynamics Tunnel.

14. SUBJECT TERMS
Aeroelasticity
Wind Tunnel
Rotorcraft

15. NUMBER OF PAGES
197

16. PRICE CODE
A09

17. SECURITY CLASSIFICATION OF REPORT	18. SECURITY CLASSIFICATION OF THIS PAGE	19. SECURITY CLASSIFICATION OF ABSTRACT	20. LIMITATION OF ABSTRACT
Unclassified	Unclassified		